Application of Thrust Vectoring to Reduce Vertical Tail Size

L.B. Timmerman

Technische Universiteit Delft

TU Delft Delft University of Technology

Challenge the future

Application of Thrust Vectoring to Reduce Vertical Tail Size

by

L.B. Timmerman

in partial fulfillment of the requirements for the degree of

Master of Science

in Aerospace Engineering

at the Delft University of Technology,

to be defended publicly on Monday May 8, 2017 at 14:00 hours.

Student number:	4420608	
Thesis registration number:	127#17#MT#FPP	
Project duration:	May 9, 2016 – May 8, 2017	
Supervisor:	Prof. dr. ir. M. Voskuijl,	TU Delft
Thesis committee:	Dr. ir. L. M. Veldhuis,	TU Delft
	Dr. ir. S. Hartjes,	TU Delft

An electronic version of this thesis is available at http://repository.tudelft.nl/.

Cover photo courtesy of www.dutch-aviation.nl

PREFACE

I am often confronted with the question, "Why do modern aircraft designs look identical to the airplanes build forty years ago?" In my opinion, this is a *trap* question because the interrogator is expecting a simple response, and most simple responses will discredit the advancements made within the aerospace industry over the past forty years. The fact is that aircraft designs have changed significantly; however, not every design improvement will be recognized by the untrained eye. During my studies, I have studied aircraft aerodynamics, propulsion systems, performance, stability, and many other aerospace disciplines. From more than six years of study, along with pure interest in aircraft design, I have just began to understand what differentiates the aircraft designs from forty years ago from modern aircraft.

To answer their question I feel compelled to list all the technological improvements made to aircraft in recent history; however, this is not a compelling way to answer their questions. After being asked this question multiple times, I feel the best answer is to discuss how the price of air travel has changed during the past forty years. Forty years ago, air travel could only be afforded by the wealthy. Nowadays, the amount of people in the world who fly each year has skyrocketed when compared to forty years ago.

This answer subtly gives credit to all the technological advancements made within the aerospace industry over the past forty years. After I finish providing my answer, the interrogator typically gains a greater appreciation for the work completed by aerospace engineers, and I am given the opportunity to discuss the future of aircraft design and aerospace engineering. For myself, discussing the future of aircraft design tends to be a more exciting discussion topic than discussing past aircraft designs. In particular, my education has provided me with the foresight relating to the design of future aircraft. With this being said, the past forty years of aerospace engineering have been thrilling; however, I am more intrigued by the next forty years of aerospace engineering.

L.B. Timmerman
Delft, May 2017

SUMMARY

The vertical tail size of a multi-engine aircraft is typically driven by the directional control requirement during one-engine-inoperative flight. This results in the vertical tail being over-sized for most regularly occurring flight conditions. By adding thrust vectoring technology to an aircraft, the vertical tail can be designed to cope with regularly occurring flight conditions rather than the one-engine-inoperative flight condition. A modern aircraft was redesigned such that it would have thrust vectoring capabilities and an unconventionally small vertical tail. The redesigned vertical tails had areas which were 85%, 70%, 60%, and 50% of the original vertical tail area, which corresponded to reductions in the vertical tail area of 15%, 30%, 40%, and 50%, respectively.

Analyses showed that the redesigned vertical tail and change in aircraft inertia due to the addition of thrust vectoring technology had a negligible impact of the aircraft's roll mode dynamics. It was also shown that the reduction in vertical tail area resulted in a degradation of the aircraft's spiral mode flight qualities. With regards to the Dutch roll motion, a reduction in vertical tail resulted in a reduction of Dutch roll damping coefficient and Dutch roll frequency. Based on the analysis of the Dutch roll mode, it has been recommended that a compromise between the 85% and 70% VT area would likely produce an acceptable compromise between the reduced VT area and Dutch roll flight characteristics; however, the aircraft design would required a yaw damper.

It is predicted that trimmed flight with one-engine-inoperative can be achieved by simultaneously using thrust vectoring technology and an unconventionally small vertical tail. Through the use of directional thrust vectoring, an aircraft's rudder deflection angle, aileron deflection angle, and bank angle may reduced during the one-engine-inoperative flight condition. Analysis of the one-engine-inoperative and crosswind flight condition shows that using thrust vectoring for directional control may allow for a reduction in trim drag; however, additional analysis of this flight condition should be competed.

Through an analysis of a vertical tail mass estimation, it has been shown that the reduction in vertical tail mass resulting from a reduction in vertical tail area is of comparable magnitude when compared to the engine mass increase due to the addition of thrust vectoring technologies. Lastly, it has been shown that an aircraft's mission fuel consumption can be reduced if the aircraft's vertical tail area is reduced and thrust vectoring flight control is implemented into the aircraft design. Reductions in mission fuel consumption greater than 1% are unlikely; however, there are feasible reductions in mission fuel mass for the proposed thrust vectoring aircraft design.

Acknowledgments

I am honored to have had the opportunity to complete a M.Sc. in Aerospace Engineering at TU Delft; however, I could not have done this without the support of many family members, friends, and colleagues. I would like to express my appreciation to the individuals who have provided support during my time spent at TU Delft.

Firstly, I would like to thank my parents, Peter and Kimberly. They have provided moral and financial support to help me reach this point in my life. I aspired to become an aerospace engineer at an early age of my life, and they allowed me to achieve this goal. My brother, Christopher and sister, Alicia, have always offered a listening ear, and for that, I would like to thank them.

There are a few individuals at TU Delft who I would like to acknowledge. In particular, my thesis supervisor, Mark Voskuijl, has provided much support during the thesis project. He was always willing to answer questions and provide guidance for the thesis research. For the thesis project I required a geometric model of the Fokker 100 aircraft. Jian Wei created the aircraft model used for the aerodynamic simulations in this thesis, and I am thankful for the work he spent making the model. I would like to acknowledge, not thank, my friend, Aljaz, for convincing me to complete multiple courses in the aerodynamics track at TU Delft. In my opinion the aerodynamics courses are what nightmares are made of; however, Aljaz helped me overcome the challenges I encountered during these courses. My friends Andrea, Dario, Reynard, and Adam have also provided lively and thought-provoking, off-the-wall conversations during my thesis studies, and for that, I would like to thank them.

If you, the reader, have made it this far into the thesis report, I wish you godspeed with the next 80 plus pages.

L.B. Timmerman
Delft, May 2017

Contents

List of Figures

List of Tables

6

NOMENCLATURE

Latin Symbol	Description	Units
A	Area	$[m^2]$
A^E	Effective area	$[m^2]$
A^G	Geometric area	$[m^2]$
b	Wingspan	$[m]$
C_D	Drag coefficient	$[-]$
C_{fg}	Thrust coefficient	$[-]$
C_L	Lift coefficient	$[-]$
C_{l_β}	Derivative of roll rate w.r.t. sideslip angle	$[-]$
C_{l_p}	Derivative of roll rate w.r.t. roll rate	$[-]$
C_{l_r}	Derivative of roll rate w.r.t. yaw rate	$[-]$
$C_{l_{\delta_a}}$	Derivative of roll rate w.r.t. aileron deflection	$[-]$
$C_{l_{\delta_r}}$	Derivative of roll rate w.r.t. rudder deflection	$[-]$
$C_{l_{\delta_{TVFC}}}$	Derivative of roll rate w.r.t. thrust vectoring deflection	$[-]$
$C\mathfrak{L}_\beta$	Derivative of aerodynamic load w.r.t. sideslip angle	$[-]$
$C\mathfrak{L}_{\delta r}$	Derivative of aerodynamic load w.r.t. rudder deflection	$[-]$
C_{n_p}	Derivative of yaw rate w.r.t. roll rate	$[-]$
C_{n_r}	Derivative of yaw rate w.r.t. yaw rate	$[-]$
C_{n_T}	Derivative of yaw rate due to inoperative engine	$[-]$
C_{n_β}	Derivative of yaw rate w.r.t. sideslip angle	$[-]$
$C_{n_{\delta_a}}$	Derivative of yaw rate w.r.t. aileron deflection	$[-]$
$C_{n_{\delta_r}}$	Derivative of yaw rate w.r.t. rudder deflection	$[-]$
$C_{n_{\delta_{TVFC}}}$	Derivative of yaw rate w.r.t. thrust vectoring deflection	$[-]$
C_{y_β}	Derivative of sideforce w.r.t. sideslip angle	$[-]$
C_{y_p}	Derivative of sideforce w.r.t. roll rate	$[-]$
C_{y_r}	Derivative of sideforce w.r.t. yaw rate	$[-]$
$C_{y_{\delta_a}}$	Derivative of sideforce w.r.t. aileron deflection	$[-]$
$C_{y_{\delta_r}}$	Derivative of sideforce w.r.t. rudder deflection	$[-]$
$C_{y_{\delta_{noz}}}$	Derivative of sideforce w.r.t. thrust vectoring deflection	$[-]$
C_p	Pressure coefficient	$[-]$
F_g	Engine gross thrust	$[\ kg \cdot m/s^2\ ]$
g	Acceleration due to gravity	$[m/s^2]$
I_{xx}	Rolling moment of inertia	$[kg \cdot m^2]$
I_{xz}	xz Product of inertia	$[kg \cdot m^2]$
I_{zz}	Yawing moment of inertia	$[kg \cdot m^2]$
k	Mass correction factor	$[-2]$
L	Rolling moment	$[kg \cdot m^2/s^2]$
$\mathfrak{L}$	Aerodynamic load (shear, bending, or torsion)	$[kg \cdot m/s^2]$ or $[kg \cdot m^2/s^2]$
m	Mass	$[kg]$
$\dot{m}$	Mass flow rate	$[kg/s]$
M	Mach number	$[-]$
M_{MO}	Maximum operating mach number	$[-]$
N	Yawing moment	$[kg \cdot m^2/s^2]$
p	Angular velocity about the x-axis	$[rad/s]$
P_e	Nozzle exit pressure	$[kg/m^2]$
P_a	Ambient pressure	$[kg//m^2]$
$\bar{q}$	Dynamic pressure	$[kg/m^2]$

r	Angular velocity about the z-axis	$[rad/s]$
S	Wing area	$[m^2]$
T_2	Time to double amplitude	$[s]$
u	Linear velocity along the x-axis	$[m/s]$
v	Linear velocity along the y-axis	$[m/s]$
V_e	Nozzle exit velocity	$[m/s]$
V_{MO}	Maximum operating speed	$[m/s]$
w	Linear velocity along the z-axis	$[m/s]$
x	Direction along the coordinate system's x-axis	$[-]$
X	Force along the x-axis	$[kg \cdot m/s^2]$
y	Direction along the coordinate system's y-axis	$[-]$
$y_{eng,c.g.}$	Distance in y-direction between engine c.g. and aircraft c.g.	$[m]$
Y	Force along the y-axis	$[kg \cdot m/s^2]$
z	Direction along the coordinate system's z-axis	$[-]$
$z_{eng,c.g.}$	Distance in z-direction between engine c.g. and aircraft c.g.	$[m]$
$z_{VT,c.g.}$	Distance in y-direction between vertical tail c.g. and aircraft c.g.	$[m]$
Z	Force along the Z-axis	$[kg \cdot m/s^2]$

Latin Symbol	**Description**	**Units**
α	Angle of attack	$[deg]$
β	Angle of sideslip	$[deg]$
γ	Ratio of specific heats	$[-]$
δ_a	Aileron deflection angle	$[deg]$
δ_r	Rudder deflection angle	$[deg]$
δ_{TVFC}	Thrust vectoring deflection angle	$[deg]$
θ	Pitch angle	$[deg]$
ς	$1 + \left(\frac{\gamma-1}{2}\right) M^2$	$[-]$
τ_{roll}	Roll mode time constant	$[s]$
ϕ	Bank angle	$[deg]$
χ	Ratio of effective area to geometric area	$[-]$
ξ	$\frac{\frac{\partial Cn}{\partial \delta_{TVFC}}}{\frac{\partial Cn}{\delta_r}} = \frac{Cn_{\delta_{TVFC}}}{Cn_{\delta_r}}$	$[-]$
ψ	Geometric angle between wing and horizontal tail	$[deg]$
ω_{DR}	Dutch roll frequency	$[rad/s]$
ζ_{DR}	Dutch roll damping coefficient	$[-]$

1
INTRODUCTION

In an effort to improve the competitiveness, performance, and sustainability of the European aviation industry, the European Commission published a document entitled *Flightpath 2050 Europe's Vision for Aviation*. The intention of the document is to inspire airliners, airports, aircraft design companies, and other aerospace related industries to develop innovative technologies and procedures aimed at reducing future greenhouse gas emissions, irrespective of the increasing air traffic growth. One specific and measurable goal stated within this document challenges the European aviation industry to reduce the present levels of CO_2 and NO_X emissions by 75% and 90%, respectively, by the year 2050 [2]. A formidable amount of innovation is required to achieve this goal, and this innovation challenge is no exception to aircraft design companies.

One technology which may be used to overcome the challenge for innovation is the thrust vectoring aircraft engine. Thrust vectoring is the concept of directing an aircraft engine's exhaust jet. By vectoring the exhaust jet, the engine's thrust can be used as a form of aircraft flight control. This concept, as shown if figure 1.1, is called thrust vectoring flight control (TVFC).

TVFC has been applied to various fighter aircraft designs to improve their maneuverability, but the technology has yet to be implemented into civil transport aircraft (CTA) designs. Typically flight control of a CTA is provided by the aircraft's ailerons, elevator, and rudder; however, the aircraft engine can also provide flight control. Because multiple methods of aircraft flight control exist, the ideal method of flight control allowing for a sustainable, efficient, and safe CTA design should be investigated.

Consider the design requirements of an aircraft's vertical tail and rudder. These aerodynamic surface are required to provide (1) static and dynamic directional stability, (2) directional control, and (3) forces and moments for flight equilibrium [3]. In particular, these surfaces must allow an aircraft to fly safely during flight conditions with large sideslip angles. Flight with large sideslip angles is commonly caused by either crosswinds or asymmetric thrust, such as a multi-engine aircraft flying with one-engine-inoperative (OEI). For many multi-engine aircraft designs, the OEI with crosswind flight condition drives the design and size of the vertical tail and rudder. This extreme flight condition seldom occurs, thus an aircraft's vertical tail and rudder may be over-sized for regularly occurring flight conditions.

By designing a multi-engine CTA with both thrust vectoring engines and an unconventionally small vertical tail and rudder, it may be possible to satisfy the aircraft's directional stability and control (S&C) requirements. The vertical tail and rudder can be designed to cope with the regularly occurring flight conditions. In the occurrence of OEI, crosswind flight, both thrust vectoring and aerodynamic control forces can be used to provide safe flight. Such an aircraft design, with TVFC and an unconventionally small vertical tail and rudder, would allow for a reduction in an aircraft's wetted surface area and parasitic drag coefficient.

In order to achieve the goals presented within *Flightpath 2050 Europe's Vision for Aviation*, it is worthwhile to investigate TVFC and the design of CTA. A review of past thrust vectoring research will be presented in order to identify the benefits and challenges associated with thrust vectoring aircraft. The review will also indicate the manner in which TVFC may be applied to the design of CTA. Next, the knowledge gained from the review will aid in the formulation of research questions and a research objective. Once the research objective is formulated, the methods and theories used to achieve the research objective will be presented. Finally, the results of thesis work will be presented in a manner which satisfies the research objective. A summary of thesis structure can be described as follows:

1. Review the history of TVFC and design criteria of CTA. This literature review occurs in chapter 2.
2. Identify the benefits and disadvantages of TVFC and how they apply to CTA. This step occurs in the opening portion of chapter 2.
3. Formulate research questions and research objectives. The research objective is presented in chapter 3.
4. Introduce the methods and theories required to accomplish the research objective. The theoretical portion of this report is presented at the beginning of chapters 4 through 8.
5. Present the results of the research and demonstrate the research objective has been accomplished. The presentation and discussion of results occurs in chapters 4 through 8; however, it is first preceded by a discussion of the relevant theories used to obtain the results.
6. Discuss the results and formulate conclusions about the feasibility of a CTA designed with TVFC and an unconventionally small vertical tail, and make recommendations for future research topics. This occurs in the final chapter, chapter 9

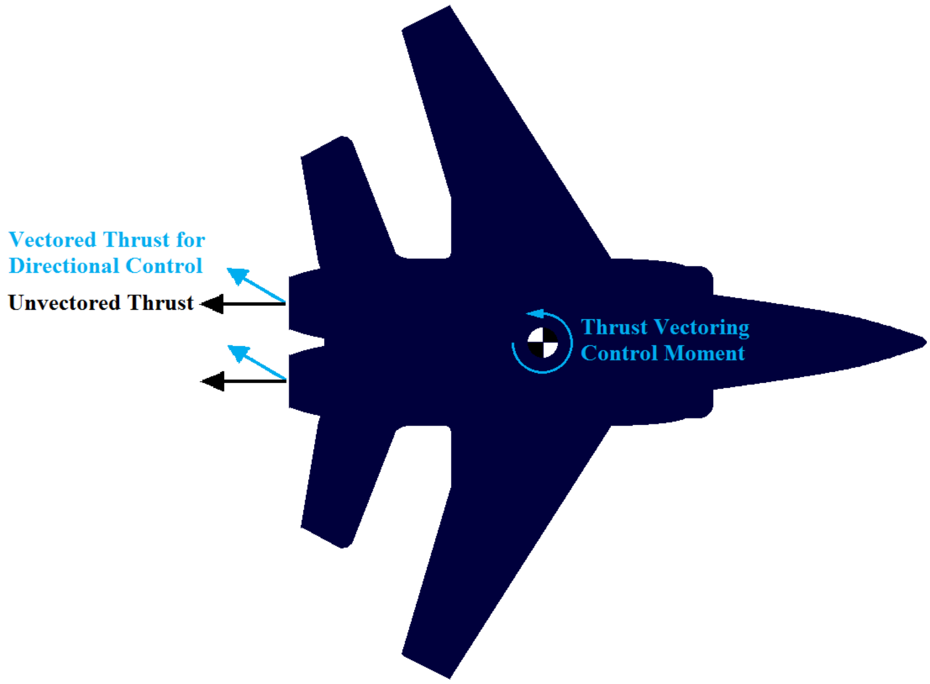

Figure 1.1: Thrust vectoring for flight control

2

Review of Thrust Vectoring Research

2.1. History of TVFC and Fighter Aircraft

The idea to use vectored thrust as form of flight control was first conceived by German missile designers during World War II. During the war, German engineers discovered that directing a missile's exhaust jet would allow for control over the missile's flight path [4]. German designed missiles required this technology because the missiles would fly at altitudes where aerodynamic control surfaces would lose their effectiveness due to low dynamic pressure. A new form of flight control was required for high altitude flight, thus the invention of thrust vectoring flight control (TVFC) came into being. Although TVFC was introduced during World War II, it wasn't until after the war that the technology was introduced into the design of manned aircraft.

The first manned aircraft designed with TVFC were fighter aircraft. According to Ray Whitford, in his book entitled *Design for Air Combat*, fighter aircraft should have high instantaneous turn rates, high control power, and short takeoff and landing (STOL) performance, among a few other design criteria. Two of the aforementioned design requirements ensure the aircraft has the ability to outmaneuver an opponent in the occurrence of air-to-air combat [5]. The STOL requirement ensures the aircraft can takeoff and land in areas which may be unreachable by other military aircraft, such as an aircraft carrier or a damaged, shorted runway. With these aircraft design criteria in mind, aircraft designers began to investigate methods to design supermaneuverable fighter aircraft with STOL performance.

In the 1950s, aircraft designers in the United States needed to design a fixed wing aircraft with STOL ability; however, the engineers desired to push this ability further, and they began designing an aircraft with vertical takeoff and landing abilities. Their efforts resulted in the design of the X-14 aircraft. The technology developed in the design of the X-14 was eventually manifested in the design of the AV-8 Harrier [4], one of the first aircraft with thrust vectoring engine capabilities. The Harrier fulfilled the STOL aircraft design criteria; however, it did not meet the supermaneuverable design criteria required from most fighter aircraft.

In the 1970s, about a decade after the Harrier's first flight, aerospace engineers began researching methods to allow fighter aircraft to maneuver in high angle of attack and/or low dynamic pressure flight conditions. Their research led to the conceptual design of a rectangular aircraft engine nozzle with the ability to vertically vector the engine's exhaust jet, as shown in figure 2.1. This thrust vectoring nozzle design improved the aircraft's maneuverability around it's pitching axis; however, this nozzle did not have the ability to vector the thrust directionally, which would improve the aircraft maneuverability around it's yawing axis. Additional thrust vectoring nozzle research resulted in the creation of a circular nozzle with both vertical and directional thrust vectoring capabilities. Figure 2.2 shows such a nozzle design.

The design of vectoring nozzles with pitch/yaw control capabilities was driven by the desire to further improve an aircraft's maneuverability by allowing for post-stall flight control. Fighter aircraft often need to maneuver at high angles of attack, which is generally a flight condition where an aircraft's tail experiences low dynamic pressure caused by flow separation on the main wing [6]. If the tail experiences a low dynamic pressure flow, then it may not provide the aircraft with sufficient directional control power. Furthermore, insufficient directional control power limits an aircraft's ability to recover from a spin. An aircraft's engine(s) can

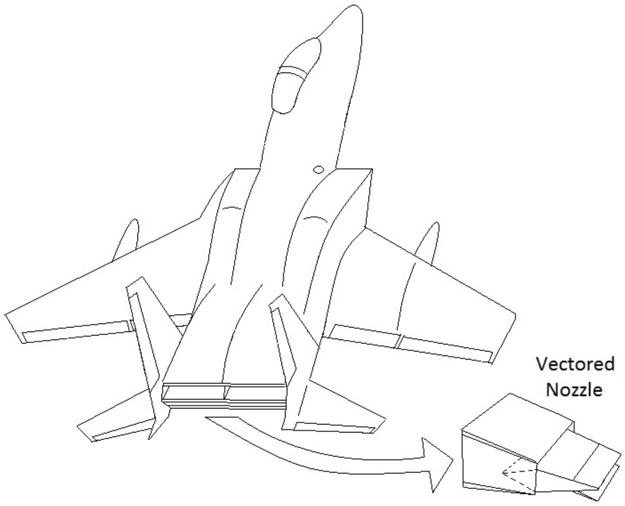

Figure 2.1: Thrust vectoring for pitch control

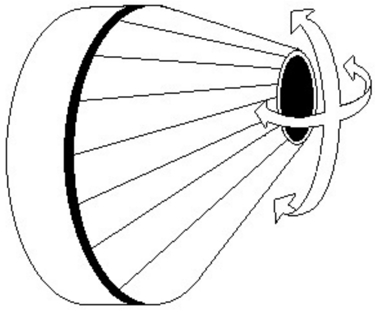

Figure 2.2: Thrust vectoring for pitch and yaw control

still function when the aircraft is flying at a high angle of attack, thus the thrust vectoring nozzle could still provide control forces when traditional aerodynamic control surfaces lose their effectiveness [7]. Through the synergistic flight control provided by aerodynamic surfaces and the thrust vectoring nozzle, it was discovered that an aircraft's maneuverability could be improved in all parts of the aircraft's flight envelope [8], and supermaneuverable aircraft were created.

An examination of figure 2.3 demonstrates why aerospace engineers have been interested in designing thrust vectoring fighter aircraft. In figure 2.3, an aircraft uses TVFC during post-stall flight conditions in order to change its heading angle by 180° and gain a positional advantage over an enemy aircraft during close-in-combat flight simulations. The maneuver demonstrated in this figure is named the Herbst maneuver, and it is an ideal example how TVFC can cause a fighter aircraft to become supermaneuverable.

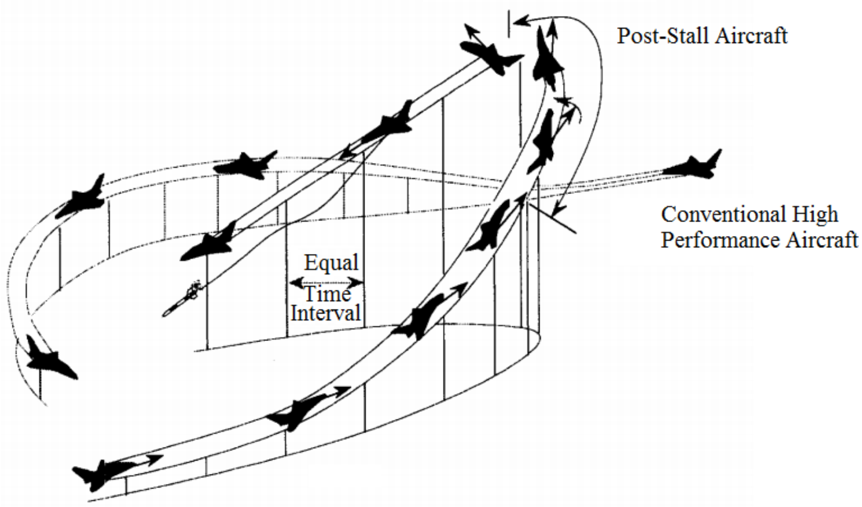

Figure 2.3: Herbst maneuver, demonstrated by thrust vectoring aircraft, in close-in-combat flight simulation [17]

The idea of thrust vectored aircraft intrigued many aircraft designers, and soon there was an abundance of research related to discovering the benefits of TVFC. Numerous benefits associated with TVFC were discovered, and table 2.1 list some of the results. The benefits listed in table 2.1 are accompanied by references. The references have been sorted into different categories which describe the type of research used for the analysis of TVFC. The categories used to sort the references include computer experiments, physical experiments, and conceptual reviews. Computer experiments include flight simulations, CFD, analytical calculations, etc.

to quantify the benefit of TVFC. Physical experiments include wind tunnel tests, physical flight tests, engine tests, etc. Conceptual reviews discuss theoretical TVFC benefits; however, conceptual reviews do not present quantitative data. For example, a conceptual review may say an aircraft's take-off run may be reduced if TVFC is used to increase the aircraft's pitch acceleration and rotation rate, but the conceptual review does not provide data validating the statement.

Benefit	**Reference**		
	Computer Experiment	Physical Experiment	Conceptual Review
Reduced Balanced Field Length (STOL)	[9]	[7] [10]	[11] [12] [13] [14] [15]
Improved Agility	[6] [8] [16] [17]	[7] [18]	[12] [15] [20]
Improved Maneuvering/ Post-Stall Maneuvering	[6] [8] [19] [16]	[7] [10] [18]	[12] [13] [14] [15] [21]
Increased Maximum Angle of Attack	[6] [16] [19] [17] [22]	[7] [18]	[14]
Improved Stealth (Reduced IR, Radar Cross-section)	[8]	-	[12] [13]
Reduced Trim and Parasite Drag	[8] [13] [23] [6] [17]	[7]	[12] [14] [20]

Table 2.1: Advantages of thrust vectoring flight control

Research which quantify a result tend to be more realiable than research which do not quantify a result. For this reason, it is beneficial to examine the research which quantify a benefit or disadvantage associated with TVFC. Table 2.2 presents quantified data associated with benefits of TVFC. The data in the table has been obtained from reference [7], and it compares the expected performance improvements of the thrust vectoring F-15 STOL/MTD (Short Take-off and Landing/Maneuver Technology Demonstrator) when compared to the standard F-15C. The data presented in table 2.2 was calculated with various computer experiments and flight simulations.

Special attention should be given to the benefits of improved stealth and reduced parasite drag. In order for these benefits to be achieved, the design of an aircraft's horizontal and vertical tail surfaces should be considered. If a traditional aircraft is designed with both TVFC and aerodynamic control surfaces, then it has redundant control surfaces. The control power required from the aircraft's elevator and rudder is reduced, because the thrust vectoring system can provide the necessary control forces and moments. This would allow for the thrust vectoring aircraft to have smaller horizontal and vertical tail surfaces when compared to an aircraft without thrust vectoring capabilities. The reduction in horizontal and vertical tail area is the cause for the improved stealth and reduced parasite drag.

Note that having redundant control surfaces can also improve the safety of an aircraft design. If an aircraft is equipped with both TVFC and traditional aerodynamic control surfaces, then in the occurrence one of the flight control system fails, the other flight control system can be used to ensure safe flight is maintained.

With the benefits of TVFC realized, many experimental and production fighter aircraft were designed with TVFC incorporated within the design. Some experimental aircraft designed with TVFC include the F-18 HARV, X-31, F-15 ACTIVE, and F-16 VISTA, and production aircraft with this technology include the Su-30 MKI, F-22, F-35 JSF, Su-27, and MIG-29 OVT [19]. The aforementioned aircraft have been designed and flown over the course of many decades. Examining only the production aircraft designed with TVFC shows how much interest the technology has received over the last half century.

Even though many successful fighter aircraft have been designed with TVFC, a full-scale CTA designed with TVFC has yet to be built and flight tested. There are multiple reasons and arguments why such an aircraft should not be designed. The argument made by those in opposition to the development of thrust vectoring CTA will now be presented.

Performance Criteria	% Change
Maximum Lift Coefficient	+78
Deceleration Rate in Flight	+72
Landing Run	-72
Roll Rate, Mach 1.4/40,000 ft	+53
Pitch Rate, Mach 0.3/20,000 ft	+33
Take-off Roll Distance	-29
Approach Speed (at constant α)	-16 kts
Acceleration Rate, Mach 1.4/40,000 ft	+30
Cruise Range	+13

Table 2.2: Expected Performance Improvements for the F-15STOL/MTD.

2.2. OPPOSITION TO TVFC

Despite the noted benefits associated with TVFC, there are arguments opposing the development of the technology. For example, there is a public perception resisting change and unconventional aircraft designs [4], and replacing convenional aerodynamic flight controls with TVFC may lead to unconventional aircraft designs. Aircraft which use engines for control, rather than aerodynamic control surfaces, may seem unsafe to the public and pilots. For example, one experienced pilot claimed TVFC disregarded everything he knew about piloting an aircraft, and another pilot claimed a thrust vectoring aircraft would disintegrate mid-flight [4]. These points of view can be understood after considering that aircraft engines are designed to propel the aircraft rather than to control the aircraft. Using an aircraft engine to control an aircraft may seem like a brute force control method.

Aerospace engineers resist the application of TVFC on CTA as well. From an aerospace engineering point of view, if an engine equipped with TVFC fails, not only is there a reduction in thrust, but the controllability of the aircraft is significantly impacted. The compounded effect of reduced thrust and control may result in a fatal aircraft crash [13].

Vectoring the nozzle will also alter an engine's performance. The fluid flow path within a deflected nozzle will differ when compared to the fluid flow path within the undeflected nozzle. This difference in fluid flow path causes a reduction in nozzle performance in the form of thrust. The extent of the nozzle performance loss is dependent on the deflection angle, and increasing the nozzle deflection angle will result in increased performance losses. These losses will be discussed and quantified at a later point.

In addition the aforementioned disadvantages, the complexity of the thrust vectoring system will increase the engine's weight and reduce the engine's reliability. It can be argued that additional complexity in an aircraft's propulsion system should be avoided. This can be understood because an aircraft's engine is already a complex and highly engineered machine. It is somewhat difficult to quantify the disadvantage of increased engine complexity because this is a subjective disadvantage. The increased engine complexity could possibly be quantified by examining either the reliability of a thrust vectoring engine or the time required to design a thrust vectoring system. Data of this type could not be found in available literature, so the disadvantage of increased engine complexity will be demonstrated through the presentation of a list of parts required to construct the General Electric Axisymmetric Thrust Reverser (GEATR) with vectoring. In table 2.3 a list of parts, materials, and percent of the engine weight corresponding to the GEATR nozzle is shown. The data has been obtained from reference [10], and the nozzle can be integrated with conventional exhaust systems, such as exhausts on the F110 and F404 which produce military thrust of 133 kN and 48.9 kN, respectively. A drawing of the GEATR is shown in figure 2.4.

From a more technical viewpoint, an aircraft engine designer will note effective TFVC requires a mixed flow turbofan engine. Using a mixed flow turbofan rather than an unmixed flow turbofan will decrease an engine's efficiency as a result of flow mixing losses, thus the engine's specific fuel consumption will increase. In reference [13], a computer generated model of the GE90 turbofan engine, which is an unmixed flow turbofan engine, was created. This engine model was modified such that it could be used for thrust vectoring. The engine was modified from unmixed flow to a mixed flow design. This particular modification reduced the engine's thrust-to-weight ratio by 11%. A comparison between the specific fuel consumption of the mixed

Part	Material	% Engine Weight
Blocker	Carbon-Carbon Titanium Aluminide	0.6
Blocker Actuation Linkage	Titanium	0.9
Cascade Frame	Titanium Aluminide Sheet Fabrication	2.1
Cascade Vanes	Titanium Aluminide SPFDB	0.5
Cascade Vane Linkage	Titanium	0.4
Casing Reinforcement	Titanium Aluminide	0.6
Casing Seal	R-41	0.1
Actuator Mounts	Polyimide‘ Graphite 15	0.2 0.2
Actuators	Aluminum	0.9
Hydraulic Tubing	Titanium	0.2
	Total	**6.5**

Table 2.3: Parts and material list for GEATR thrust vectoring/reversing nozzle [10]

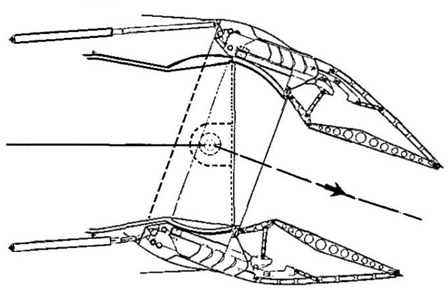

Figure 2.4: GEATR engine nozzle with thrust vectoring/reversing capabilities [10]

and unmixed flow engine designs was not presented in reference [13]; however, it was noted the mixed flow engine design will have the higher specific fuel consumption of the two engines.

As one can see, there are various arguments opposing the advancement of TVFC. Safety is an arguing point used by both the support and opposition of TVFC. Redundant flight control systems, thrust vectoring flight control and aerodynamic flight control, make for a safer aircraft; however, the failure of an engine, along with its thrust vectoring abilities, raises safety concerns among aerospace engineers, pilots, and the public. Additionally, the weight and complexity associated with thrust vectoring technology concerns aircraft engine designers. In table 2.4, a summary of the disadvantages associated with TVFC are listed. The references which analyzed the disadvantages of TVFC have been sorted according the type of research used for the analysis.

Based on the aforementioned opposing arguments, the implementation of TVFC in an aircraft's design should demonstrate a level of safety comparable to modern aircraft. The TVFC system should not significantly increase an engine's weight while simultaneously reducing an engine's efficiency. With knowledge of the opposing arguments, it is beneficial to review research which refute the opposing arguments. A review of the CTA designed with TVFC will now be presented.

2.3. CIVIL TRANSPORT AIRCRAFT AND THRUST VECTORING

Civil transport aircraft have significantly different design criteria when compared to fighter aircraft. Firstly, the flight envelopes for the two aircraft types differ from each other. Maneuvering at high angles of attack and completing high-g maneuvers is not a design criteria for a CTA. Short takeoff and landing distances may be required for CTA; however, the requirement is less confining when compared to the takeoff and landing distances a fighter aircraft must achieve. Since the two aircraft have different design requirements, it is beneficial to examine design requirements for CTA. Such an examination will show how TVFC may allow for an improvement in a CTA's design.

Typical design requirements for CTA may include carrying a payload for a specific distance, such as trans-

Disadvantage	Reference Computer Experiment	 Physical Experiment	 Conceptual Review
Negative Public Perception			[4] [13]
Reduced Engine Performance	[24] [25] [26]	[6] [23]	[7] [8] [12] [9] [15]
Increased Engine Complexity	-	-	[7] [9] [27]
Reduced Engine Thrust-to-Weight Ratio	[25] [21] [13] [10]	[6] [23]	[7] [8] [12] [9] [27] [15]
Mixed Flow Turbofan Design Required	[13]	-	-
Wing/Tail Aerodynamic Flows Modified	-	-	[9]

Table 2.4: Disadvantages of thrust vectoring flight control for CTA

porting 200 passengers a distance of 1,500 kilometers at a cruise Mach number of Mach 0.70. Economic or sustainability criteria may also imposed on an aircraft design. In addition to the aforementioned design criteria, the safety of the passengers is one of the utmost important CTA design requirements. The importance of the safety requirement has inspired aerospace engineers to research how TVFC can make aircraft safer, thus aerospace engineers are confronted with the task to convert the supermaneuverability capabilities of fighter aircraft to improved safety standards on CTA.

As mentioned earlier, TVFC shows its usefulness in low dynamic pressure flows, which is the area of the flight envelope when aerodynamic control surfaces lose their effectiveness. For CTA, this area of the flight envelope occurs during takeoffs and landings, and in some extreme situations, low dynamic pressures may be encountered during post-stall fight or spins [22]. Before testing the effectiveness of TVFC in low dynamic pressure flight conditions, the technology should first be rigorously tested in safe flight conditions, such as during high dynamic pressure flight tests. In the occurrence TVFC does not provide adequate flight control, the traditional aerodynamic control surfaces can be used to safely control the aircraft.

2.3.1. Flight Test of a Scaled B-727 with TVFC

On 12 May, 1995, a flight test was conducted to analyze the controllability of a thrust vectoring CTA. For the flight test, a dynamically scaled model of a Boeing 727 successfully demonstrated the ability to perform turning maneuvers using only TVFC. A Boeing 727 was selected for the test flights due the location of its three engines. The distance between the aft-mounted engines and the aircraft's center of gravity created long moment arms which aided in the pitch and yaw control effectiveness of the TVFC [20]. It was not stated if the thrust vectoring prototype was flown in adverse flight conditions, such as crosswind flight; however, the successful demonstration of controlled flight using only vectored thrust establishes the feasibility of CTA equipped with TVFC.

In the aforementioned flight test, the aircraft could use both vectored thrust and aerodynamic surfaces for flight control. For such an aircraft design, if one of the control systems fails, then the other system could provide the forces and moments required to trim and control the aircraft. This redundancy in flight control systems improves the safety of an aircraft design. To demonstrate the safety benefits, flight tests or simulations should be conducted demonstrating the ability of an aircraft to continue flying safely after one of its control systems fails. In reference [22] computer simulations were completed to analyze the safety benefits of redundant control systems. For the computer simulations, recovery of aircraft flight control using TVFC was demonstrated after an aircraft's elevator, rudder, and ailerons have all failed.

These simulations were conducted using a F-15B fighter aircraft; however, some of the general knowledge gained from the simulations can be applied to CTA. In the article, it is noted that having (1) multiple engines, (2) a large distance between the aircraft's center of gravity and engine nozzle exit, and (3) distributing the engine position about the aircraft is important for successful TVFC. This knowledge can be applied to CTA because it indicates what aircraft engine configurations are most suitable for TVFC. Aircraft with aft mounted engines, such as the B-727, MD-88, or Fokker 100 can possibly benefit from TVFC . For the B-747 and A-340, aircraft, engine's are wing mounted both ahead and aft of the aircraft's center of gravity, and thrust vectoring may be used to improve the pitch, yaw, and roll control for these aircraft [22].

thisas well as aircraft with engines mounted both ahead and aft of the aircraft's c.g., such as the B-747 and A-340,

2.3.2. DC-10 AND PROPULSION CONTROLLED AIRCRAFT

So far, only deflection of the engine's exhaust jet has been discussed as a form of TVFC; however, aircraft can also be controlled using differential thrust. The concept of controlling an aircraft with differential thrust, also know as propulsion controlled aircraft, was tested by NASA in the 1990s. The inspiration for propulsion controlled aircraft came after multiple aircraft crashed due to major flight control systems failure.

One of the crashes resulting from failure of aerodynamic control surfaces occurred on 19 July, 1989. On this day, shortly after takeoff, the fan in a DC-10's aft-mounted engine disintegrated. Debris from the failure was not contained within the engine's nacelle, and the debris punctured the tail and the hydraulic systems, including backup systems, located within the tail. Shortly after the puncture occurred, the fluids within the hydraulic system completely drained. Nearly all control of the aircraft was lost; however, the pilots still had some control over the aircraft. Due to the damaged tail, the aircraft had a tendency to yaw right. The pilots used this yawing tendency to change the aircraft's heading angle. To achieve a constant heading angle, the pilots applied different throttle settings to the left and right wing-mounted engines, and the differential thrust corrected the yawing tendency. The pilots also discovered an increase in the engines' throttle would increase the aircraft's pitch angle, and a decrease in pitch angle would occur when the engines' throttle was reduced [33].

With the unconventional aircraft control method, the pilots attempted to align the aircraft with the runway and land. What further intensified the challenge of landing was the approach speeds required for the landing. Because elevator control was lost, the aircraft could not flare during the landing. The high speed landing caused the aircraft to break apart after touchdown. Despite the crash landing and ensuing fire, 184 of the 296 total people survived the crash [33]. The flight crew made use of the available resources, and they demonstrated the feasibility of propulsion controlled aircraft. Additionally, the pilots demonstrated the safety benefit of redundant flight control systems, even though the engines were never intended to control the aircraft.

As one can see, it is feasible for an aircraft to be controlled with differential thrust and vectored thrust. There are considerable challenges hindering the development of propulsion controlled aircraft; however, TVFC remains as a feasible form of control. It should be noted that for TVFC to be a feasible form of control, the technology must demonstrate safety comparable to conventional nozzles.

2.3.3. RELIABILITY OF THRUST VECTORING NOZZLES

For the aforementioned DC-10 crash, the fracture of an engine's fan blade caused the loss of aircraft control. The addition of a thrust vectoring nozzle will add complexity to the aircraft engine design, and this results in a reduction in engine reliability. As more parts are added to the engine, there is an increased chance of parts failing during flight. Care must be given to ensure a thrust vectoring nozzle design doesn't fail. This presents a challenge since the nozzle is required to vector the hot gases exiting the engine.

Designing a nozzle capable of withstanding the flow of hot gases should not be a concern for CTA. Considering that military engines with afterburning capabilities have been designed with thrust vectoring nozzles, one would expect that engines designed for CTA could be readily designed with thrust vectoring nozzles. The turbofan engines designed for CTA typically have much higher bypass ratios when compared the the bypass ratio of military aircraft engines. This indicates that civil aircraft engines have a larger ratio of cool air mixing with the hot core gases when compared to military aircraft engines; therefore, one may expect that the civil aircraft engines would have the lower nozzle flow temperature. Decreasing the nozzle flow temperature will improve the reliability of the nozzle; however, no data was found to support this claim. The main argumentation point is that since thrust vectoring nozzles have been added to military aircraft engines, the technology can be readily added to civil aircraft engines, and the reliability issues can be overcome.

The previous argument may be considered presumptuous since CTA are flown much more frequently than military aircraft. This is important to consider; however, one researcher claims that the engine complexity associated with thrust vectoring technology is not significant. In fact, the complexity of TVFC systems is similar to that of thrust reversing systems [21]. This statement is promising, because many modern aircraft engines already employ thrust reversing technology, thus the design of thrust vectoring systems seems to be a challenge aircraft engine designers can readily overcome. With these arguments, one would expect that the mechanical design of thrust vectoring nozzles can achieve the reliability required for modern CTA.

2.3.4. B-777 AND SAFETY OF THRUST VECTORING AIRCRAFT

Another argument opposing the development of TVFC was related to the safety of the technology. In reference [13], the feasibility of a modified B-777 aircraft using only vectored thrust for longitudinal and directional control was researched. For the study, the aircraft's entire tail was removed, and the aircraft engines' mounting location was moved from underneath the wings to the aft section of the fuselage. These modification required the aircraft's wings to be moved so to accommodate the center of gravity shift. A summary of the modifications made to the B-777 aircraft are shown in figure 2.5.

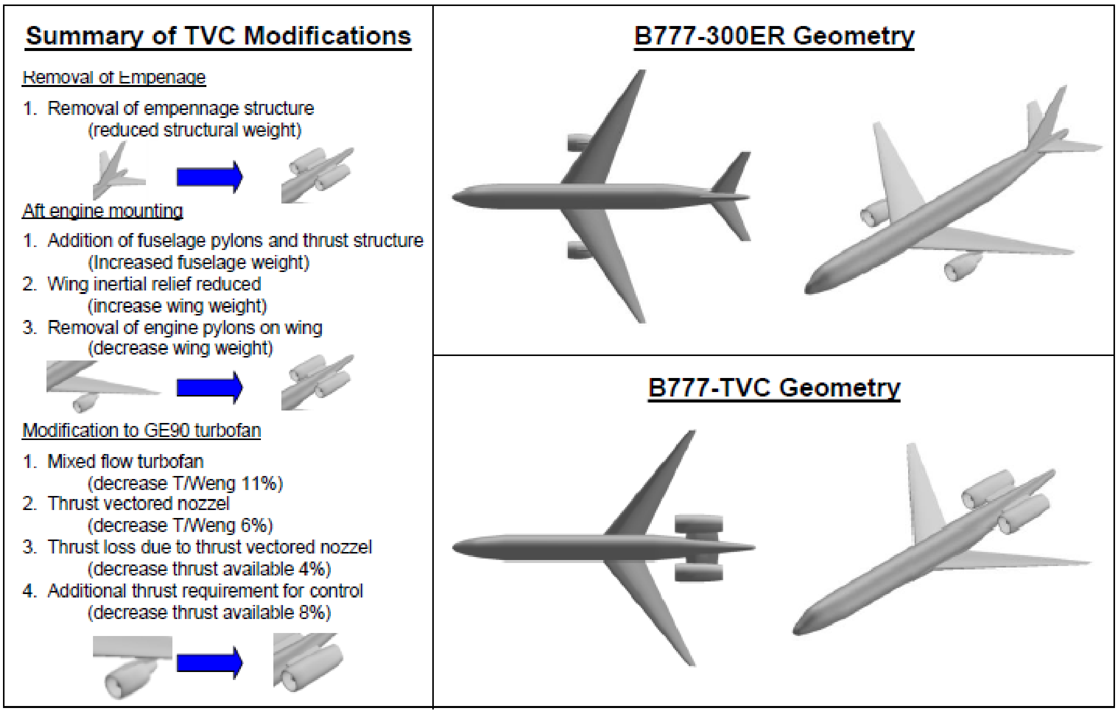

Figure 2.5: Modifications made to a B-777 aircraft to create a thrust vectoring variant in reference [13].

Results of the study showed the thrust vectoring variant of the B-777 had improved aerodynamic efficiency and lower weight when compared to the original B-777. These benefits resulted from a reduction in parasite drag and weight associated with the tail surfaces; however, the performance benefits came at the expense of safety and controllability. The results showed a tailless aircraft, as shown in figure 2.5, could not achieve statically stable flight. Furthermore, the OEI flight condition was shown to be uncontrollable.

This modified B-777 designed in reference [13] was shown to have unsafe stability characteristics; however, this does not prove TVFC is less safe than using aerodynamic control surfaces. In fact, it is not surprising the tailless, thrust vectoring B-777 variant was unsafe because the movement of the engines and wing shifted the aircraft's center of gravity aft. The aft movement of the center of gravity would intensify the destabilizing yaw moment caused by the fuselage.

Additionally, when examining figure 2.5, one can assume the directional control arm lengths of the two aircraft designs differ considerably. For example, the directional control arm of the thrust vectoring design is

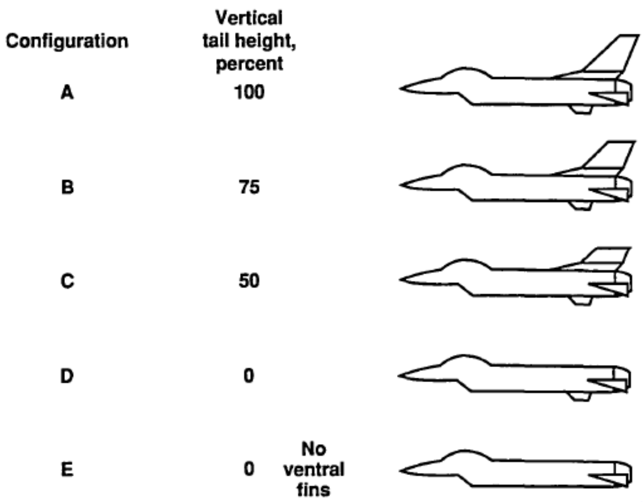

Figure 2.6: Vertical tail designs of an F-16 designed with TVFC used for a stability analysis in reference [8]

roughly the distance between the wing's mean aerodynamic center and the nozzle exit, whereas the distance between the mean aerodynamic centers of the wing and vertical tail represents the directional control arm length for the original design. The effectiveness of a control system in generating a yaw moment about the aircraft's center of gravity is proportional to the directional force generated by the control system and the control arm length. The thrust vectoring B-777 could not generate the required directional control forces and moments; however, thrust vectoring on other CTA design may fulfill the directional control requirements.

Perhaps the most crucial result of the aforementioned study comes in the form of a recommendation. It was recommended an aircraft designed with TVFC and a reduced tail area may revolutionize the performance of CTA by reducing the aircraft's weight [13]. Though this recommendation was made, Omoragbon *et al.* have yet to publish results of such a study. A study of aircraft designed with TVFC and reduced tail areas may demonstrate the ability of a safe and controllable aircraft design. In fact, such a study was completed by NASA in the 1990s.

2.3.5. CONTROL USING TVFC AND REDUCED VERTICAL TAIL SIZE

For NASA's study, presented in [8], NASA analyzed the S&C of a thrust vectoring F-16 aircraft with various tail sizes. The analysis was completed with the vertical tail heights of 100, 75, 50, and 0 percent of the baseline F-16 aircraft. The various tail designs are shown in figure 2.6. One important conclusion gathered from the study showed the vertical tail height could be reduced to a height between 0 and 50 percent and still be statically stable. The F-16 designs with reduced vertical tail areas fulfilled the static stability requirements, but it is also important to examine the dynamic stability of the various F-16 designs.

Regarding the aircraft's dynamic stability, the impact of the vertical tail design on dynamic stability was not thoroughly discussed in reference [8]. It was mentioned that reducing the vertical tail area will result in a reduction of Dutch roll handling qualities, and control systems would need to be designed in order to maintain acceptable handling qualities for the reduced vertical tail areas.

The added mass and inertia from the thrust vectoring system will also impact an aircraft's dynamic stability, and this was demonstrated in reference [8]. It was shown that the added mass and inertia impacted the aircraft's Dutch roll mode but not the rolling and spiral modes. For the Dutch roll mode, the thrust vectoring F-16 had a lower Dutch roll frequency when compared baseline F-16. The Dutch roll damping was also impacted. At Mach numbers below Mach 0.8, the thrust vectoring F-16 had higher Dutch roll damping, and the opposite was true for Mach numbers above Mach 0.8.

In figure 2.6, it can be seen that aircraft configuration has no vertical tail or ventral fins. Reference [8] did not discuss how an aircraft's landing performance is impacted after the removal of the vertical tail and ventral fins. During landing, aircraft have their thrust set to idle in order to minimize the landing speeds and distance. If the thrust is set to idle during landing, then the aircraft yaw control would be reduced. One may expect that the crosswind landing performance of aircraft configuration E would be impacted since it does not have a vertical tail or ventral fins.

The results obtained from the thrust vectoring F-16 study are promising because it is shown the aircraft can still have stable flight characteristics with a reduced vertical tail size. It should be noted that the F-16 has only one engine, and the OEI flight condition was not analyzed within the study. To convince those unsure about the safety of thrust vectoring aircraft, the OEI flight condition should be analyzed for multi-engine CTA.

Even though the OEI flight condition was not analyzed for the single-engine F-16, one of the study results may be related to the OEI flight condition of multi-engine aircraft. Consider figure 2.7 which shows the dimensional yawing coefficient for the rudder and thrust vectoring nozzle. This coefficient is used to determine the yaw moment generated for a given rudder or nozzle deflection angle. Larger dimensional yaw coefficients indicate more efficient directional control. Earlier it was mentioned TVFC may be an effective form of control in low dynamic pressure flows. This concept is verified by examining the rudder and nozzle dimensional yawing coefficients for flows below about Mach 0.3. At Mach numbers below Mach 0.3, the thrust vectoring of an F-16 engine operating at full throttle is more efficient than the rudder in generating directional control moments. It should be noted that since figure 2.7 plots the thrust vectoring dimensional yawing coefficient for a full throttle, the dimensional yawing coefficient is likely greater than the thrust vectoring dimension yawing coefficient calculated using the thrust required for trimmed flight.

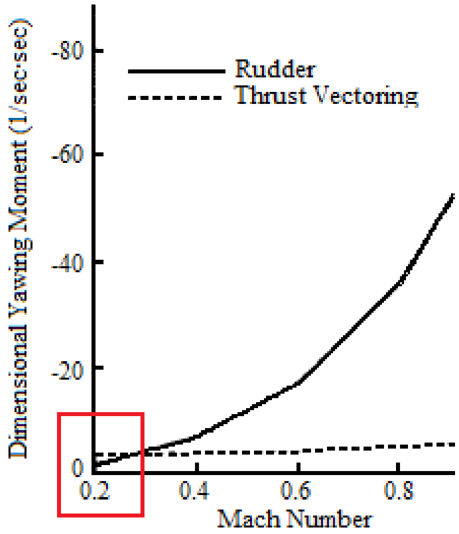

Figure 2.7: Dimensional yawing coefficient for rudder and nozzle of a F-16 at sea level [8].

If a multi-engine aircraft is attempting to achieve trimmed flight during the OEI flight condition, then using the TVFC to correct the yawing moment due to asymmetric thrust may be more effective that the rudder. This statement is valid as long as there is sufficient thrust to maintain the required trim velocity and to correct the yawing moment. This demonstrates the feasibility of an aircraft to achieve trimmed, OEI flight using vectored thrust. It should be noted that the data presented in figure 2.7 has be calculated at sea level. Since the thrust of jet engines decreases as altitude increases, the thrust vectoring dimensional yawing coefficient will decrease as altitude increases, and using TVFC to generate yawing moments may not be beneficial as high altitudes.

2.4. APPLICATION OF TVFC TO CTA

A summary of this chapter will be given. The summary of the data will be presented in a manner such that benefits of TVFC can be directly related to CTA.

The concept of TVFC was first applied to fighter aircraft in the 1950s. This technology was used to create so-called *supermaneuverable* aircraft. Along with the benefit of improved maneuverability, fighter aircraft designed with TVFC possibly had reduced parasite drag, among other benefits. Based on the design requirements of CTA, this reduction in parasite drag can be applied to CTA. A reduction in parasite drag would allow for a reduction in fuel consumption for a CTA. This is particularly beneficial for CTA, because this may allow for a possible reduction in greenhouse gas emissions.

By using this knowledge, a research project can be designed which analyzes the design of thrust vectoring CTA. The next section will use the knowledge obtained from the literature review to create a research objective related to TVFC and the design of CTA.

3

Thrust Vectoring Research Project

Within the previous chapter, the benefits and disadvantages of TVFC have been identified. Views and arguments held by those who oppose the design of thrust vectoring CTA have been presented. Now the problem at hand is to formulate a research objective which exploits the potential benefits of TVFC while being constrained to appease those opposing arguments.

After the presentation of the research objective, an overview of the steps required to accomplish the research objective will discussed. This overview will use a flow chart to serve as a guide for the research. The individual research steps will be introduced in this section; however, detailed attention regarding each step is provided at later points within the report.

3.1. Research Objective Formulation

As has been discussed, thrust vectoring has the potential of being an innovative form of aircraft flight control. Aircraft require roll, pitch, and yaw control, which correspond to control around an aircraft's lateral, longitudinal, and directional axes, respectively. Since TVFC will be implemented into the design of a CTA, it must be determined if the TVFC will provide lateral, longitudinal, or directional control. The impact of adding TVFC on an aircraft's design will now be examined for the cases for lateral, longitudinal, or directional control.

Lateral control is typically achieved by deflecting an aircraft's ailerons. The ailerons are aerodynamic control surfaces located at the outboard wing position, near the wing tip. In order for thrust vectoring to provide efficient lateral control, the aircraft's engines should also be mounted on the aircraft's wing, far away from the fuselage. Wing mounted engines are commonplace on modern CTA; however, mounting a engine near with wing tip will likely incur a significant wing structural mass increase. When comparing aileron and thrust vectoring engine lateral control moment arm, the ailerons will have the larger of the two. Since the moment arm of a wing mounted engine is relatively short, it is unlikely that replacing ailerons with TVFC will improve the lateral control on a CTA design; therefore, the implementation of thrust vectoring for lateral control will not be researched.

Longitudinal control is typically achieved by deflecting an aircraft's elevator. Elevators are typically located on an aircraft's horizontal tail. This position creates a long control moment arm between the aircraft's elevator and center of gravity, and efficient longitudinal control requires this moment arm to be as large as feasibly possible. In addition to providing longitudinal control, the elevator, in conjunction with the horizontal tail, provides longitudinal trim moments. Many CTA are designed to have a positive static margin, which indicates that an aircraft's horizontal tail and elevator must provide longitudinal trim moments to balance the inherent nose-down pitching moment caused by the forward location of the aircraft's center of gravity relative to the aerodynamic center. It is important to note that the horizontal tail and elevator must provide longitudinal trim forces during cruise conditions.

Earlier it was shown that TVFC can be an efficient form of control in low dynamic pressure flows. This concept was validated with the aid of figure 2.7, which demonstrated that an F-16's thrust vectoring nozzle can be more efficient than the rudder in generating directional control moments at Mach numbers below Mach 0.3. Since CTA spend a large percentage of their flight duration at cruise conditions, where the dynamic pressure is relatively large, one would expect the elevator to be more efficient at providing longitudinal trim moments than thrust vectoring. If thrust vectoring is used to provide longitudinal trim during cruise flight conditions, the nozzle deflection angle required for trimmed flight will likely be larger than the required elevator deflection angle. This is a concern because the aircraft engine's thrust and specific fuel consumption are reduced as nozzle deflection angle increases. If the nozzle deflection angle required for longitudinal trim is too large, then the aircraft will likely have worse cruise fuel consumption than if the elevator was used to trim the aircraft.

It is possible that thrust vectoring could improve the takeoff performance of a CTA. If vectored thrust is used to improve the pitch rate of an aircraft's rotation during takeoff, then the aircraft's takeoff distance can be reduced. This is a benefit of thrust vectoring for longitudinal control; however, applications of thrust vectoring which may improve an aircraft's cruise performance should be investigated since CTA spend majority of a flight at the cruise condition. Based on the aforementioned arguments, other control applications of thrust vectoring, such as directional control, should be researched before the benefits of thrust vectoring for longitudinal control is researched.

Lastly, it is possible for thrust vectoring to provide directional control. Before determining if thrust vectoring should be used for directional control, the design requirements of the vertical tail and rudder, now to be referred together as VT, should be reviewed. These aerodynamic surfaces are required to provide (1) static and dynamic directional stability, (2) directional control, (3) forces and moments for flight equilibrium [3]. In particular, the VT must allow an aircraft to achieve directional trim during flight conditions with large sideslip angles. For multi-engine aircraft, the flight condition which produces the largest sideslip angle is typically the one-engine-inoperative (OEI) with crosswind condition. Furthermore, a multi-engine aircraft which experiences an engine failure after the takeoff decision speed is in a relatively low dynamic pressure flow. This particular flight condition typically drives the VT design of a multi-engine aircraft. For flight conditions differing from the OEI, crosswind condition, the VT is typically over-designed.

If thrust vectoring is used to provide directional control, then the vectored thrust can assist the VT in providing the directional trim forces required for OEI, crosswind flight at low dynamic pressures. This statement is intriguing since vectored thrust appears to be an effective form of control at low dynamic pressures. If TVFC is used in the aforementioned manner, the directional control power required from the aircraft's VT is relieved. A reduction in a VT's directional control power requirement would necessitates a redesign of the VT, and the size of the VT may be reduced. One may be tempted to fully remove the VT in favor of TVFC; however, it is important to reiterate that reference [13] discovered a B777 had unsafe stability characteristics if the VT was entirely removed.

By designing an aircraft with both thrust vectoring engines and a VT, an aircraft can potentially fulfill the directional stability and control (S&C) requirements necessary for safe flight. With such a design, the VT can be designed to cope with the regularly occurring flight conditions. In the occurrence of OEI, crosswind flight, both thrust vectoring and aerodynamic control forces can be used to achieve trimmed flight. A CTA design with TVFC and an unconventionally small VT is expected to have a lesser wetted surface area than a comparable, conventional CTA design. The reduction in wetted surface area would likely be accompanied by a reduction in parasitic drag coefficient. The final result may reveal aircraft performance benefits in the form of reduced mission fuel consumption.

One should be reminded that the addition of thrust vectoring technology to an aircraft is accompanied by an increase aircraft mass. This is undesirable because increasing an aircraft's mass will result in increased fuel consumption. However, by using thrust vectoring for directional control, the aircraft's VT area can be reduced, and reduced VT area may be be accompanied by a reduction in the VT's structural mass. With this realization, it is important to research how an aircraft's empty operational mass is effected by the addition of TVFC and a reduction in VT area.

It is also important to recognize efficient directional control requires the engines to be placed at the aft location of the fuselage. This engine position maximizes the directional control arm of the thrust vectoring engines. Earlier it was mentioned that effective longitudinal control also requires aft engine placement. Redesigning the horizontal tail rudder due to the addition of TVFC will not be researched; however, the engine placement allows for takeoff performance benefits associated with TVFC to be analyzed if the thrust vectoring is used for longitudinal control during takeoff.

Finally, the analysis of aircraft S&C is typically separated into two categories. One category is longitudinal S&C and the other category is lateral-directional S&C. For symmetric aircraft designs, the aircraft's longitudinal equations of motion can be analyzed independently from the lateral and directional equations of motion; however, an aircraft's lateral and directional equations of motion are coupled. Although thrust vectoring for lateral control is of little interest, an aircraft's lateral stability needs due to the VT redesign and application of thrust vectoring for directional control.

By using the knowledge discussed in this chapter, a research objective can be formulated to investigate the benefits and disadvantages of designing an aircraft with TVFC and an unconventionally small VT. The research objective is stated as follows:

> *The research object is to investigate how the (1) lateral-directional stability and control, (2) parasite drag, (3) mission fuel consumption, and (4) empty operational weight of civil transport aircraft designed with thrust vectoring flight control and an unconventionally small vertical tail differ from a comparable, conventional civil transport aircraft design.*

To achieve the goals stated in the research objective, knowledge of the following aircraft related disciplines is required: design, aerodynamics, S&C, structures, and performance. Brief overviews pertaining the to various aerospace disciplines and their relation to achieving the research objective will be provided in the following section, and the discussion will serve as a roadmap to guide the reader through the report.

3.2. RESEARCH PROJECT OVERVIEW

To research the feasibility of a CTA designed with TVFC and an unconventionally small VT requires a multidisciplinary research plan. Figure 3.1 shows a flowchart used to assess the feasibility of a thrust vectoring CTA design. Many of the blocks in the flowchart correspond to an unique aerospace engineering discipline. The purpose of the flowchart blocks will be briefly described. In particular, the relation between the blocks and the research objective will be described. The blocks in the flowchart will serve as a road-map when the core portion of the thesis is presented.

The first step in the research plan, labeled as block 1, is to design an aircraft which will be used for the study. Rather than designing an entirely new aircraft with TVFC, an existing aircraft will be modified to include TVFC. Since the thrust vectoring will be used for directional control, the VT control power requirements will be reduced, and aircraft's VT must be redesigned to accommodate the change in required control power. Within this *aircraft design* block are sub-steps which must be completed in order to create the aircraft model. These sub-steps include (1) creating a thrust vectoring engine model, (2) creating an aerodynamic database containing S&C derivatives, and (3) calculating the aircraft's mass and inertia. Once the aircraft model is created, the next step can be started.

The next step in achieving the research objective is to analyze the aircraft's lateral and directional static stability. Blocks 2 is used to complete this step. Since the aircraft's VT area will be reduced, it is important to ensure the aircraft exhibits lateral and directional stability after redesign of the VT. To complete this task, the aircraft's lateral and directional stability derivatives will be examined. If the aircraft design exhibits lateral and directional stability, then step 3 can be completed; otherwise, the aircraft design will be considered as unfeasible.

Block 3 is used to analyze the aircraft's lateral and directional dynamic stability. Aircraft have three different lateral-directional dynamic modes, which are the roll mode, spiral mode, and Dutch roll mode. The mass and inertia addition of the thrust vectoring system as well as the redesign of the VT will impact the aircraft's dynamic modes. Block 3 is used to ensure the aircraft's three modes are stable. In addition to checking for lateral-directional dynamic stability, the aircraft's airworthiness will be examined. If the aircraft design fulfills the dynamic stability and airworthiness requirements, the a trim analysis can be completed. An aircraft design which does not fulfill these requirements will be deemed as an unfeasible aircraft design.

Following the dynamic stability analysis is a trim analysis, which occurs in block 4. In the formulation of the research objective, it was stated that thrust vectoring and aerodynamic control forces can be used to trim the OEI, crosswind flight condition. The validity of this statement must verified. If the redesigned VT is too small, then it may not be able to provide the directional trim force required for trim. Additionally, large nozzle deflection angle will result in a reduction of axial thrust, and the axial thrust required for trimmed flight may be insufficient. There are criteria to be examined during the trim analysis, but these will be discussed at a later point. Depending on the trim analysis, either the aircraft design will be deemed as unfeasible or the next aircraft design analysis can be completed.

If the aircraft design fulfills the acceptance criteria established in the trim analysis, then a deep stall analysis will be completed. Block 5 is used to complete this task. Deep stall is a phenomenon occurring when the wake generated by a stalled wing encapsulates the horizontal tail. In the occurrence of deep stall, the elevator loses its ability to create longitudinal control moments, and this will prevent the aircraft from recovering from the stall. At this point, the purpose of a deep stall analysis will not be explained because the impact of the VT design on the horizontal tail position has yet to be discussed; however, the reader should be informed of this safety related analysis.

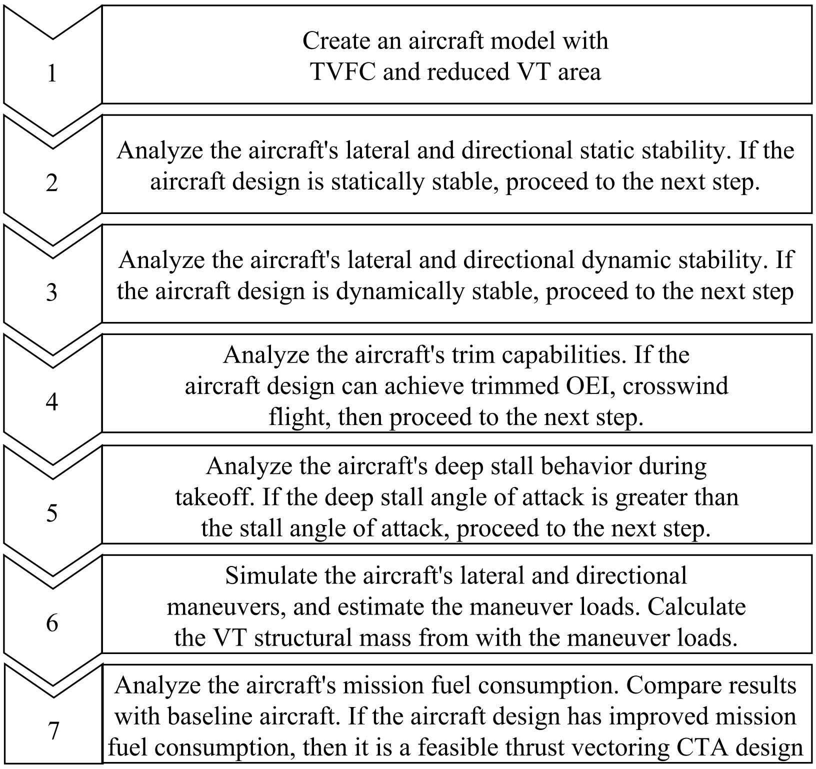

Figure 3.1: Flowchart to determine a feasible thrust vectoring aircraft design

After the deep stall analysis is completed, the VT weight analysis will be completed. Block 6 denotes this step. For this step, the worst case load acting on the VT must be determined, and the VT's structure must be designed to withstand this load. During this step, the structural mass of the redesigned VT will be compared to the structural mass of the baseline aircraft's VT. At this point, the potential reduction in VT structural mass will be realized.

The final analysis needed to accomplish the research objective is a performance analysis. In this analysis, denoted by block 7, the aircraft's parasite drag coefficient will be estimated. The parasite drag influences the aircraft's mission fuel consumption. The mission fuel consumption of the thrust vectoring CTA design will be estimated and compared to the baseline aircraft's mission fuel consumption. At this point, the feasibility of a CTA designed with thrust vectoring engines and a reduced VT size will be determined.

Before the research methodologies and theories are presented, a summary of the discussed topics will be presented. In order to improve the competitiveness, performance, and sustainability of the European aviation industry, innovative aircraft designs must be researched. An aircraft designed with TVFC and an unconventionally small VT may may be used to overcome this challenge for innovation. A research objective has be formulated to investigate the safety and aircraft performance benefits of the proposed aircraft. The aircraft safety aspects to be analyzed include lateral and directional stability and control, OEI trimmed flight, and deep stall. The aircraft performance aspects to be analyzed include mission fuel consumption, which is dependent on the aircraft's weight and parasitic drag, and takeoff performance.

Now the research methodologies and theories used to accomplish the research objective will be presented.

4

Designing a Thrust Vectoring Aircraft

4.1. Designing a Thrust Vectoring Aircraft

In order to achieve the research objective, a thrust vectoring aircraft must be designed for the study. The primary function of the thrust vectoring system is to provide directional control. To maximize the potential benefits offered by the TVFC, the engine position must be selected carefully. CTA typically have engines mounted either under the wings or at the aft part of the fuselage, near the tail surfaces. To maximize the directional control arm, an aircraft with aft mounted engines will be used.

For the analysis, a thrust vectoring aircraft must be either newly designed, or an existing aircraft's engine and VT can be modified. The decision to modify an existing aircraft was selected. By modifying an existing aircraft design, the stability, control, performance, etc. of the baseline and modified aircraft designs can be compared. This allows for the potential benefits and disadvantages of the modified aircraft to be realized.

The aircraft selected for modification is the Fokker 100. An image of the Fokker 100 is shown in figure 4.1. This aircraft was selected for the analysis for a variety of reasons. Firstly, the Fokker 100 fulfills the aft-mounted engine requirement. Secondly, a significant amount of studies have been completed with regards to the Fokker 100, and there is an abundance of information related to the design, performance, S&C, etc. of this aircraft. Lastly, a geometric model of the Fokker 100 was readily available. The geometric model has been designed for use in an aerodynamic simulation software called VSAERO. Modifications, such as redesigning the aircraft's VT, could be readily made to the Fokker 100 computer model, and aerodynamic simulations can be completed to obtain the lateral-direction S&C derivatives of the redesigned Fokker 100.

Figure 4.1: Fokker 100 aircraft. Image courtesy of flyfokker.com

4.2. VERTICAL TAIL DESIGN METHOD

Part of the research objective requires a redesign of the Fokker 100's VT. The VT redesign results from the addition of thrust vectoring engines. For a multi-engine aircraft, the VT size is commonly driven by the requirement to provide sufficient directional control in the occurrence of OEI and crosswind flight conditions. With the addition of TVFC, the directional control power required from the aircraft's VT is relieved. Reducing the VT's directional control power requirement necessitates a redesign of the VT. In the end, the size of the vertical tail and rudder may be reduced.

Since the VT of the Fokker 100 needs to be redesigned, a strategy to design the VT must be developed. A design strategy which simply scales the VT's span, root chord, and tip chord equally was selected. With the scaling of these VT design parameters, the redesigned VTs will have the same aspect ratio, taper ratio, and sweep angle as the original VT design. Maintaining the overall planform of VT helps ensure the stall angle, lift coefficient, drag divergent Mach number, etc. are relatively consistent for each VT design. Scaling factors were selected so to allow the redesigned VTs to have 85%, 70%, 60%, and 50% area of the original VT area. By using the Fokker 100 with five different VT designs, including the original and four scaled variants, the impact of the TVFC and VT redesign on the Fokker 100's lateral-directional S&C can be seen. Figures 4.2-4.2 shows the Fokker 100 model and various VT designs.

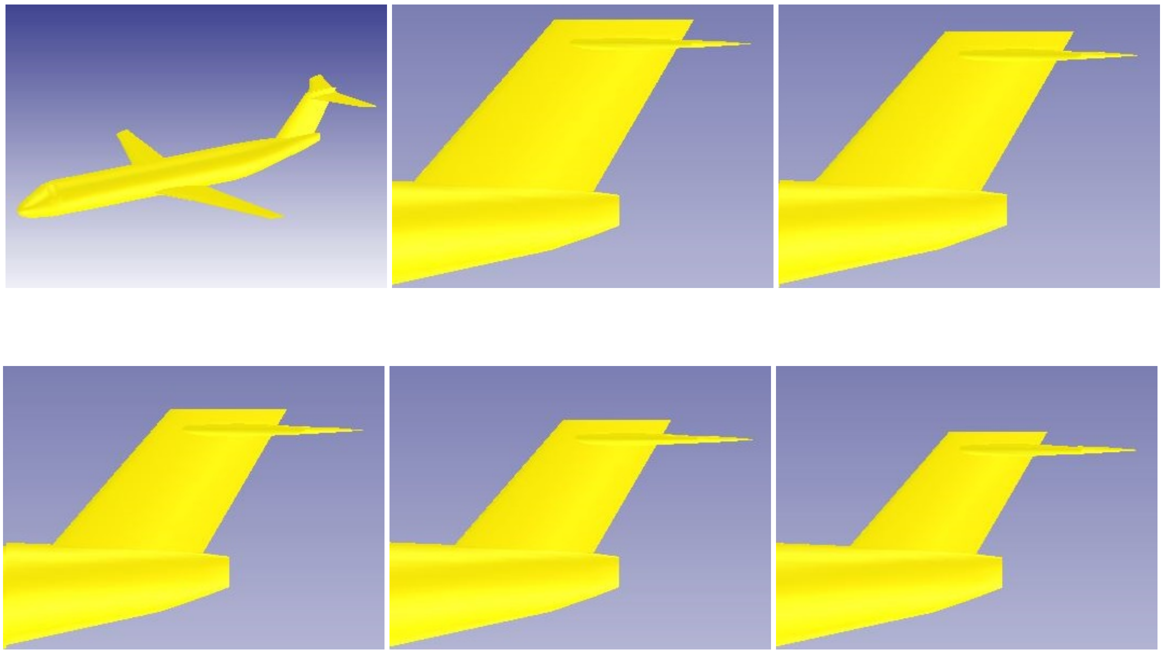

Figure 4.2a: Fokker 100 models and various VT designs

Note the computer model does not include the engine. VSAERO, the software used for the aerodynamic simulations, uses a panel method for the simulations. The interaction between the vectored thrust and the fuselage is expected to be highly complex. Modeling the flow field is further complicated by the relatively close proximity of the VT and potentially deflected rudder. It is determined that a detailed study the aircraft's aerodynamics in the area of the fuselage, vectored thrust, and VT should be completed using an aerodynamic modeling method of higher fidelity than panel method codes. For this reason, the engine was not added to the Fokker 100 computer model. Future studies should be completed to analyze the aerodynamics of the aft portion of the aircraft.

As one can see if figure 4.1, the Fokker 100 aircraft has a T-tail configuration, thus a redesign of the VT will impact the aircraft's horizontal tail (HT). For example, a reduction in the VT's tip chord reduces the area used to connect the VT and HT. This will impact the HT's structure and weight. Additionally, reducing the VT's span will change the location of the HT in relation to the aircraft's wing. If the VT span is reduced significantly, then the HT may lose its ability to generate the control power required to recover from a deep stall. Such design concerns were considered when the VT redesign method was selected. Attention to these design concerns will be provided at a later point.

With the selection of the Fokker 100 and various VT designs completed, an accurate model of the aircraft designs must be created. The first part of the aircraft to be modeled is the aircraft's engine and thrust vectoring performance. Modeling the engine will be the next topic of discussion.

4.3. THRUST VECTORING ENGINE MODEL

The Fokker 100 is equipped with two Rolls-Royce Tay 650 turbofan engines. Modeling the Tay 650 engine is required to analyze how the addition of thrust vectoring technology will impact the engine's performance. First, a Tay 650 engine without thrust vectoring capabilities will be modeled. Upon completion of this step, the engine model will be expanded to include thrust vectoring capabilities. Modeling a Tay 650 engine with thrust vectoring capabilities will now be discussed.

4.3.1. BASELINE ENGINE MODEL

A model of the Tay 650 engine without thrust vectoring capabilities must be modeled. In order to create the engine model, information about the engine's design parameters, such as bypass ratio and turbine inlet temperature and performance, such as takeoff thrust, must be known. Engine manufacturing companies, including Rolls-Royce, are selective in which engine design parameters and performance criterion are released to the public. For this reason, the actual Tay 650 engine performance, except for the engine design point condition, is unknown. However, Rolls-Royce has published some of the Tay 650 engine design parameters and performance data in reference [28]. Data published within this document can be used to create an engine model similar to the actual Tay 650 engine.

A model of the Tay 650 engine was developed using the data provided in reference [28] and a program named Gas turbine Simulation Program (GSP). Table 4.1 displays the engine performance and engine design point data used to create the Tay 650 model. A comparison between the takeoff thrust, cruise thrust, and cruise specific fuel consumption (SFC) of the actual Tay 650 engine and the modeled engine is presented as well.

	Design Point Performance				
	Tay 650	Model Engine	Error	Takeoff Design Point Inputs	
Takeoff Thrust, [kN]	67,200	67,000	0.30%	Bypass Ratio	3.10
Cruise Thrust, [kN]	18,200	18,100	0.59%	Inlet Mass Flow Rate	$193\,\mathrm{kg\,s^{-1}}$
Cruise SFC, [kg/(N h)]	0.0714	0.0631	12%	Overall Pressure Ratio	16.4
				Low Pressure Rotor Speed	8,015 RPM
				High Pressure Rotor Speed	12,560 RPM
$\text{Error} = \frac{Tay\,650\ value - Model\ Value}{Tay\,650\ Value} \cdot 100$				Turbine Inlet Temperature	1,369 K

Table 4.1: Design point performance and inputs for the Tay 650 and developed engine model

As one can see, the takeoff and cruise thrust of the two engines are in close agreement; however, the cruise SFC values for the two engines differ by more than 10%. The possible cause for this discrepancy is because bleed air flows were not included in the engine model. By not modeling the bleed air flows, one would expect the developed engine model to have lower a SFC than the actual Tay 650, and the data presented in table 4.1 supports this thought. The difference in SFC between the two engines will likely be noticeable when the mission fuel weight is calculated in the performance analysis. This difference will need to be addressed during the appropriate section.

With the errors between the two engine's design point performance analyzed, the developed engine model can be deemed as acceptable, and an off-design performance analysis can be completed. GSP was also used to calculate the engine's off-design performance. For the off-design performance analysis, performance maps of the engine's gross thrust, SFC, etc. can be created for any engine operating condition. An engine operating condition consists of an altitude, Mach number, and throttle setting. Off-design operating conditions were calculated at altitudes of 0, 1, ..., 10 km, Mach numbers of 0, 0.1, ..., 0.7, and 0.77, and throttle settings of 10, 20, ..., 100%. The engine performance can be calculated for any combination of altitude, Mach, and throttle setting within the specified specified limits, and interpolation methods can be used to obtain engine performance data for flight conditions not explicitly calculated. Figure 4.3 shows a flowchart of how the engine performance can be obtained for a given operating point.

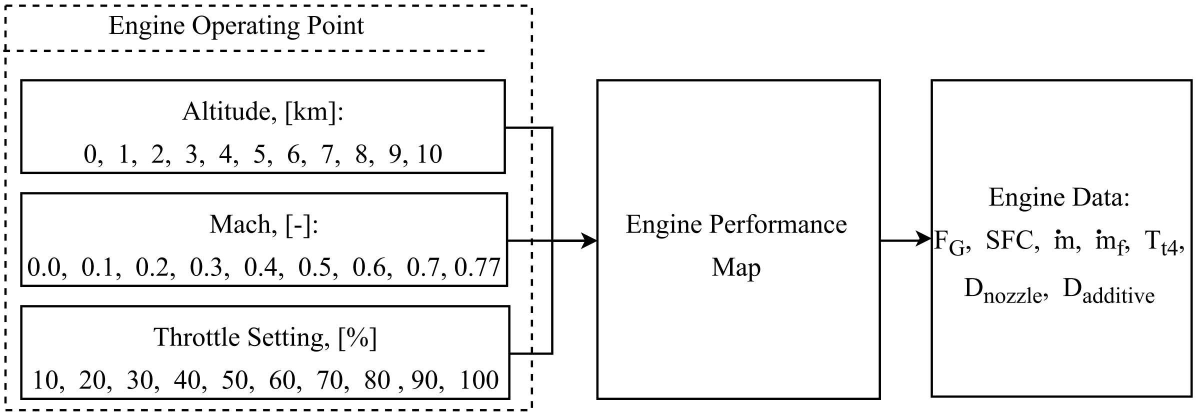

Figure 4.3: Flow chart to obtain engine performance data

In figure 4.4, an engine performance map is shown which relates TSFC, uninstalled engine thrust , and flow Mach number for sea-level flight conditions. Figure 4.4 can be used to determine the aircraft's TSFC for a specified trim condition at sea-level. Note that thrust equals drag in order for trimmed flight to be achieved. If the aircraft's total drag is known for a given Mach number at sea-level, then the engine's TSFC can be determined. Similar plots can be created for various altitudes, such as shown in figure 4.5 which plots the engine performance map at an altitude of 10,000 meters.

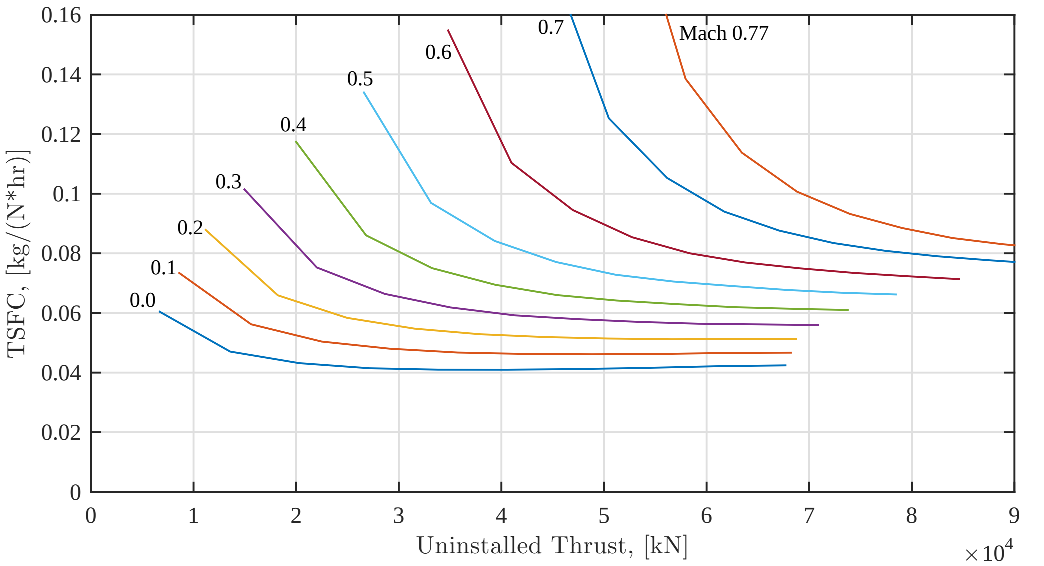

Figure 4.4: Engine partial-throttle performance map at sea-level conditions.

After the creation of the baseline Tay 650 engine model, the model can be further developed to include the impact of thrust vectoring. Modeling the effects of thrust vectoring on engine performance will now be discussed.

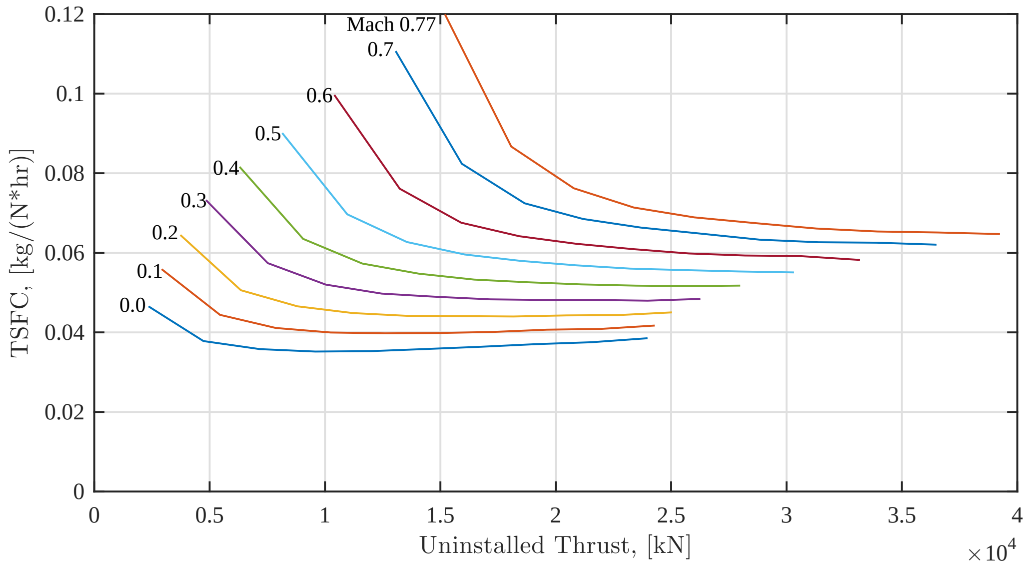

Figure 4.5: Engine partial-throttle performance map at an altitude of 10 kilometers.

4.3.2. THRUST VECTORING LOSSES MODEL

With the addition of thrust vectoring technology, the engine's performance will be altered. Deflecting the nozzle causes the fluid flow path inside the nozzle to differ when compared to the unvectored nozzle condition. In particular, the deflection will change the area at each section along the nozzle's length. Losses in nozzle performance result from this change in nozzle geometry. From an aerodynamic viewpoint, losses can also be caused by a thickening of the flows boundary layer due to vectoring, and for large deflection angles, internal flow separation may cause a reduction in the engine nozzle performance.

To further demonstrate how a nozzle's cross-sectional area depends upon its deflection angle, figure 4.6 will be used. For a nozzle which provides longitudinal and directional control, two deflection angles are required to describe the nozzle's position. The angles δ_y and δ_z are used to describe the nozzles deflection angle in the yaw and pitch planes, respectively. As seen in figure 4.6, the upper image represents a convergent-divergent nozzle without a deflection angle, ($\delta_y = 0,\ \delta_z = 0$), and the lower image represents the nozzle deflected with an angle of δ_z, ($\delta_y = 0,\ \delta_z \neq 0$).

In figure 4.6, A_t^G and A_e^G represent the geometrical areas of the nozzle's throat and exit, respectively, and A_t^E and A_e^E represent the effective area of the nozzle's throat and exit, respectively. What differentiates the geometric area from the effective area is how the nozzle's area is perceived by the flow. The geometric area is defined by physical, solid boundaries, whereas the effective boundary is defined by the flow's actual path and behavior through the nozzle. In reference [7], the effective and geometric areas of the nozzle throat and exit are related to the nozzle deflection angle with the following equation:

$$\frac{A_t^E}{A_t^G} = \cos\delta_y \cdot \cos\delta_z \tag{4.1a}$$

$$\frac{A_e^E}{A_e^G} = \cos\delta_y \cdot \cos\delta_z \tag{4.1b}$$

In reference [29], a more vigorous derivation of the relationship between the nozzle areas and deflections angles is introduced. The equations resulting from the derivation in reference [29] are as follows:

$$\frac{A_t^E}{A_t^G} = \cos\delta_y \cdot \cos\delta_z \cdot (\cos^2\delta_y + \sin^2\delta_y \cos^2\delta_z)^{-1/2} \tag{4.2a}$$

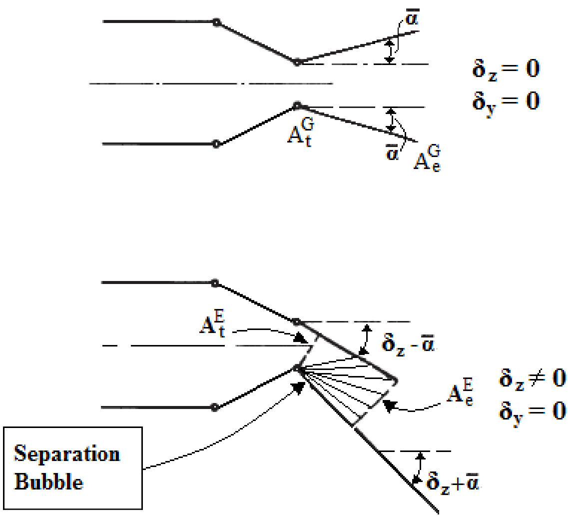

Figure 4.6: Vectored and unvectored nozzle geometry with corresponding geometric and equivalent areas [7]

$$\frac{A_e^E}{A_e^G} = \cos\delta_y \cdot \cos\delta_z \cdot (\cos^2\delta_y + \sin^2\delta_y \cos^2\delta_z)^{-1/2} \tag{4.2b}$$

To simplify the writing of the effective to geometric area ratio, the following variable is introduced:

$$\chi = \cos\delta_y \cdot \cos\delta_z \cdot (\cos^2\delta_y + \sin^2\delta_y \cos^2\delta_z)^{-1/2} \tag{4.3}$$

Because the nozzle's geometric and effective areas vary for different deflection angles, the nozzle performance is dependent on the deflection angle. To fully understand the benefits stemming from the addition of TVFC in a CTA design, the nozzle's performance must be modeled for all possible flight conditions and nozzle deflection angles. In open literature, nozzle performance models have been created through the use of empirical coefficients [7] [36] [37]. Numerical methods can also be used to model the change in performance for a vectored nozzle [52].

Past research has used empirical and numerical methods to model the performance of nozzles; however, a knowledge gap exists between the two models. For example, there is a gap in correlating empirical equations with nozzle performance of compressible flows [24]. Numerical solutions have been proven to accurately model the performance of compressible flows in nozzles, but numerical methods require a relatively large amount of time and computing resources when compared to an empirical method. To bridge this knowledge gap, an analytical model should be used.

An analytical solution allows for more versatility when compared to empirical models, and implementing the analytical solution is generally simpler than developing a numerical solution. In reference [24], compressible flow equations for nozzles are used to derive an analytical equation expressing the performance of a vectored nozzle. For the derivation, it is shown that the nozzle performance is dependent on the nozzle's friction and change in area. It is important to consider the nozzle friction because boundary layer growth within the nozzle is dependent on friction, and the boundary layer influences the effective area of the nozzle. Before the analytical solution is presented, the nozzle thrust coefficient will be introduced. The nozzle thrust coefficient, $C_{fg,nozzle}$, is represented by the following equation:

$$C_{fg,nozzle} = \frac{F_{g,a}}{F_{g,i}} = \frac{\dot{m}_a V_{e,a} + A_e(P_e - P_a)}{\dot{m}_i V_{e,i}} \tag{4.4}$$

In equation 4.4, F_g is nozzle's gross thrust and the subscripts a and i represent the actual and ideal nozzle flow condition, respectively. The variable $\dot{m}$ is the nozzle's mass flow rate, and V_e is the flow velocity flowing through the nozzle's exit area, A_e. Lastly, P_e and P_a represent the fluid's static pressure at the nozzle exit and the ambient pressure, respectively.

The nozzle thrust coefficient is the ratio of a nozzle's actual thrust to its ideal thrust. By examining equation 4.7, it can be seen that the thrust coefficient depends upon the nozzle's exit area and exhaust flow velocity. Based on the continuity equation, one can realize that changing the geometric and effective areas of a nozzle will result in a change of the flow velocity within the nozzle; therefore, deflecting the nozzle will change the nozzle's thrust coefficient.

In equations 4.1, the relationship between the geometric and effective areas and the nozzle deflection angle was introduced. Since the nozzle thrust coefficient depends upon these variables, it is beneficial to relate the thrust coefficient to these variables. This task is completed in reference [24], and the analytical equation used to calculate the thrust coefficient of a vectored nozzle is the following equation:

$$C_{fg,TVFC} = \frac{A_t^E}{A_t^G}\left\{\frac{M_a}{M_i}\sqrt{\frac{\varsigma_i}{\varsigma_a}} + \frac{A_e^E}{A_t^E}\frac{\sqrt{\varsigma\left(\frac{\gamma+1}{2}\right)^{(\gamma+1)/(\gamma-1)}}}{\gamma M_i}\left(\frac{P_e}{P_a}-1\right)\right\} \tag{4.5a}$$

where

$$\varsigma = 1 + \left(\frac{\gamma-1}{2}\right)M^2 \tag{4.5b}$$

In equation 4.5a, is the flow Mach number, and γ is the specific heat capacity of the nozzle fluid flow.

Equation 4.5a is for convergent-divergent nozzles; however, most CTA have only convergent nozzles. This equation can still be used for convergent nozzles, but it should be realized the flow exits the nozzle at the throat because there is no divergent section, thus the nozzle's exit area is if fact the throat area. This results in the area ratio $\frac{A_e^E}{A_t^E}$ being equal to one. After $\frac{A_e^E}{A_t^E}$ is set equal to one and equation 4.1 is substituted into equation 4.5a, the final thrust coefficient equation can be written as:

$$C_{fg,TVFC} = \left\{\frac{M_a}{M_i}\sqrt{\frac{\varsigma_i}{\varsigma_a}} + \frac{\sqrt{\varsigma\left(\frac{\gamma+1}{2}\right)^{(\gamma+1)/(\gamma-1)}}}{\gamma M_i}\left(\frac{P_e}{P_a}-1\right)\right\}\cdot\chi \tag{4.6}$$

In reference [24], the analytical solution used to calculate the vectored nozzle thrust coefficient has been with compared to vectored nozzle thrust coefficients obtained using a numerical solutions and experimental measurements. The comparison was completed for multiple nozzle pressure ratios (NPR) and nozzle deflection angles. The results of the comparison are plotted in figure 4.7. The legend in figure 4.7 shows the numerical solution and analytical solutions were completed for a nozzle surface roughness of 30 μm and 15 μm, respectively. The surface roughness of the nozzle used for the experiments had a maximum surface roughness of 30 μm, but ideally the entire nozzle was to have a surface roughness of 15 μm.

It can be seen the analytical equation calculates a thrust coefficient closely agreeing with the experimental thrust coefficient, thus calculating the nozzle's thrust coefficient using the analytical solution will provide results with accuracy sufficient for a feasibility study of a thrust vectoring CTA.

To calculate $C_{fg,TVFC}$, the flow's actual and ideal Mach number must be known at the nozzle's exit. The static pressure at the nozzle's exit must also be known to calculate $C_{fg,TVFC}$. The necessity to know these variables creates complications when calculating the vectored nozzle thrust coefficient coefficient. To avoid this complication, a simplification will be made which assumes the static pressure at the nozzle exit, P_e is nearly equal to the ambient static pressure, P_a. This can be reasonably assumed because large changes in pressure cannot occur over short distances for subsonic flows. By using the assumption $P_e \approx P_a$, equation 4.6 can be reduced to the following:

$$C_{fg,TVFC} = \frac{A_t^E}{A_t^G}\frac{M_a}{M_i}\sqrt{\frac{\varsigma_i}{\varsigma_a}}\cdot\chi \tag{4.7}$$

This equation can be further simplified by assuming boundary layer growth and flow separation in the nozzle is negligible. This assumption is generally not valid; however, calculating the boundary layer thickness

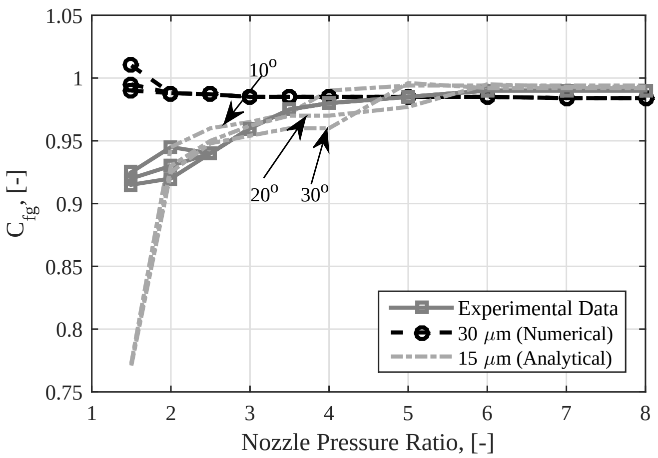

Figure 4.7: Nozzle thrust coefficient as a function of nozzle pressure ratios for three vectoring angles [24]. (μm - nozzle surface roughness)

and flow extent of flow separation in the nozzle can be quite complex. For example, the nozzle pressure ratio, deflection angle, and Reynolds number can all influence the boundary layer development. To avoid this complication, the nozzle will be considered as an ideal nozzle. With this assumption, the vectored nozzle thrust coefficient is treated as a conventional convergent nozzle thrust coefficient which is corrected to account for the change in effective nozzle area due to the nozzle deflection angle. The following equation results from these assumptions:

$$C_{fg,TVFC} = C_{fg,nozzle} \cdot \chi \tag{4.8}$$

Figure 4.8 plots the value of the nozzle thrust coefficient as a function of nozzle deflection angle. It can be seen that the thrust coefficient has a value equal to one, i.e. no losses due to vectoring, at a nozzle deflection angle of 0°. At the maximum nozzle deflection angle of 20°, the thrust coefficient is approximately 0.94.

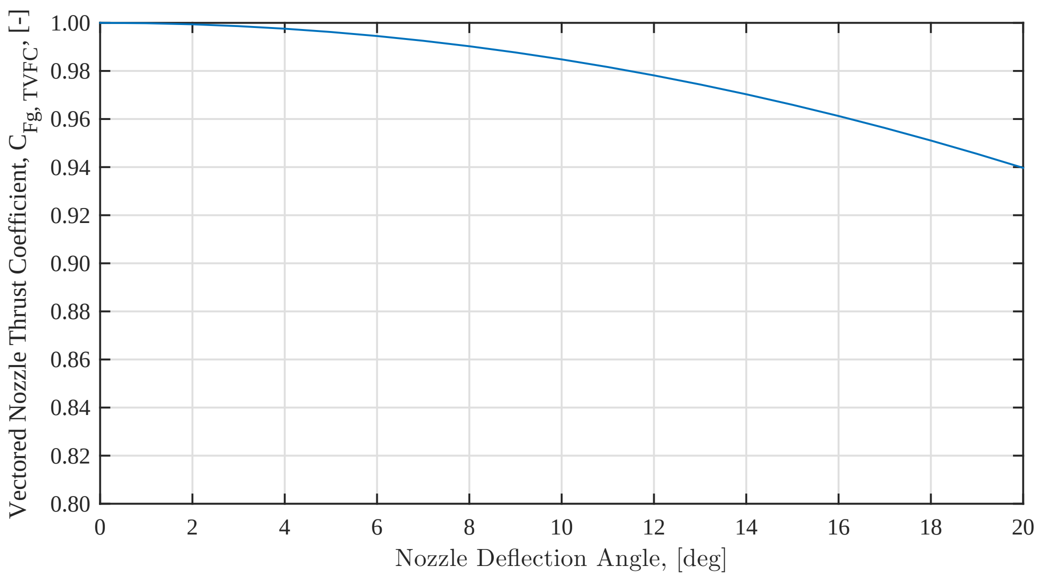

Figure 4.8: Thrust coefficient for a vectored nozzle.

Once the vectored nozzle thrust coefficient is known, the axial, lateral, vertical components of the vectored thrust can be calculated. To complete this task, the effective thrust vectoring angle must be known.

4.3.3. EFFECTIVE NOZZLE DEFLECTION ANGLE

What differentiates the effective thrust vectoring angle from the nozzle deflection angle is the possibility of boundary layer growth and flow separation within the nozzle. According to reference [7], the difference between the effective thrust vectoring angle and the nozzle deflection angles can differ by 4° for subsonic nozzle flows. In references [6] and [53], it stated the effective thrust vectoring angles are generally equal, within 1°, to the nozzle deflection angle. Since the effective thrust vectoring angle and nozzle deflection angle differ by a few degrees or less, these two angles are assumed to be equal.

With the aforementioned assumption, the vectored thrust components can be calculated with the following equations:

$$F_{g,x} = F_{g,i} \cdot C_{fg,TVFC} \cdot \cos\delta_y \cdot \cos\delta_z \tag{4.9a}$$

$$F_{g,y} = F_{g,i} \cdot C_{fg,TVFC} \cdot \sin\delta_y \cdot \cos\delta_z \tag{4.9b}$$

$$F_{g,z} = F_{g,i} \cdot C_{fg,TVFC} \cdot \cos\delta_y \cdot \sin\delta_z \tag{4.9c}$$

4.3.4. ENGINE MASS INCREMENT DUE TO THRUST VECTORING

There is a lack of modern information related to the engine mass increment caused by the addition of TVFC; however, some thrust vectoring nozzle mass data dating back to the 1980s and 1990s can found in available literature. Due to the age of the data, attention has to be given to ensure the data can be applied to modern thrust vectoring nozzle designs.

In reference [23], a spherical convergent flap nozzle was designed. Figure 4.9 shows the geometry of the design. The nozzle mass for this design was estimated to be about 600 lbs (272 kg); however, this nozzle mass does not properly represent the thrust vectoring nozzle mass used on a CTA. Firstly, due to the challenge of integrating an engine with an aircraft's airframe, the rectangular nozzle shape suggests that it was designed for a military aircraft rather than a CTA. Secondly, the nozzle was designed to vector thrust in the pitch plane and not the yaw plane. The nozzle to be equipped on the Fokker 100 should have the ability to vector the thrust in both the pitch and yaw planes. Lastly, the type of engine for which the nozzle was designed is unknown. Information about the engine's thrust or mass should be known before this nozzle mass estimate is applied to the Tay 650 engine. Based on these reasons, other references should be used to estimate the mass increment resulting from the thrust vectoring nozzle design.

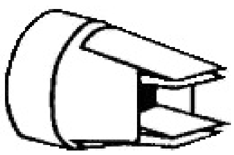

Figure 4.9: Spherical convergent flap nozzle [23]

Reference [10] also presents thrust vectoring nozzle mass data. Figure 4.10 displays the expected engine mass increase due to the addition of thrust vectoring and thrust reversing nozzle designs. This data has been specifically calculated for the General Electric Axisymmetric Thrust Reverser nozzle shown in figure 2.4. This nozzle design can vector thrust in both the pitch and yaw planes, which fulfills one of the thrust vectoring nozzle requirements. Since the GEATR nozzle has a circular cross section, rather than a rectangular cross section, the mass increments shown in figure 4.10 can be assumed to be the more reliable thrust vectoring nozzle mass estimation when compared to mass estimation of the previously discussed spherical convergent flap nozzle.

Since the data in figure 4.10 is presented as a percent engine mass increment, it can be reasonably assumed to be applicable for engines of varying thrust, mass, and thrust-to-weight ratios; however, this statement should be verified. To verify this statement, reference [10] states that the GEATR nozzle can be fitted to the General Electric F110 and F404 engine models. The thrust, masses, and thrust-to-weight ratios for these two engines are displayed in table 4.2, and the two engines can be seen to differ significantly. Since the GEATR can be fitted to these different nozzles, the mass estimation data in figure 4.10 can be assumed to apply to the Tay 650 engine. It should be noted that Rolls-Royce designed the Tay 650 engine, and the GEATR nozzle was designed by General Electric. The assumption that the GEATR mass can be applied to the Tay 650 is not completely verified.

-	F110-GE-129	F404-102/402
Engine Mass, [kg]	1,805	1,035
Engine Thrust, [kN]	131	78.7
Engine Thrust-to Weight, [-]	7.40	7.75

Table 4.2: General Electric engine data [41] [42]

One should also recognize that the GEATR nozzle is a convergent-divergent nozzle. This indicates that the nozzle has been designed to achieve supersonic flow velocities at the nozzle exit. Convergent-divergent nozzles are typically equipped on supersonic aircraft, whereas convergent nozzles are equipped on subsonic aircraft [37]. Due to the divergent nozzle section, convergent-divergent nozzles tend to be longer than nozzles with only a convergent section; therefore, it is reasonable to assume the mechanical design of convergent-divergent nozzles requires more material than a simple convergent section. Since the data in 4.10 is presented for a convergent-divergent nozzle, one could expect that it overestimates the thrust vectoring nozzle mass for a convergent nozzle. With this realization, the data presented in table 4.10 may be considered as a conservative mass estimate for a convergent thrust vectoring nozzle.

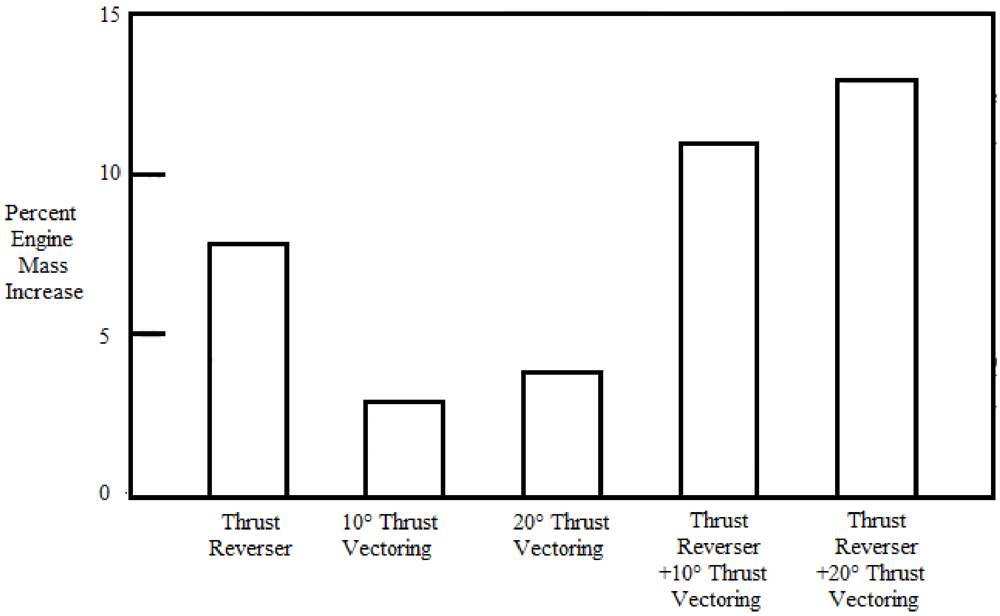

Figure 4.10: Mass of thrust reversing and thrust vectoring system for the GEATR nozzle [10]

Based on the aforementioned reasons, the thrust vectoring nozzle mass data presented in figure 4.10 will be used to estimate the thrust vectoring nozzle mass of the Tay 650 engine. The Fokker 100 has thrust reversing abilities, so the Tay 650 engine mass with thrust reversing abilities must be calculated to estimate the baseline engine mass. The engine mas with thrust reversing and either 10° or 20° thrust vectoring must also be estimated. The difference between the baseline engine mass and the mass of the engine with either 10° or 20° nozzle deflection abilities will be used to estimate the engine mass increment due to the TVFC addition.

The Fokker 100 has thrust reversing abilities, and the thrust reversing system can be seen in figure 4.11. Data regarding the mass of this type of thrust reversing system could not be found in literature, so the thrust reversing nozzle will be estimated to increase the Tay 650 mass by 8%. This value was selected based on the thrust reversing data presented in figure 4.10. It must be noted that the thrust reversing system equipped on the Fokker 100 differs from the GEATR thrust reversing nozzle, and the 8% mass increment applies specifically to the GEATR nozzle design. This statement is affirmed through a comparison of the thrust reversing systems shown in figures 4.11 and 4.12. Although the mechanical design of the nozzles differ, their masses will be considered as comparable due to a lack of information about thrust reversing system equipped on the Fokker 100.

Figure 4.11: Fokker 100 thrust reverser nozzle. Image courtesy of *Wikipedia Commons*

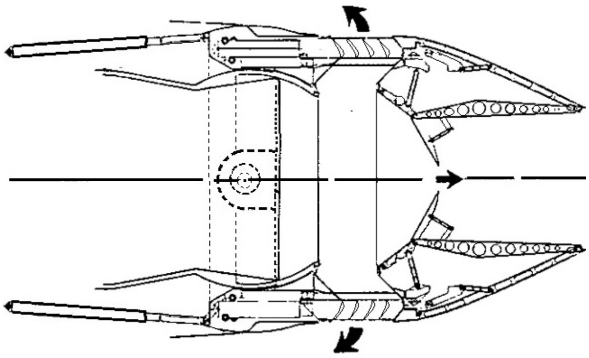

Figure 4.12: GEATR thrust vectoring and thrust reversing nozzle. [10]

In table 4.3, the Tay 650 mass and the estimated mass of the thrust vectoring and thrust reversing systems have been displayed. This data has been calculated from knowledge of the baseline Tay 650 engine mass [28] and figure 4.10. Since the Fokker 100 has fitted the Tay 650 engine with a thrust reversing system, engine 2 is used to estimate this mass. A thrust vectoring system capable of achieving either 10° or 20° nozzle deflection angles will be added in addition to the thrust reversing system, and engine 3 and 4 estimate this engine mass. The difference between the engine 2 mass and either the engine 3 or 4 mass is the estimated mass increase due to thrust vectoring. The percent mass increase due to the addition of thrust vectoring has also be displayed in table 4.3. Since the Fokker 100 has two engines, the estimate mass of the thrust vectoring system shown in table 4.3 must be added to the Fokker 100 twice.

	Percent Engine Mass Increase due to Nozzle	Engine Mass Estimate [kg]
Engine 1: Tay 650	-	1,595
Engine 2: Tay 650 + Thrust Reverser	8.0%	1,723
Engine 3: Tay 650 + Thrust Reverser + 10° Thrust Vectoring	11%	1,770
Engine 4: Tay 650 + Thrust Reverser + 20° Thrust Vectoring	13%	1,802
Mass Difference between Engine 2 and Engine 3 [kg]:	47	
Percent Mass Difference between Engine 2 and Engine 3:	2.7%	
Mass Difference between Engine 2 and Engine 4 [kg]:	79	
Percent Mass Difference between Engine 2 and Engine :	4.6%	

Table 4.3: Tay 650 engine and estimated nozzle mass

It is important recognize the significance of the data presented in table 4.3. In the formulation of the research objective, it was stated that the mass increment due to the addition of thrust vectoring should not be greater than the mass decrement resulting from the VT redesign. It is therefore desirable to reduce the VT weight between 94 kg (2 x 47) and 158 kg (2 x 79 kg) in order to achieve a reduction in the Fokker 100 empty operational mass. A reduction in empty operational mass is expected to reduce the estimated mission fuel consumption; however, the nozzle masses are relatively small when compared to the aircraft's empty operational mass of 24,600 kg [56]. A reduction in parasite drag, which is associated with the reduction in VT area, may impact the aircraft's mission fuel mass more than the slight change in empty operational mass.

One final comment must be made in regards to the mass estimation procedure. It is likely that the thrust vectoring engines impact the engine's pylon mass. For example, if the vectored thrust is used for directional control, then the engine pylon will experience either tensile or compressive forces, and the pylon's structure must be strengthened to account for these additional forces. This would result in an increase in engine pylon mass; however, the mass increment due to pylon strengthening will be neglected.

4.4. AIRCRAFT MASS AND INERTIA

As has been discussed, a Fokker 100 aircraft will be fitting with a TVFC system and its VT will be redesigned. The methods and theories used to redesign the VT and model the thrust vectoring engine model have been discussed. It is now important to present other data required to complete the Fokker 100 model. The Fokker 100 mass and inertia will now be presented.

Due to the data available in open literature, the mass and inertia for the Fokker 100 corresponding to the empty operational aircraft structure was used. Reference [56] provides the Fokker 100 empty operational mass, and reference [54] provides the Fokker 100 empty operational inertia. Table 4.4 presents a summary of this data.

Fokker 100 Structural Variable	Value
Mass	2.46×10^4 kg
I_{xx}	2.53×10^5 kgm^2
I_{yy}	1.67×10^6 kgm^2
I_{zz}	1.85×10^6 kgm^2
I_{xz}	8.72×10^4 kgm^2

Table 4.4: Fokker 100 mass and inertia data [56] [54]

Since the aircraft's empty operational inertia will be used for the S&C analyses, it is important to consider how this influences the results presented in later sections. Inertia is the tendency of an object to resist changes in its state of motion. In order to alter an object's state of motion, a force must be applied. When applying the concept of inertia to aircraft, an empty operational mass aircraft would have the lesser inertia when compared to the same aircraft at its maximum operational mass. With this realization, one would expect the rotational rates induced by a control input to be larger for the empty operational aircraft. For this example, the rotational rate represents a change in an aircraft's change in motion, and the control input is force used to create the change in motion. To summarize this point, the empty operational mass aircraft would be more agile when compared to the maximum operational mass aircraft.

It is also beneficial to examine the mass and inertia effects from an aircraft dynamics viewpoint. It will later be discussed that CTA have specific dynamic modes. The lateral and directional dynamic modes of a CTA include the roll mode, spiral mode, and Dutch roll mode, and the aircraft's inertia will influence these dynamic modes. In particular, the Dutch roll mode is an oscillatory dynamic mode where an aircraft yaws and rolls in an out-of-phase sequence. This motion is undesirable from an aircraft handling viewpoint, and aerodynamic forces should dampen this oscillatory motion. For a given aircraft design, one would expect the aerodynamic forces to be more effective in damping the Dutch roll motion for an aircraft flying at its empty operational mass and inertia when compared to the same aircraft flying at it maximum operational mass and inertia.

When analyzing the influence of the aircraft's mass on its trim conditions, an aircraft flying at its empty operational mass will require lesser lift to achieve trimmed flight when compared to an aircraft flying at its maximum operational mass. From a drag viewpoint, induced drag increases with lift, so increasing an aircraft's mass will result in an increase in induced drag; therefore, thrust must increase to achieve trimmed flight. For one-engine-inoperative flight, the aircraft's operative engine may produce sufficient thrust for trimmed flight for the empty operational mass aircraft, but single operative engine may not produce sufficient thrust for the maximum operational mass aircraft.

These are initial considerations related to the selected Fokker 100 mass and inertia, and the implications on the design feasibility of a thrust vectoring aircraft with an unconventionally small VT must be understood.

4.5. Control Effector Limits and Rates

To complete the Fokker 100 trim assessment and flight simulations, the control surface deflection limits and rates must be specified. For the maximum rudder, elevator, and aileron deflection angles, data corresponding to the Fokker 100 has been found in reference [44]. These values are summarized in the first few rows of table 4.5. For the aircraft's maximum rudder, elevator, and aileron deflection rates, reference [47] recommends values of $\pm 60^\circ$/sec.

Control Effector	Maximum Deflection Angle	Maximum Deflection Rate
Rudder	20°	60°/s
Elevator	22° down, 25° up	60°/s
Aileron	20° down, 25° up	60°/s
Nozzle	20°	60°/s

Table 4.5: Maximum deflection angle and deflection rate for the aircraft's control effectors

For the maximum nozzle deflection angle, an angle of 20° in any direction will be used. This value has been chosen because multiple references, such as references [6], [23], and [10], have researched thrust vectoring nozzle designs with this nozzle deflection capability.

For the nozzle deflection rate, a value of $\pm 60^\circ$ will be used. This nozzle deflection rate was based on a nozzle designed in reference [6]. This thrust vectoring nozzle had the ability to provide pitch plane thrust deflection at a rate of 60°/sec, and yaw plane thrust deflection at a rate of 40°/sec. The research in reference [6] was published in 1989, so one can assume modern technology can achieve pitch and yaw plane deflection rates of 60°/sec, thus this deflection rate was used for the thrust vectoring nozzle model.

It is important to compare the deflection rate limits of the rudder and nozzle since they will both provide directional control. Based on the data presented in table 4.5, the rudder and nozzle have identical maximum deflection rates. Note that it is beneficial from an aircraft control viewpoint to have large deflection rates for the control devices because an aircraft's maximum rotational rates increase when deflection rates increase.

4.6. Aircraft Model Recommendations

The methods used to model the thrust vectoring Fokker 100 aircraft have been discussed. There are limitations with the aircraft model, and these limitations will be addressed.

It was been stated that the aircraft will use both thrust vectoring and aerodynamic control surfaces to trim the aircraft in the occurrence of OEI flight conditions. If the engine fails during the aircraft's takeoff, then the engine's thrust will be deflected in the yaw plane to balance the moment created by the asymmetric thrust. By vectoring the thrust to allow for yaw control, the axial thrust used to accelerate the aircraft during takeoff is reduced. This will impact the aircraft's takeoff performance and balanced field length. An analysis of the aircraft's takeoff performance with OEI should be completed; however, limitations in the aircraft model will not allow for this analysis to be completed. In order to analyze an aircraft's takeoff performance, the Fokker 100 landing gear and high lift devices must be modeled. Neither the Fokker 100 landing gear or high lift devices have been included in the aircraft model.

The significance of this model limitation can be understood through knowledge of aircraft airworthiness standards. In the Federal Aviation part 25 section 121 (FAR 25.121), airworthiness standards are established for transport aircraft takeoff and climb performance with OEI. For example, the FAR states a two-engine aircraft must have a positive climb gradient with OEI and it landing gear extended for the critical takeoff configuration. When the landing gear is retracted, the takeoff climb gradient of two-engine aircraft may not be less than 2.4 percent with OEI. Based on these airworthiness standards, the takeoff performance analysis requires landing gear and high lift systems to be modeled.

To fully demonstrate the feasibility of the proposed aircraft design, a detailed analysis of the OEI takeoff performance should be analyzed; however, the discussed limitations in the aircraft model prevent the completion of this analysis.

5

Aerodynamic Analysis

The Fokker 100 with five different VT designs, including the original design and four scaled variants, will be used to evaluate the S&C of an aircraft designed with TVFC and an unconventionally small VT. To complete this evaluation, aerodynamic simulations must be completed to estimate the aircrafts' S&C derivatives. In addition to estimating S&C derivatives, aircraft performance coefficients, such as C_L and C_D, must be estimated with the aerodynamic simulations. An aerodynamic analysis program named VSAERO was used to obtain the required S&C derivatives and performance coefficients for the various Fokker 100 aircraft designs. The importance of the S&C derivatives will be discussed at a later section, but they are first introduced in the aerodynamic analysis because they are used to demonstrate the capabilities and limitations of the Fokker 100 model.

Since VSAERO was used to complete the aerodynamic analysis, the theory of VSAERO will be briefly discussed. This allows the capabilities and limitations of VSAERO to be recognized.

5.1. VSAERO - Theory, Capabilities, and Limitation

VSAERO is a computer program which models aerodynamic flows. VSAERO uses a first-order panel method with nonlinear aerodynamic extensions to calculate the aerodynamic characteristics around arbitrary bodies. Examples of nonlinear aerodynamic calculations offered within VSAERO include integral viscous boundary layer calculations, compressibility correction factors, and Trefftz plane analysis for induced drag calculations. The algorithm used by VSAERO allows for low run-times while maintaining an accuracy level suitable for preliminary aircraft design analysis [39].

As mentioned, VSAERO uses a first-order panel method to calculate a flow's aerodynamics. Panel methods are based on the Laplace equation, which assume the flow is incompressible and irrotational. This indicates potential flow theory is used.

To include the effects of the flow's viscosity, an iterative solution can be used to model boundary layers near the aircraft's surface. By using a transpiration velocity boundary condition, the viscous boundary layer can be modeled. The transpiration velocity can be imagined as a distribution of sources placed on the surface of a body, and the sources push the inviscid streamlines away from the body so to align the streamlines with the boundary layer thickness [40]. The VSAERO user manual, reference [57], and reference [45] provide a more detailed explanation of transpiration velocities.

VSAERO offers a variety of compressibility correction factors, such as the Prandtl-Glauert and Karman-Tsien correction factors; however, most of the aerodynamic simulations will be completed in relatively low dynamic pressure flows where compressibility is not significant. As has been discussed in previous sections, aerodynamic control surfaces lose their effectiveness in low dynamic pressure flows, whereas thrust vectoring is expected to be an effective form of control in low dynamic pressure flows. This is the reason why primarily low Mach number, below Mach 0.6, aerodynamic simulations are required. It should be noted that the Prandtl-Glauert correction factor gives "reasonable behavior for the lift of an elliptical wing" [57], which suggest that the high Mach aerodynamic simulation results must be verified before they are considered to be accurate.

Lastly, VSAERO has the ability to predict the drag of arbitrary bodies. Viscous effects and boundary layers methods can be included in the aerodynamic analysis, and this allows for the possibility of viscous drag calculations. For induced drag calculations, a Trefftz plane analysis is used. It should be noted drag caused by shock wave and boundary layer interactions are not possible.

The panel method used by VSAERO as well as its additional non-linear calculations make it a program suitable for calculating the aircraft's various S&C derivatives. Now it is beneficial to discuss the various flight conditions for which the derivatives should be calculated.

5.2. AERODYNAMIC MODEL

For the aerodynamic analyses, the Fokker 100 aircraft was discretized into more than 14,000 panels. The wake was also modeled for the aerodynamic simulations, and more than 10,000 panels where used to model the wake. It must be noted that the author of the thesis did not create the body mesh and wake mesh. J.H. Wei, the author of reference [55], created the Fokker 100 body mesh and wake mesh algorithms. Figure 5.1 shows the fully meshed Fokker 100 model along with wake streamlines, and figures 5.2 and 5.3 show the wing and tail meshes, respectively.

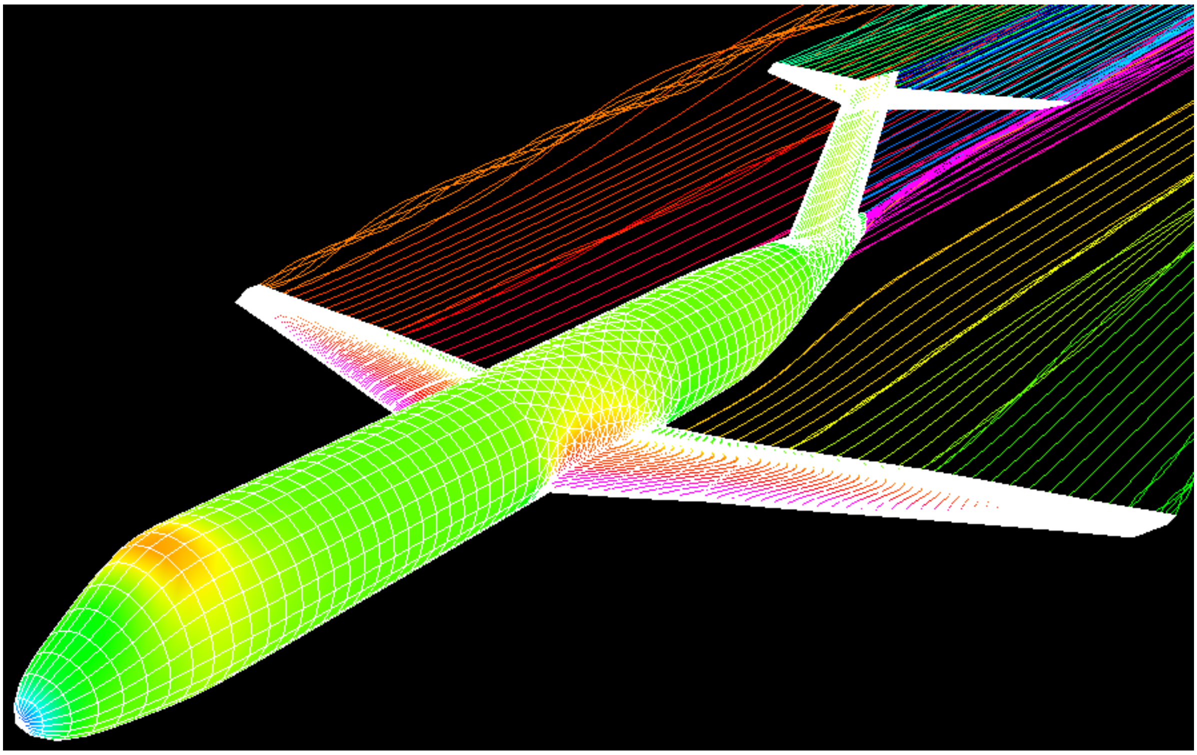

Figure 5.1: Mesh of the Fokker 100 aircraft with wake streamlines in VSAERO

In reference [55], the VSAERO simulation results are validated for the Fokker 100 aircraft and wake model. This validation is shown in table 5.1, and the validation compares lateral-directional S&C derivatives of the Fokker 100 obtained from an internal document with the same derivatives calculated from VSAERO simulations. The validation data shown in table 5.1 has been completed at an altitude of 2000 meters, Mach number of 0.3, and an angle of attack of 5°.

The validation results in table 5.1 do show a few inaccuracies in the Fokker 100 model. In particular, the errors in calculated values of $Cn_{\delta a}$ and $Cl_{\delta r}$ are large; however, one should recognize the physical meaning of these derivatives. $Cn_{\delta a}$ is the change in yaw moment due to the aileron deflection, and this moment is primarily caused by asymmetric drag created when one aileron is deflected with its trailing edge up and

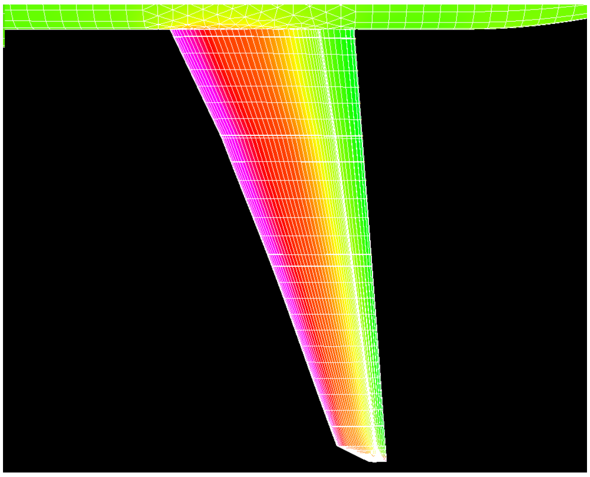

Figure 5.2: Mesh of the Fokker 100 wing in VSAERO

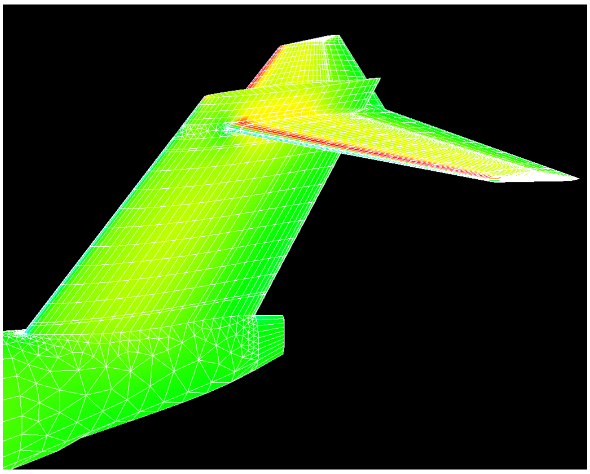

Figure 5.3: Mesh of the Fokker 100 tail in VSAERO

Derivative	Reference Value	Calculated Value	Difference
Cy_β	-0.707	-0.594	15.9%
Cl_β	-0.089	-0.100	12.6%
Cn_β	0.107	0.122	13.7%
Cy_p	0.345	0.198	42.5%
Cl_p	-0.467	-0.451	3.50%
Cn_p	-0.098	-0.069	30.3%
Cy_r	0.835	0.461	44.8%
Cl_r	0.187	0.226	21.2%
Cn_r	-0.199	-0.165	17.0%
$Cy_{\delta a}$	0.000	0.024	-
$Cl_{\delta a}$	-0.152	-0.196	29.3%
$Cn_{\delta a}$	0.001	0.004	542%
$Cy_{\delta r}$	0.127	0.168	32.3%
$Cl_{\delta r}$	0.011	0.019	72.8%
$Cn_{\delta r}$	-0.066	-0.085	29.0%

Table 5.1: Validation of the Fokker 100 VSAERO model obtained from reference [55]

the other aileron is deflected with its trailing edge down. The ailerons are not designed to produce yawing moments, and one can see the value of $Cn_{\delta a}$ is considerably smaller than the coefficient representing the yawing moment produced by a rudder deflection, $Cn_{\delta r}$. The value of $Cn_{\delta a}$ can be considered as negligible when compared to $Cn_{\delta r}$.

A similar argument can be used for $Cl_{\delta r}$. The rudder is not designed to produce rolling moments; however, since its aerodynamic center is located above the aircraft's center of gravity, it will produce some small rolling moment. The ailerons are the control surface primarily used to create a rolling moment, and this concept can be verified since $Cl_{\delta a}$ is larger than $Cl_{\delta a}$. Since the derivatives show the ailerons are the control surface most effective at producing a rolling moment, the error in the rolling moment created by the rudder can be considered as acceptable.

5.3. AERODYNAMIC SIMULATION RESULTS

Aerodynamic simulations at various altitudes and Mach numbers must be completed in order to analyze how the various VT designs effect the aircraft aerodynamics, stability, and controllability. By varying the air flow's angle relative to the aircraft, aerodynamic data can be obtained for various angles of attack, α, and angles of sideslip, β. Quasi-steady aerodynamic simulations can also be completed for aircraft roll, pitch, and rates. The roll, pitch, and yaw rates are denoted with the variables p, q, and r, respectively.

Completing aerodynamic simulations for various altitudes, Mach numbers, flow angles, and angular rotation rates allows for the calculation of the S&C derivatives for each aircraft configuration. This process of completing aerodynamic simulations to obtain S&C derivatives requires a significant amount of computing effort; therefore, selection of the simulation altitudes and Mach numbers should be done intelligently to reduce the required computing time.

Earlier it was stated that VSAERO uses compressibility correction factors and integral boundary layer methods to improve the accuracy of the results; however, how compressibility and boundary layers impact the aerodynamic results is unknown. For example, assume the flow's Reynolds number does not have a noticeable impact on the aerodynamic results. If this statement is valid, then aerodynamic simulations only need to be completed for varying Mach number and not for varying Reynolds number. In such an occurrence, the amount of required aerodynamic simulations can be significantly reduced.

To reduce the required simulation computing time, a study was completed to assess the impact of the flow's Reynolds number and Mach number on the aerodynamic results. For the analysis, simulations of the original Fokker 100 design were completed for 16 different Mach number and altitude combinations. Note that for a constant Mach number, a flows Reynolds number changes with altitude. Flow Mach numbers of 0.25, 0.42, 0.58, and 0.75 and altitudes of 0, 2,000, 6,000, and 10,000 meters were used to obtain the aerodynamic data set. By calculating the S&C derivatives for the 16 different Mach number and altitude combinations, the impact of the Mach number and Reynolds can be analyzed. The results of the aerodynamic analysis and calculation of the S&C derivatives are shown in figures 5.5 through 5.7. The derivatives were calculated at α=0° and β=0°. Since the study being presented is concerned with lateral and directional S&C, only the derivatives pertaining to this study are presented.

From an examination of the plots, a correlation between the values of the lateral-directional S&C derivatives and the flow's Mach number is noticeable. This indicates that the flow's compressibility does have an impact on the aerodynamic simulation results. When completing the aerodynamic analysis for the five Fokker 100 designs, aerodynamic simulations must be completed for various Mach numbers.

When examining how the S&C derivatives vary with altitude, it is difficult to establish a correlation. One would expect the S&C derivatives to vary with changes in altitude and Reynolds number, but this idea is not supported by the data shown in figure 5.5 through 5.7. This lack of correlation between the values of the S&C derivative and altitude may result from an insufficient amount of panels on the Fokker 100 aircraft. Increasing the amount of panels on the Fokker 100 body may prove that the lateral-directional S&C derivatives are impacted by the flow's Reynolds number.

Since a correlation between the flow's Reynolds number and the value of the S&C derivatives has not been established, aerodynamic simulations will not be completed for varying altitudes and Reynolds numbers. It can be presumed that for a constant Mach number, the flow's Reynolds number will not have a noticeable impact on the calculation of the lateral-directional S&C derivatives.

Using this aforementioned knowledge allows for the determination of the flight conditions used to obtain the S&C derivatives. For the aerodynamic simulations, an altitude of 2,000 meters is used, and flow Mach numbers of 0.30, 0.42, 0.58, and 0.75 are used for the aerodynamic simulations. The lowest Mach number used for the simulations in Mach 0.3. This value was selected because it was assumed to be near the stall Mach number for the Fokker 100 flying at its empty operational mass without high-lift devices. An upper Mach number of Mach 0.75 was selected because it corresponds to the maximum operational Mach number of the Fokker 100. These altitude and Mach number combinations were used to complete the aerodynamic simulations for the five various Fokker 100 aircraft designs.

5.4. AIRCRAFT FLIGHT ENVELOPE

After the aerodynamic simulations are completed, the aircraft's flight envelope can be predicted. Once the flight envelope is predicted, the domain used to analyze the aircraft's stability, control, OEI flight, and performance is defined. The following criteria have been used to predict the flight envelope of the Fokker 100:

- Minimum Mach number corresponding to stalled flight conditions

- Maximum altitude corresponding the the maximum cabin overpressure
- Maximum operational mach number, M_{MO}, corresponding to engine limitations
- Maximum operating speed, V_{MO}, corresponding to structural limitations

A brief explanation will be given to each of the criteria used to define the flight envelope.

To establish the minimum Mach number for a given altitude, stall criteria had to be established. The stall criteria was defined when the aircraft's trimmed angle of attack was 8°. This value was selected because VSAERO is limited in the modeling of separated flows, and the accuracy of the aerodynamic simulation results at high angle of attacks would required a detailed analysis before they can be considered as acceptable. It is also important to reiterate that the aircraft model does not include high lift devices or landing gear models; therefore, the minimum Mach number corresponds to a 'clean' aircraft configuration. Since the aircraft's stability and control analyses will be completed using the aircraft's empty operational mass and inertia, it was determined that the aircraft's empty operational mass should also be used to define the minimum airspeed.

For the aircraft's ceiling, which is the maximum altitude, an altitude of 10,000 meters was selected. This altitude has been determined with the assumption that the cabin's overpressure is the limiting factor. The aircraft could achieve trimmed flight at higher altitudes; however, stability, control, performance, etc. analyses where not completed above 10,000 meters.

The maximum operational Mach number corresponds to the limitations of the Tay 650 engine. This Mach number has been defined by the manufacturers of the Tay 650 engine. It is also important to note that the ability of VSAERO to produce accurate results at high Mach numbers has not been investigated. Additionally, many of the analyses will be completed at lower Mach numbers, when the freestream dynamic pressure is relatively low.

Lastly, the maximum operating speed corresponds to the aircraft's structural limits. A calibrated airspeed of 400 knots was selected for this limit. The actual Fokker 100 maximum operating speed was not found in literature however, according to reference [3], the A300 has a maximum dive speed of 425 knots. The maximum operating speed for the Fokker 100 was selected such that it is lower than the maximum dive speed of another transport aircraft.

By using the described criteria, the flight envelope of the Fokker 100 can be created. Figure 5.4 shows the resulting flight envelope. Note that this flight envelope shown in figure 5.4 will be used throughout the report, and the criteria used to define the boundaries should be kept in mind.

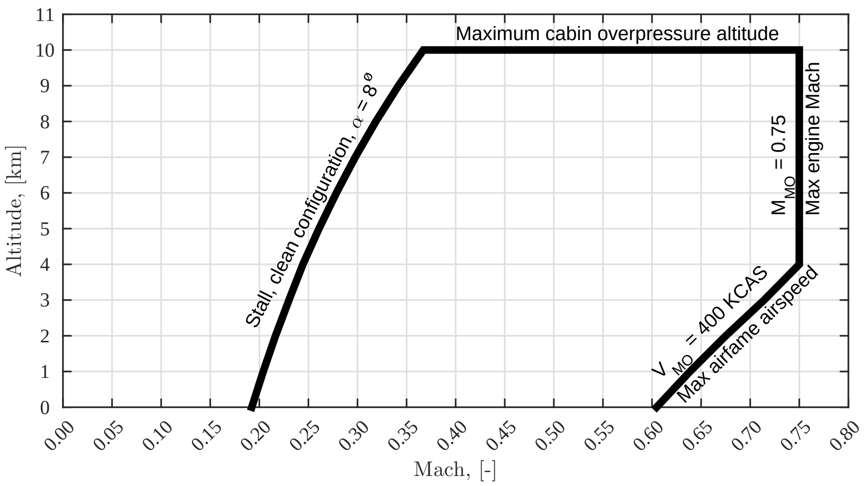

Figure 5.4: Predicted Fokker 100 flight envelope

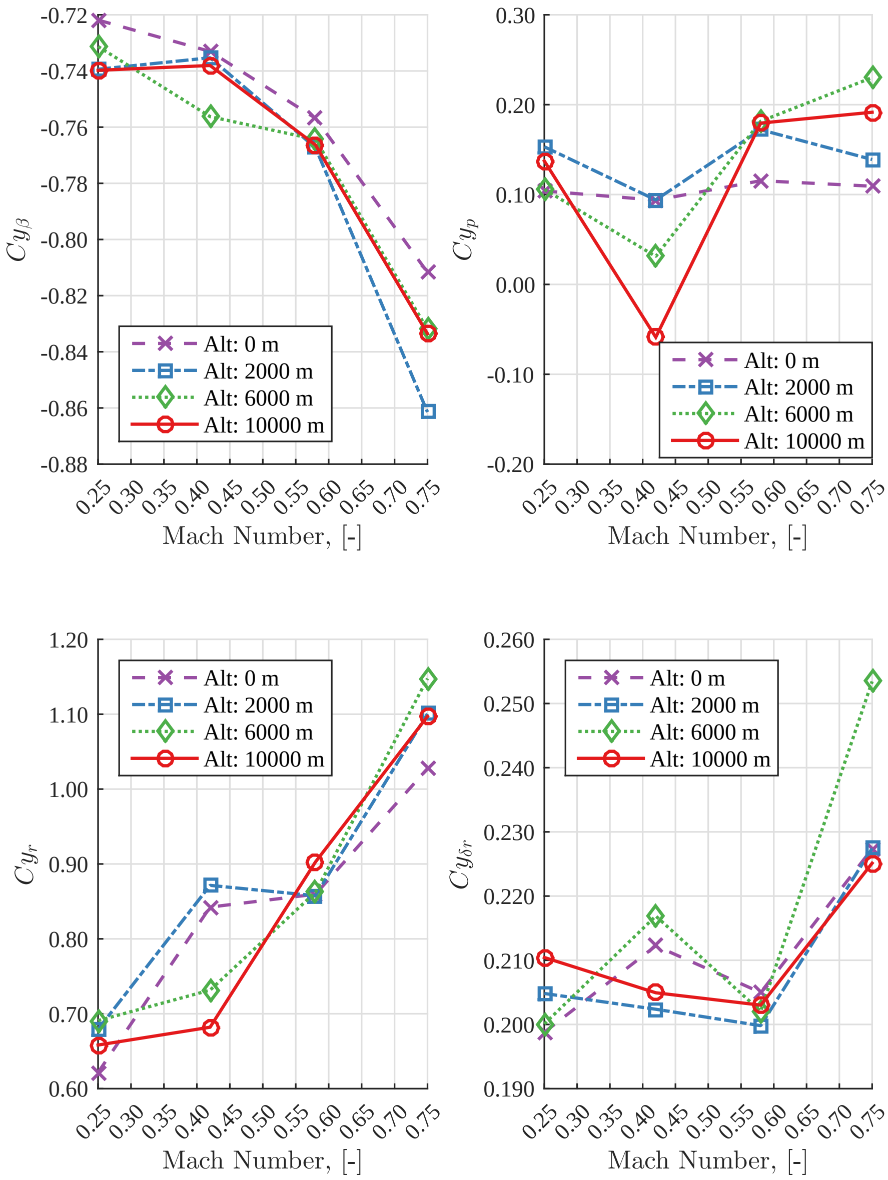

Figure 5.5: Fokker 100 stability and control derivatives with respect to sideforce, Cy

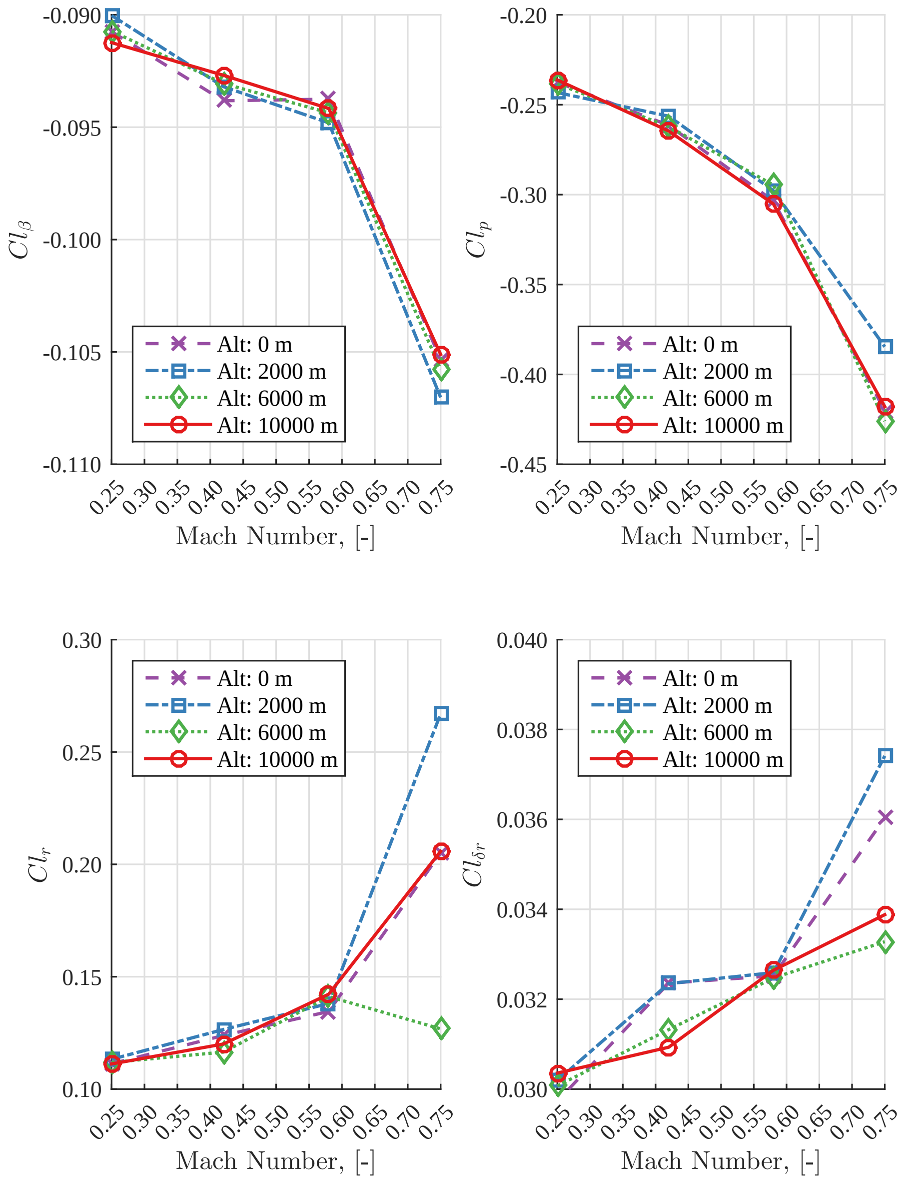

Figure 5.6: Fokker 100 stability and control derivatives with respect to rolling moment, Cl.

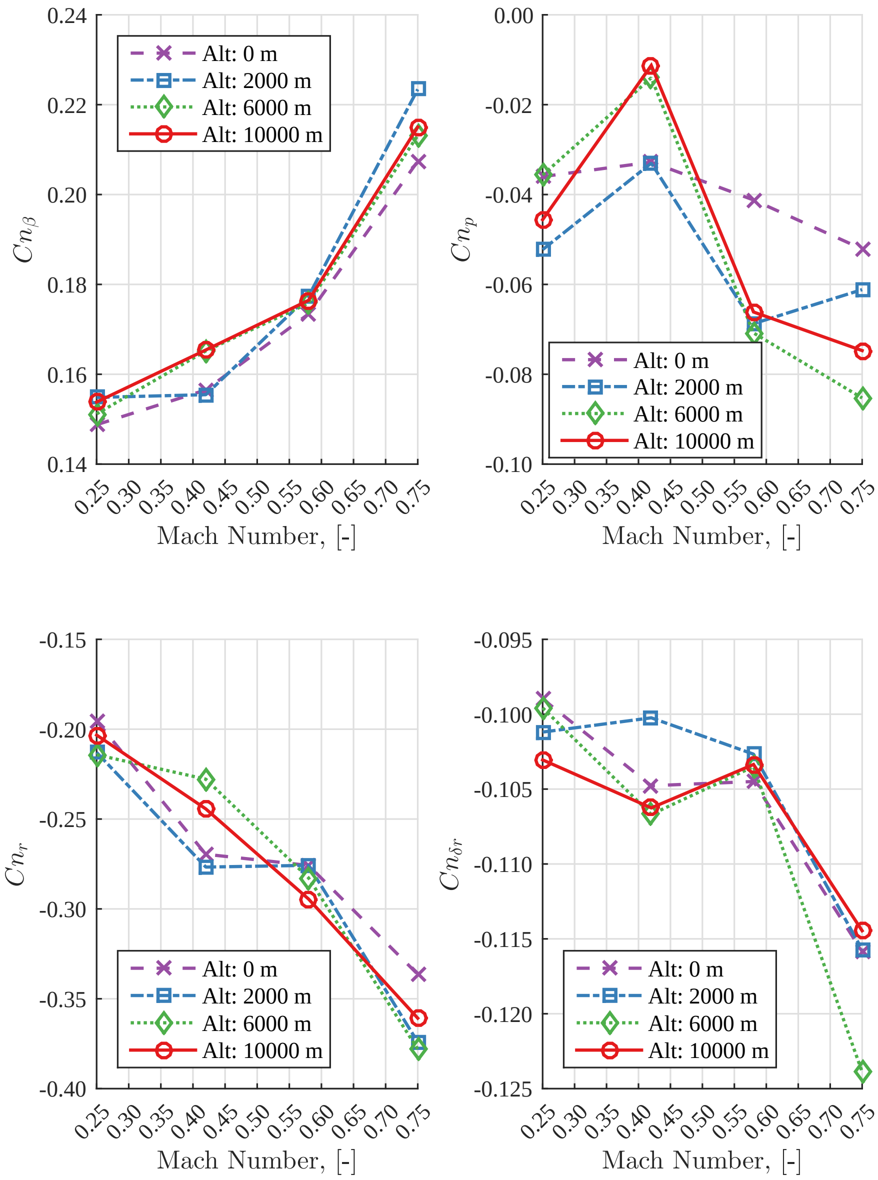

Figure 5.7: Fokker 100 stability and control derivatives with respect to yawing moment, Cn

6

Stability and Control Analyses

Aircraft stability is related to an aircraft's ability to maintain an equilibrium flight condition. Stability is often separated into two different categories: static stability and dynamic stability. Both static and dynamic stability analyses for the thrust vectoring Fokker 100 aircraft with various VT designs will be presented in this section.

Stability of an aircraft can be analyzed for its rolling, pitching, and yawing motions. For many aircraft designs, roll and yaw motions are coupled, thus aircraft lateral and directional stability often studied simultaneously. Due to the symmetrical shape of most aircraft, an aircraft's pitching motion is often independent of the aircraft's roll and yaw motions, thus longitudinal stability analyses is often completed independently. A redesign of the Fokker 100 VT will impact the aircraft's lateral and directional stability; however, the VT redesign is not expected to have a significant impact on the aircraft's longitudinal stability. Therefore, lateral-directional stability analyses will be discussed, whereas longitudinal stability analyses will be neglected.

For the stability analysis, a coordinate system must be defined so forces, moments, angles, and velocities are know to be either negative or positive. Figure 6.1 shows coordinate system as well as the notation required to explain the S&C analysis. The coordinate system is body fixed with the origin of the coordinate system placed at the aircraft's center of gravity, and the x-axis passes through the nose of the aircraft. The right-hand-rule can be used to orientate the coordinate system. The notation shown in 6.1 is as follows:

1. X, Y, Z are forces
2. u, v, w are linear velocities
3. L, M, N are moments
4. p, q, r are angular velocities

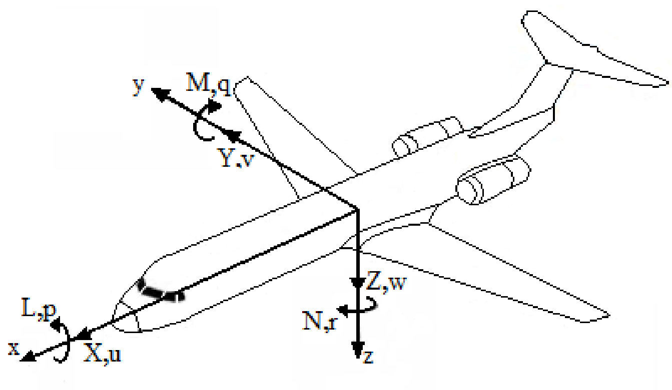

Figure 6.1: Stability axis coordinate system and S&C nomenclature

6.1. LATERAL-DIRECTIONAL EQUATIONS OF MOTION

In order to analyze an aircraft's stability, whether static or dynamic, the aircraft's equations of motion must be derived. A thorough derivation of an aircraft's EOM can be found in many books and peer reviewed journal articles covering the topic of aircraft stability and control, such as in references [8], [34], and [35]; however, only the final equations of motion resulting from the derivation will be discussed. It should also be noted that multiple assumptions have been used during the derivation to simplify the equations of motion. The assumptions used during the derivation are listed as follows:

- Aircraft has a rigid body
- Aircraft has a constant mass
- Earth is flat and non-rotating
- Aircraft is located within a constant gravity field
- Rotating mass effects are negligible (engine blade rotation negligible)
- Aircraft has a plane of symmetry such that I_{xy} and I_{yz} are equal to zero
- Aircraft's center of gravity lies within the assumed plane of symmetry

The lateral-directional equations of motion are as follows:

$$\Sigma Y = \left(Cy_\beta\beta + Cy_p\frac{pb}{2u} + Cy_r\frac{rb}{2u} + Cy_\delta\delta\right)\overline{q}S + mg\sin\phi\cos\theta = m(\dot{v} + ru - pw) \tag{6.1a}$$

$$\Sigma L = \left(Cl_\beta\beta + Cl_p\frac{pb}{2u} + Cl_r\frac{rb}{2u} + Cl_\delta\delta\right)\overline{q}Sb = I_{xx}\dot{p} + (I_{zz} - I_{yy})qr - I_{xz}(\dot{r} + pq) \tag{6.1b}$$

$$\Sigma N = \left(Cn_\beta\beta + Cn_{T_\beta}\beta + Cn_p\frac{pb}{2u} + Cn_r\frac{rb}{2u} + Cn_\delta\delta\right)\overline{q}Sb = I_{zz}\dot{r} + (I_{yy} - I_{xx})pq - I_{xz}(\dot{p} - qr) \tag{6.1c}$$

In these equations, S&C derivatives are introduced to indicate how the forces and moments acting on the aircraft change as the aircraft's flight condition changes. δ refers to the deflection of a control device, such as the rudder or thrust vectoring nozzle. Cn_{T_β} represents the change in yawing moment coefficient due to thrust with sideslip angle. Some derivations of the lateral-directional equations of motion neglect this variable because it is assume to have a negligible impact on the aircraft's yawing moment; however, since the OEI flight condition is being analyzed, this term is included in the lateral-directional equations of motion. The other variable nomenclature in equations represent aircraft parameters commonly used in the discipline of aircraft stability and control. The nomenclature is widely used and accepted; however, a full description of each variable can be seen in nomenclature table presented at the beginning of this report.

6.2. PHALANX

The lateral-directional equations of motion, shown if equation set 6.1, along with the longitudinal equations of motion can be used to analyze the flight mechanics and dynamics of the various aircraft designs. In order to analyze the aircraft flight mechanics, a program named Phalanx (Performance, Handling Qualities and Load Analysis Toolbox) will be used.

Phalanx is aircraft flight mechanics toolbox developed by Mark Voskuijl, an assistant professor at Delft University of Technology. The program models an aircraft's flight mechanics through the creation of multibody dynamic systems. By integrating data from various aerospace disciplines, Phalanx can develop nonlinear aircraft models [39]. Phalanx is suitable for various flight mechanics analyses, and some of its flight mechanics analyses include the following:

- Trim assessment
- Control law design
- Aeroelastic effects

- Handling qualities assessment
- Virtual time domain flight tests
- Aircraft response to atmospheric turbulence
- Loads prediction (e.g. pull-up manuever loads)
- Performance analysis (e.g. takeoff and cruise performance)

In the following sections, various analyses will be presented which are related to aircraft mechanics and dynamics. Some of the analyses will include trim analyses, Dutch roll analyses, aircraft maneuvering analyses, mission performance analyses, among others. A full-order, nonlinear model for each of the discussed aircraft designs was created within Phalanx, and Phalanx was used to complete the aircraft mechanics and dynamics analyses. Note that full-order means the aircraft's longitudinal equations of motion were included in the analyses; however, a discussion of the aircraft's longitudinal flight mechanics and dynamics will not be discussed.

6.3. STATIC STABILITY

For an aircraft to possess stable flight characteristics, an aircraft flying in an equilibrium position must return to its original equilibrium position after experiencing a disturbance, such as a crosswind. When an aircraft experiences a disturbance, aerodynamic forces and moments must allow for equilibrium to be achieved. By analyzing the lateral-directional stability derivatives, particularly the sign each derivative, the aerodynamic forces and moments can be seen to either stabilize or destabilize the aircraft. For example, if an aircraft experiences a disturbance which causes the aircraft to roll, then a moment must be created so wings-level flight may be obtained.

In order for an aircraft to have positive lateral-directional stability, the lateral-directional stability derivatives must abide to the following inequalities:

$$\begin{array}{lll} Cn_\beta > 0 & Cn_p < 0 & Cn_r < 0 \\ Cl_\beta < 0 & Cl_p < 0 & Cl_r > 0 \\ CY_\beta < 0 & & \end{array}$$

For the Cn_p and Cl_r, static stability does not require the inequalities to be true; however, it is conventional for S&C derivatives to abide by the presented inequalities. Also, the stability derivatives of Cy_p and Cy_r are shown in equation 6.1a, but their contribution to an aircraft's static stability is typically of minor importance [35]. Requirements on the sign of Cy_p and Cy_r will not be used to assess the static stability of the aircraft designs.

With the requirements for lateral-directional static stability in mind, it is beneficial to examine how reducing the VT area influences the S&C derivatives. Figures 6.2 through 6.4 contain plots of the lateral-directional S&C derivatives for the various VT sizes. From the figures, it can be seen that reducing the VT size causes the magnitude of the S&C derivatives to approach zero. This indicates a deterioration in the lateral-directional static stability as the VT area is reduced. Special consideration should be given to the smallest of the VT designs, which is the 50% VT area, because it is the design most likely to not fulfill the static stability criteria. When examining the stability derivatives for the 50% VT area, it can be noticed the derivatives fulfill the aforementioned stability criteria. The larger VT designs also fulfill the static stability criteria. Based on this realization, the VT area can be further reduced and the static stability criteria can still be fulfilled.

Showing that the all the VT designs fulfill the static stability criteria is an important result; however, figures 6.2 through 6.4 should be more closely examined. For nearly every lateral-directional S&C derivative, the value of the derivatives approaches zero as the Mach number is decreased, and the value of the derivatives may even change sign if the Mach number becomes low enough. This indicates the aircraft has relatively poor static stability at low Mach number. Based on this trend, one would expect that the dynamic stability of the aircraft designs deteriorates as the freestream Mach number is reduced.

It should be noted that the cause for the improvement in static stability as the freestream Mach number increases explained by the Prandtl-Glauert rule. The Prandtl-Glauert states the pressure coefficient for a

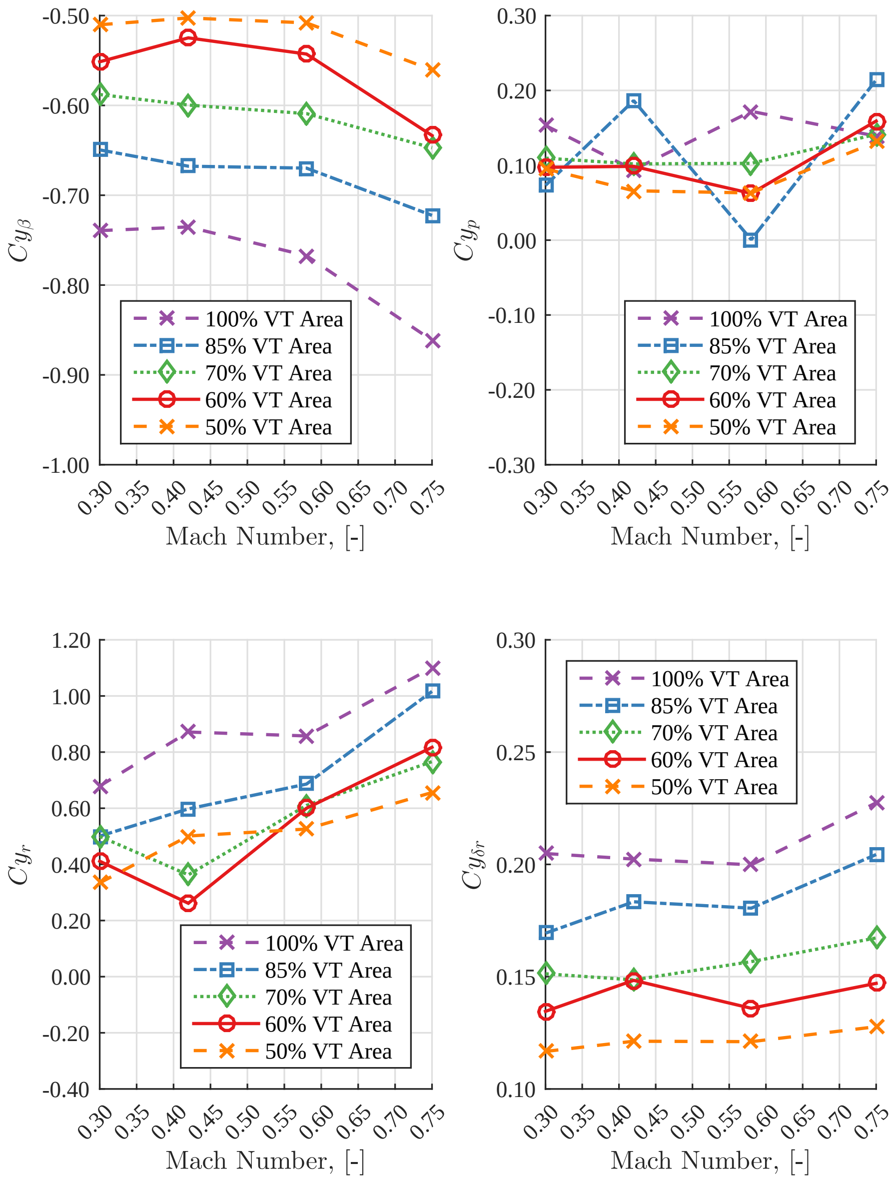

Figure 6.2: Fokker 100 stability and control derivatives with respect to sideforce, Cy, all VT designs

compressible flow, C_p, is related to the pressure coefficient of an incompressible flow, $C_{p,0}$ multiplied by a correction factor. The following equation demonstrates the Prandtl-Glauert rule:

$$C_p = \frac{C_{p,0}}{\sqrt{1 - M_\infty^2}} \tag{6.2}$$

Since all the VT designs meet the static stability criteria, it is beneficial to examine the dynamic stability of all the VT designs. The following section discusses the influence of the VT design on the aircraft's lateral-directional dynamic stability, and the discussion will be used to determine which VT designs provide acceptable S&C.

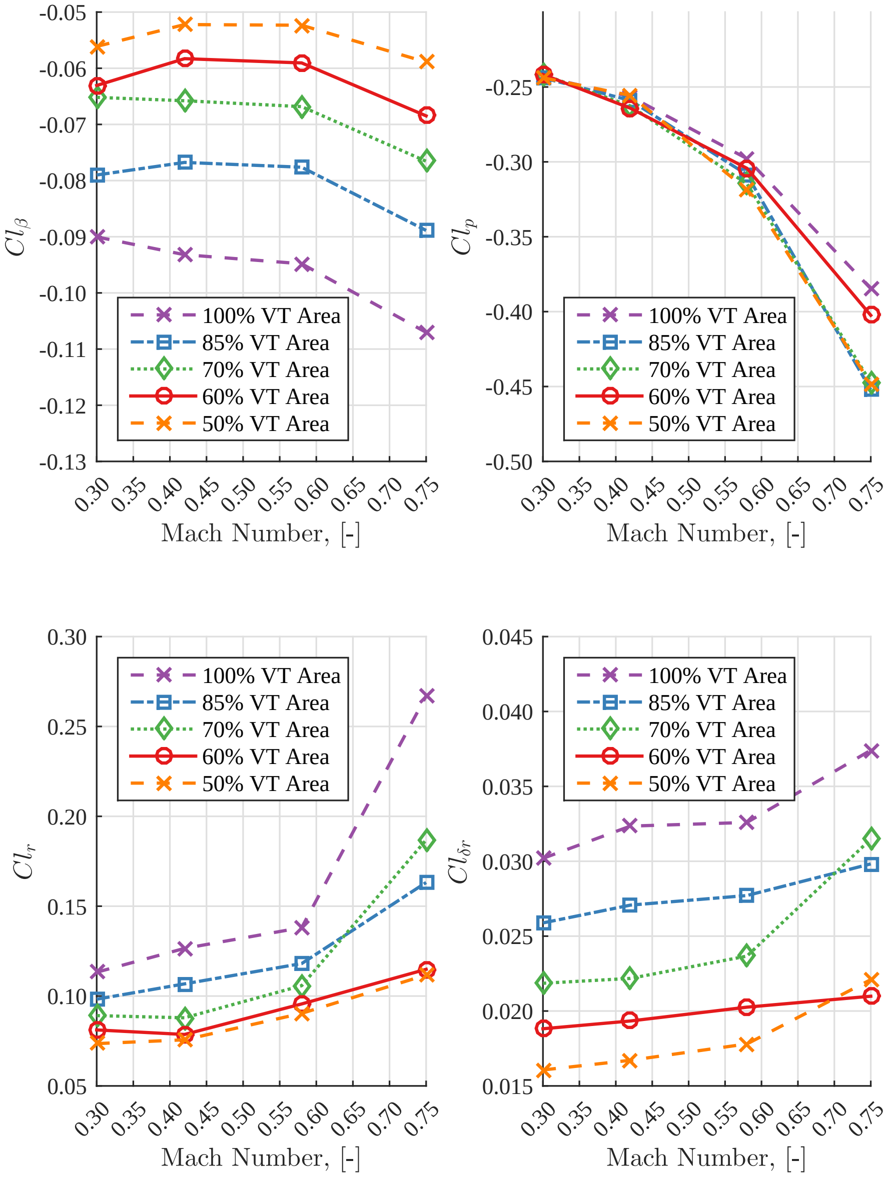

Figure 6.3: Fokker 100 stability and control derivatives with respect to rolling moment, Cl, all VT designs

6.4. DYNAMIC STABILITY

The aircraft's lateral-directional equations of motion are presented in equations 6.1a through 6.1c, and these equations can be used to analyze an aircraft's motion after a disturbance, such as a control deflection. To analyze an aircraft's dynamics, the aircraft must be perturbed around a reference flight condition. Many aircraft motions can be considered as small deviations from steady-level flight, and linearizing an aircraft's equations of motion around the steady-level flight condition is possible. Having linear equations of motion is beneficial, because it is possible to use analytical methods, including the Laplace-transform, to solve the equations of motion [35]. For steady-level flight, the following conditions are valid:

$$v_0 = 0; \quad w_0 = 0; \quad p_0 = 0; \quad q_0 = 0; \quad r_0 = 0$$

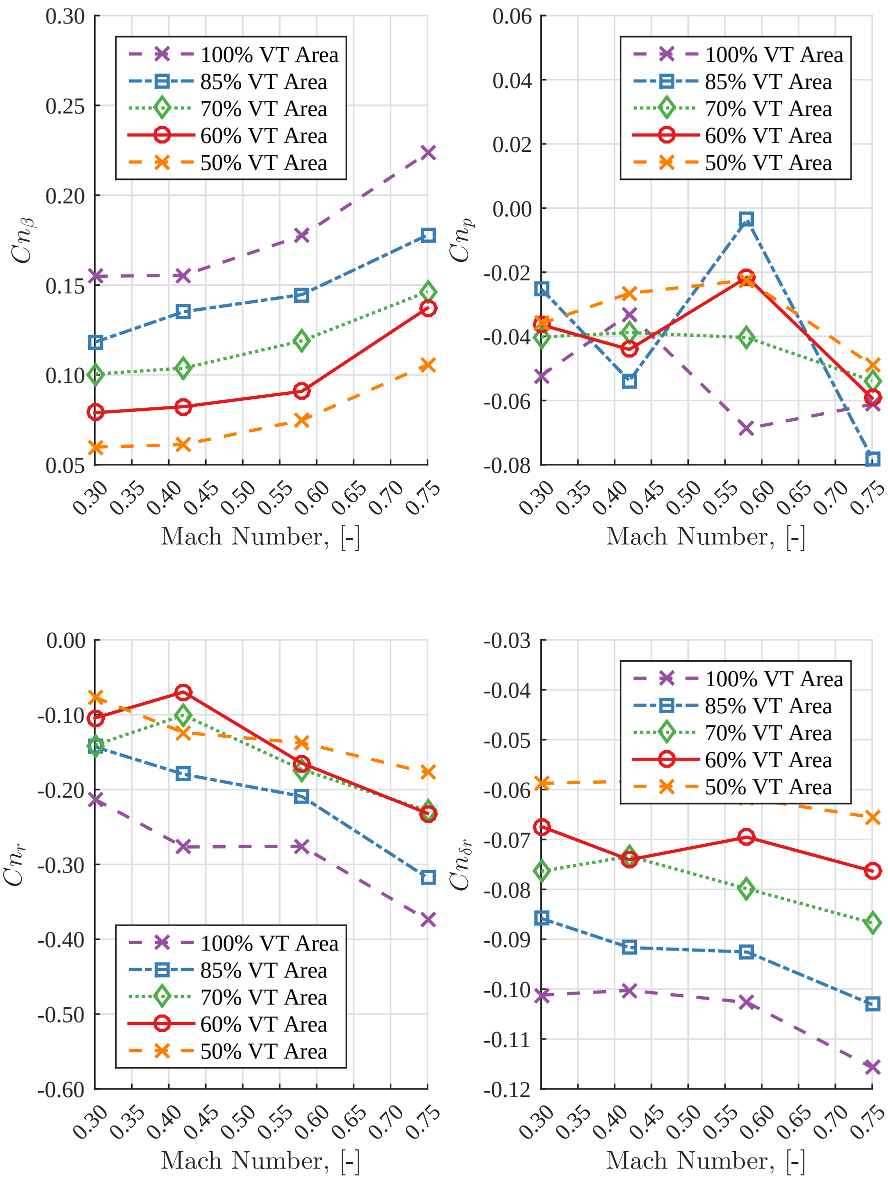

Figure 6.4: Fokker 100 stability and control derivatives with respect to yawing moment, Cn, all VT designs

For an aircraft slightly perturbed from a steady-level flight condition, the aircraft's linear and angular velocities are as follows:

$$
\begin{aligned}
u &= u_0 + \varepsilon u_1 \quad & v &= v_0 + \varepsilon v_1 \quad & w &= w_0 + \varepsilon w_1 \\
p &= p_0 + \varepsilon p_1 \quad & q &= q_0 + \varepsilon q_1 \quad & r &= r_0 + \varepsilon r_1
\end{aligned}
$$

Assuming the perturbations are small, such that $\varepsilon \ll 1$, the products of the perturbations could be approximated as zero. Once again, the perturbations must be small in order for the equations of motion to be linearized. By assuming small perturbation, equations 6.1 can be simplified to the following:

$$Y = \left(C_{y_\beta}\beta + C_{y_p}\frac{pb}{2u} + C_{y_r}\frac{rb}{2u} + C_{y_\delta}\delta\right)\overline{q}S + mg\sin\phi\cos\theta = m(\dot{v} + ru) \tag{6.3a}$$

$$\Sigma L = \left(C_{l_\beta}\beta + C_{l_p}\frac{pb}{2u} + C_{l_r}\frac{rb}{2u} + C_{l_\delta}\delta\right)\overline{q}Sb = I_{xx}\dot{p} - I_{xz}\dot{r} \tag{6.3b}$$

$$\Sigma N = \left(C_{n_\beta}\beta + C_{n_{T_\beta}}\beta + C_{n_p}\frac{pb}{2u} + C_{n_r}\frac{rb}{2u} + C_{n_\delta}\delta\right)\overline{q}Sb = I_{zz}\dot{r} - I_{xz}\dot{p} \tag{6.3c}$$

Through the use of equations 6.3, the lateral-directional dynamic stability and response can be analyzed. Before this analysis is examined, three modifications can be made which allow the physical characteristics of these equations to be better understood. First, the following geometrical relations should be realized.

$$p \approx \dot{\phi} \tag{6.4a}$$

$$r \approx \dot{\psi} \tag{6.4b}$$

$$v \approx u\beta \tag{6.4c}$$

$$sin\phi \approx \phi \tag{6.4d}$$

By using these relations, the lateral-directional equations of motion can be written in terms of β, ϕ, ψ.

It is also common to divide the side force equation by the aircraft's mass, m. This allows the terms in the side force equation to have units of linear acceleration. A similar process can completed by dividing the rolling and yawing moment equations by I_{xx} and I_{zz}, respectively. This allows the terms in the moments equations to have units of angular acceleration [34].

After dividing the lateral-direction equations of motion by their respective mass and inertia terms, new dimensional coefficients can be created. To illustrate the creation of the dimensional coefficients, an example will be provided. Consider the term $\frac{C_{n_\beta}\overline{q}Sb\beta}{I_{zz}}$ in equation 6.3c which can be rewritten as $N_\beta\beta$. Other dimensional coefficients can be created in a similar process, which results in the following equations:

$$Y_\beta\beta + Y_p\dot{\phi} + Y_r\dot{\psi} + Y_\delta\delta + g\phi\cos\theta = u\dot{\beta} + u\dot{\psi} \tag{6.5a}$$

$$L_\beta\beta + L_p\dot{\phi} + L_r\dot{\psi} + L_\delta\delta = \ddot{\phi} - \frac{I_{xz}}{I_{xx}}\ddot{\psi} \tag{6.5b}$$

$$N_\beta\beta + N_{T_\beta}\beta + N_p\dot{\phi} + N_r\dot{\psi} + N_\delta\delta = \ddot{\psi} - \frac{I_{xz}}{I_{zz}}\ddot{\phi} \tag{6.5c}$$

These dimensional coefficients and their magnitudes provide insight regarding the aircraft's lateral-direction stability. Consider the coefficient N_β. The meaning of this coefficient indicates the aircraft's yaw angular acceleration for unit change in the aircraft's sideslip angle [34]. For the other dimensional coefficients, a similar physical meaning can be discovered.

To solve the linearized equations of motion, it is possible to use the Laplace-transform. After applying the Laplace-transform and rearranging the equations of motion, so to have the terms associated with a control deflection on one side of the equation, the following equations are derived:

$$\left(sU - Y_\beta\right)\beta(s) - \left(sY_p + g\cos\theta\right)\phi(s) + s\left(U - Y_r\right)\psi(s) = Y_\delta\delta(s) \tag{6.6a}$$

$$-L_\beta\beta(s) + \left(s^2 - L_p s\right)\phi(s) - \left(s^2\frac{Ixz}{I_{xx}} + sL_r\right)\psi(s) = L_\delta\delta(s) \tag{6.6b}$$

$$-\left(N_\beta + N_{T_\beta}\right)\beta(s) - \left(s^2\frac{I_{xz}}{I_{zz}} + N_p s\right)\phi(s) + \left(s^2 - sN_r\right)\psi(s) = N_\delta\delta(s) \tag{6.6c}$$

Equations 6.6 can be divided by $\delta(s)$, which allows for the creation of the aircraft's open loop transfer functions $\frac{\beta(s)}{\delta(s)}$, $\frac{\phi(s)}{\delta(s)}$, and $\frac{\psi(s)}{\delta(s)}$. The equations can then be assembled into matrix format, and the transfer functions can be considered as variables which can be solved using matrix algebra.

$$\begin{bmatrix} (sU - Y_\beta) & -(sY_p + g\cos\theta) & s(U - Y_r) \\ -L_\beta & (s^2 - L_p s) & -\left(s^2 \frac{Ixz}{I_{xx}} + sL_r\right) \\ -\left(N_\beta + N_{T_\beta}\right) & -\left(s^2 \frac{I_{xz}}{I_{zz}} + N_p s\right) & (s^2 - sN_r) \end{bmatrix} \begin{pmatrix} \frac{\beta(s)}{\delta(s)} \\ \frac{\phi(s)}{\delta(s)} \\ \frac{\psi(s)}{\delta(s)} \end{pmatrix} = \begin{Bmatrix} Y_\delta \\ L_\delta \\ N_\delta \end{Bmatrix} \tag{6.7}$$

By taking the determinate of the matrix on the left and setting it equal to zero, the so-called characteristic equation is formed. The characteristic equation is a fourth order polynomial, and it takes the following form:

$$As^4 + Bs^3 + Cs^2 + Ds + E = 0 \tag{6.8}$$

The roots of the characteristic equation, called eigenvalues, determine the dynamic stability characteristics of the aircraft. For most aircraft, the solution to the characteristic equation reveals two real eigenvalues and one pair of complex eigenvalues. The real eigenvalues correspond to the aircraft's spiral mode and roll mode, and the complex eigenvalues correspond to the Dutch roll mode. Once these eigenvalues are known, the frequency behavior of the Dutch roll mode can be determined, and the time-constant behavior of the roll mode and spiral mode can be determined.

It has been shown that an aircraft has three separate lateral-directional dynamic modes. The three modes include the roll mode, spiral mode, and Dutch roll mode. Before the analysis of the lateral-direction dynamic modes is presented, a brief discussion about the impact of the aircraft's inertia on dynamic stability will be presented.

6.4.1. EFFECT OF INERTIA ON AIRCRAFT STABILITY

In order to analyze the aircraft's lateral-directional dynamic modes, the mass and inertia of the aircraft must be known. This poses a challenge in the present study, because the mass of the VT is unknown at this point, and a change in the VT mass will influence the aircraft's inertia. To determine the VT mass, a maneuvering and dynamic loads analysis must be completed, and these loads are influenced by the aircraft's inertia. There is clearly a mutual dependency between the aircraft's structural mass and the aircraft's dynamics.

To solve this problem, an iterative method should be used. Consider the dynamic analysis for the VT which has an area 70% of the original VT area. This VT design is shown in figure 4.2. The mass of the 70% VT area is unknown; however, one can assume the VT structural mass scales linearly with VT area. This would indicate the 70% VT area design would have a mass which is 70% of the original VT mass. In other words, there is a 30% mass reduction. As will be shown later, this assumption is not valid, but it allows for an acceptable first approximation of the VT mass. With this VT mass estimation, the aircraft's inertia can be updated, and the aircraft's maneuvering and dynamic load can be calculated. After the calculation of the VT loads is completed, the VT mass can be estimated, and the aircraft's inertia can be updated. The aforementioned process should be repeated until convergence of the VT mass is achieved.

This iterative process of determining the VT mass is theoretically correct; however, it is not practical for the conceptual aircraft design study being presented. Completing aircraft dynamics analysis, estimating VT loads, and estimating the VT weight is a time consuming process. For this reason, the iterative process was not used. The VT mass was assumed to scale linearly with area, and the aircraft dynamics and loads analysis was completed once for each VT design. The estimated VT mass using the load analysis results was not much different from the initial, guessed mass, and it was determined that a second iteration was not needed. This validity of this process will be readdressed when the results of the VT mass analysis are presented.

6.4.2. ROLL MODE

The roll mode is highly damped motion which tends to restore equilibrium to a rolling aircraft. As the aircraft rolls, the wing going down will have an increased angle of attack when compared to the relative angle of attack for flight without a roll rate. The increased angle of attack will result in an increase in lift. The opposite will occur for the wing going up. The restoring roll moment is caused by differential lift on the aircraft's wings.

The roll mode is highly dependent on the stability derivative Cl_p. The value of Cl_p is primarily influenced by the design of the wing, and it should not significantly change as the VT area is modified. The plot of Cl_p in figure 6.3 confirms this statement. For this reason, the change in stability derivatives resulting from the VT area reduction will likely not influence the aircraft's roll mode.

Reducing the VT's mass and increasing the engines' mass will slightly change the aircraft's inertia around the roll (longitudinal) axis. If the weight reduction of the VT redesign is equal to the weight addition of the TVFC system, then the aircraft's empty operational mass will remain constant and the inertia about the roll axis will decrease. This reduction in inertia can be understood by knowing the center of mass locations for the VT and engines. Table 6.1 shows the distance between the aircraft's roll axis and the center of gravity for the VT and engine. The VT center of mass is directly vertical of the roll axis, and this distance is represented by the variable $z_{VT,c.g.}$. The engine center of gravity has a slight vertical and lateral displacement relative to the roll axis, and these displacements are represented by $z_{eng,c.g.}$ and $y_{eng,c.g.}$. The VT is assumed to have a uniform mass distribution, and assumption was used to determine the VT's center of mass. The engine is assumed be a point mass and its center of gravity lies in the geometric center of the engine.

VT Area % of original	VT Mass [kg]	$z_{VT,c.g.}$ [m]	Engine Mass [kg]	$y_{eng,c.g.}$ [m]	$z_{eng,c.g.}$ [m]	Distance from engine center of gravity to roll axis, [m]
100	365.0	3.50	1628	1.20	2.80	3.05
85	310.3	3.34	1683	1.20	2.80	3.05
70	255.5	3.17	1738	1.20	2.80	3.05
60	219.0	3.05	1774	1.20	2.80	3.05
50	182.5	2.92	1811	1.20	2.80	3.05

Table 6.1: Distance between the aircraft's roll axis and the center of gravity for the VT and engines

The data in table 6.1 indicates that the VT mass is decreasing as the VT area is reduced. This causes the VT's center of mass to move closer to the roll axis. In order for the aircraft's empty operational mass to remain constant, the mass reduction of the VT is added to the engine. This indicates that the VT's mass is reduced and the engine's mass is increased. By comparing the center of mass location relative to the roll axis for the VT and engine, it can be seen that engine's center of mass is closer to the roll axis. By reducing the VT mass and increasing the engine mass, more mass will be located near the aircraft's roll axis. Since the aircraft's empty operational mass remains constant, the results in table 6.1 would indicate a reduction in the aircraft's moment of inertia about the x-axis when the VT mass is decreased and the engine mass is increased.

The impact of the change in moment of inertia on the aircraft's roll mode is shown in table 6.2. In this table, the aircraft's roll mode time constant, τ_{roll}, for the five VT designs at an altitude of 2000 m and four different Mach numbers.

	Roll Mode Time Constant, τ_{roll}			
VT Area % of original	2000 m Mach 0.30	2000 m Mach 0.42	2000 m Mach 0.58	2000 m Mach 0.75
100	1.51	1.13	0.77	0.59
85	1.52	1.13	0.75	0.54
70	1.56	1.11	0.76	0.56
60	1.56	1.13	0.77	0.59
50	1.60	1.20	0.76	0.53
Level 1 Handling Qualities: $\tau_{roll} \leq 1.4$				
Level 2 Handling Qualities: $1.4 \leq \tau_{roll} \leq 3.0$				
Level 3 Handling Qualities [59]: $3.0 \leq \tau_{roll} \leq 10$				

Table 6.2: Roll mode time constant for all VT designs. Empty operational mass and inertia.

When examining the data presented in table 6.2, the value of τ_{roll} changes slightly as the VT area is reduced; however, a trend which correlates the value of τ_{roll} to the reduction in VT area and mass is not readily recognized. This is because the change in moment of inertia around the roll axis is relatively small. The difference between the mass of the 100% VT area and 50% VT area is about 180 kg, and the movement of mass from the

VT to the engine relative to the roll axis is less than one meter. This statement is verified by the data presented in table 6.1. Simply adding fuel to the aircraft will have a more noticeable impact on the value of τ_{roll} when compared to impact of the VT mass reduction. Any differences in the value of τ_{roll} could also be caused by slight differences in the value of Cl_p for the various VT designs. Based on these realizations, the change in aircraft inertia caused by the VT mass reduction and engine mass increase can be considered as negligible for the current study.

It should be noted that the airworthiness requirements in reference [59] state that a light to medium transport aircraft should have a value of τ_{roll} of 1.4 or less. This criteria is reflective of level 1 flight qualities as specified within reference [59], which is formally known as MIL-STD-1797A. This document states that level 2 flight qualities are achieved if τ_{roll} is less than 2. Level 1 flight qualities indicate that the aircraft can be flown without causing large pilot workloads, and level 2 flight qualities indicate a slight increase in pilot workload and some degradation in flight qualities. With the relation between τ_{roll} and the aircraft's flight qualities understood, each of the five VT designs are considered to have adequate flight qualities with respect to the roll mode.

6.4.3. SPIRAL MODE

If an aircraft's directional stability, Cn_β, is strong compared to its lateral stability, Cl_β, then it is possible for an aircraft to have an unstable spiral mode. A divergent spiral mode occurs when the aircraft's directional stability aligns the aircraft with the relative freestream; however, the relatively weak dihedral effect is slow to restore lateral balance. Because of the yaw velocity induced by Cn_β, the wing on the outside of the yawing motion travels faster than the inside wing. This results in asymmetric lift, and aircraft's bank angle increases with outer wing moving up. While this occurs, the directional stability aligns the aircraft with the relative wind, and this forces the aircraft nose to a lower pitch attitude.

Redesigning the VT will impact both the aircraft's lateral and directional stability, and it will therefore impact the aircraft's spiral stability. It is common for aircraft to have an unstable spiral mode; however, the divergence of the spiral mode often occurs slowly. Due to the slow divergent nature of an unstable spiral mode, it acceptable to have some degree of spiral instability. Nonetheless, a criteria should be used to determine if an unstable spiral mode produces acceptable flight qualities. Typically, the criteria used to determine the acceptability of an unstable spiral mode is the spiral's time-to-double amplitude, T_2. If T_2 is greater than 20 seconds, then the aircraft is considered to have level 1 handling qualities [59].

The spiral stability for each of the five Fokker 100 designs was initially analyzed for various combinations of altitude and Mach number. The calculated value of T_2 varied significantly for each VT design and flight condition. An easily recognized correlation between the VT area and the spiral mode's T_2 was not found. Based on the physical explanation of the spiral mode, one can presume the VT area will impact the stability of the spiral mode, thus an alternative method should be used to determine how the VT area effects the spiral mode.

It is important to recognize the spiral mode generally has either negative damping or lightly positive damping. Due to the dynamic behavior of this mode, small errors and uncertainties in the S&C derivatives will influence the eigenvalue corresponding to the roll mode, and these errors may cause T_2 to vary significantly for the VT designs and flight conditions. In order to establish a correlation between the VT design and the spiral mode's T_2, a sensitivity analysis was completed. For the sensitivity analysis, the value of each lateral-directional stability derivative was increased by 10% while the values of the other stability derivatives were held constant, and the spiral mode's T_2 was the determined. This allows for the sensitivity of T_2 with respect to each lateral-directional stability derivative to be determined.

This sensitivity analysis was completed for the 100% VT area at an altitude of 0 meters and Mach 0.30. Table 6.3 displays the results of the sensitivity analysis. Note that negative values of T_2 represent a stable spiral mode.

In table 6.3, the first data line shows the T_2 value which has been calculated with the unmodified stability derivatives. This indicates the first data line contains the baseline T_2 value. For the other data lines, the value of a single lateral-directional stability derivative was increased by 10%, and the change in T_2 was determined.

VT Area & of original	Sensitivity Variable	% Change of Stability Derivative	Spiral Mode T_2, [s]
100	**-**	**-**	**-179**
100	Cl_β	+10	-69.4
100	Cn_β	+10	260
100	Cy_β	+10	-179
100	Cl_p	+10	-194
100	Cn_p	+10	-180
100	Cy_p	+10	-178
100	Cl_r	+10	295
100	Cn_r	+10	-63.4
100	Cy_r	+10	-177

Table 6.3: Spiral mode time to double amplitude sensitivity analysis. Altitude: 0 m, Mach 0.30, empty operational mass and inertia, empty operational mass and inertia

Based on the sensitivity analysis, one can see that T_2 is relatively sensitive to changes in Cl_β, Cn_β, Cl_r, and Cn_r. This conclusion can be established because T_2 changed significantly when the values of these stability derivatives were individually increased by 10%. In fact, increasing Cn_β and Cl_r by 10% caused T_2 to become positive, meaning the spiral mode became unstable. The other lateral-directional stability have a minor or negligible impact on the value of T_2. This result is not particularly surprising, because reference [35] states an aircraft's spiral mode will be stable if the following inequality is fulfilled:

$$Cl_\beta Cn_r - Cn_\beta Cl_r > 0 \tag{6.9}$$

Based on this inequality, one would expect that varying the values of Cl_β, Cn_β, Cl_r, and Cn_r would have a noticeable impact of the spiral mode's T_2.

With the aforementioned knowledge, a Monte Carlo simulation was completed to analyze the impact of Cl_β, Cn_β, Cl_r, and Cn_r on the value of T_2. The premise of the Monte Carlo simulation is that by simultaneously applying random errors to Cl_β, Cn_β, Cl_r, and Cn_r, a correlation between the VT area and T_2 can be discovered.

In table 5.1, the calculated values of Cl_β, Cn_β, Cl_r, and Cn_r had respective errors of 12.6%, 13.7%, 21.2% and 17.0% with respect to the reference values. Using this data, it was determined that a random error between -15% and +15% should be added to each of the lateral-directional stability derivatives which influence the value of T_2. The error added to each stability derivative is more representative of an uncertainty in the calculation of each stability derivatives. The uncertainty in the stability derivatives then manifests uncertainty in the calculation of T_2. These uncertainties are assumed to be the reason why a correlation between the VT area and spiral mode's T_2 is difficult to recognize.

For the Monte Carlo analysis, a random error was between -15% and +15% added to Cl_β, Cn_β, Cl_r, and Cn_r for each VT design. The other stability derivatives were unaltered. Note that the errors added to the stability derivatives were independent of each other. After the error was added to the stability derivatives, the value of T_2 was calculated. For example, errors of 8%, -2%, 13%, and 1% could be added to the values of Cl_β, Cn_β, Cl_r, and Cn_r, respectively, for each VT design. After the random error is applied, the value of T_2 can be calculated for each VT design. This process was completed 1,250 times at an altitude of 0 meters and Mach 0.30. Table 6.5 displays the results.

In table 6.5, the spiral mode's T_2 has been separated into four different categories. One category is for T_2 values less that 20 seconds. This would indicate the aircraft has unacceptable spiral mode flight qualities according to reference [59]. One category represents T_2 values which are negative, and this indicates a stable spiral mode. The other two categories represent unstable spiral modes as well as how 'fast' the aircraft is estimated to enter a spiral.

Since a Monte Carlo analysis was used to create figure 6.5, the y-axis shows the percent of Monte Carlo analyses each VT design produced a specific T_2 value. An example will be provided to clarify this plot and explana-

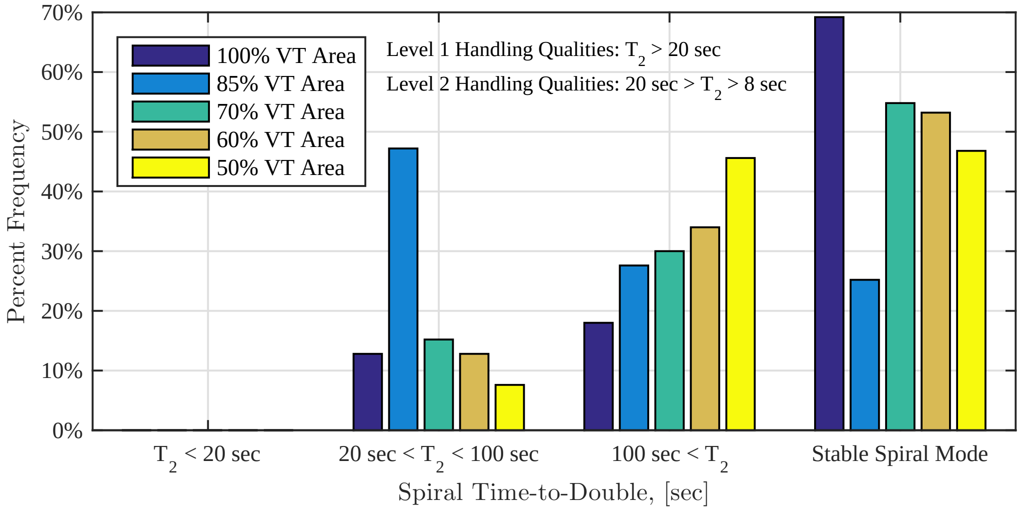

Figure 6.5: Monte Carlo analysis of the spiral time to double amplitude. Altitude: 0 m, Mach 0.30, empty operational mass and inertia.

tion. Consider the data displayed for the original, 100% VT area. It can be seen that for the stable spiral mode, nearly 70% of the 1,250 Monte Carlo simulations resulted in a stable spiral mode, and slightly under 20% of the simulation resulted in an unstable spiral mode having a T_2 value greater than 100 seconds. With the 100% VT area, one can be quite confident that this Fokker 100 aircraft will have either a slow divergent spiral more or a stable spiral mode.

When comparing the T_2 data for the five different VT designs, some trends are noticeable. Firstly, note that all VT designs are either stable or have a T_2 value greater than 20 seconds. This indicates that every VT design has acceptable spiral mode behavior. Now examine the stable spiral mode data. As one can see, as the VT area is reduced, the percent frequency the VT design produces a stable spiral mode decreases. This indicates the 100% VT area is the VT design most likely to produce a stable spiral mode. This also indicates a reduction in VT area will likely worsens the aircraft's spiral behavior. Although the spiral mode's behavior worsens as the VT area is reduced, this is not a major concern since a majority of the Montro Carlo simulations resulted in a stable or relatively slow divergent spiral mode for each VT design.

In table 6.3, it can be seen that the 85% VT area produces the worst spiral mode behavior of all VT designs. The possible cause for this behavior may be shown in the S&C derivatives plots shown in figures 6.3 and 6.4. In particular, examine the plots of Cl_β, Cn_β, Cl_r, and Cn_r at a Mach number of 0.30. For each of the plots, a noticeable correlation between the VT area and the value of the stability derivatives can be recognized, and this correlation is expected. However, special attention should be given to the plot of Cn_r. When examining the data plotted at Mach 0.30, it can be seen that the value of Cn_r for the 85% VT area possibly has a large error . Based on the trend of the data, the value of Cn_r should likely be in between the values of Cn_r corresponding to the 70% and 100% VT areas. This is expected to be the cause of the relatively poor spiral behavior for the 85% VT area.

Lastly, it is important to remember the spiral stability analysis has be presented for the empty operational mass and corresponding inertia aircraft configuration. It is important to consider how this spiral mode will be affected if the aircraft's inertia is increased. By increasing the aircraft's inertia the aircraft will resist a change in motion, meaning the an increase in inertia causes the aircraft to resist entering a spiral. One would expect that an increase in inertia is accompanied by an increase in T_2; therefore, an increase in inertia is beneficial when analyzing the aircraft's spiral stability.

To summarize this section, the spiral mode behavior is sensitive to the stability derivatives Cl_β, Cn_β, Cl_r, and Cn_r. Reducing the VT area will impact the value of these four derivatives; therefore, the spiral mode behavior of the aircraft will be impacted by the design of the VT. Reducing the VT area will likely worsen the spiral mode behavior of the aircraft; however, the spiral mode stability for all five VT designs is deemed as acceptable.

Analyses have been completed for the roll and spiral modes. Based on these analyses, each of the five different Fokker 100 designs have been shown to demonstrate acceptable roll and spiral stability behavior. Now it is beneficial to examine how the VT design impacts the aircraft's Dutch roll stability.

6.4.4. DUTCH ROLL MODE

A dynamic mode which is highly by an aircraft's VT design is the Dutch roll. The Dutch roll mode is an oscillatory dynamic mode where an aircraft yaws and rolls in an out-of-phase sequence. This motion is due to the coupling of the aircraft's lateral and directional stability, and it is highly undesirable from an aircraft handling viewpoint. The VT is the primary contributor to the damping and stability of the Dutch roll motion. Reducing the VT size will cause the Dutch roll damping ratio, ζ_{DR} to decrease, which indicates the motion is becoming less stable.

To analyze the Dutch roll damping, full order, nonlinear simulations of the aircraft's dynamics were completed. It is important to know that if the ζ_{DR} becomes negative, then the Dutch roll motion is unstable. Figure 6.6 shows the results of the Dutch roll simulations. In the figure, lines are plotted for each of the VT designs which indicate ζ_{DR} is equal to zero. In dynamic stability terms, a damping ratio equal to zero indicates neutral stability.

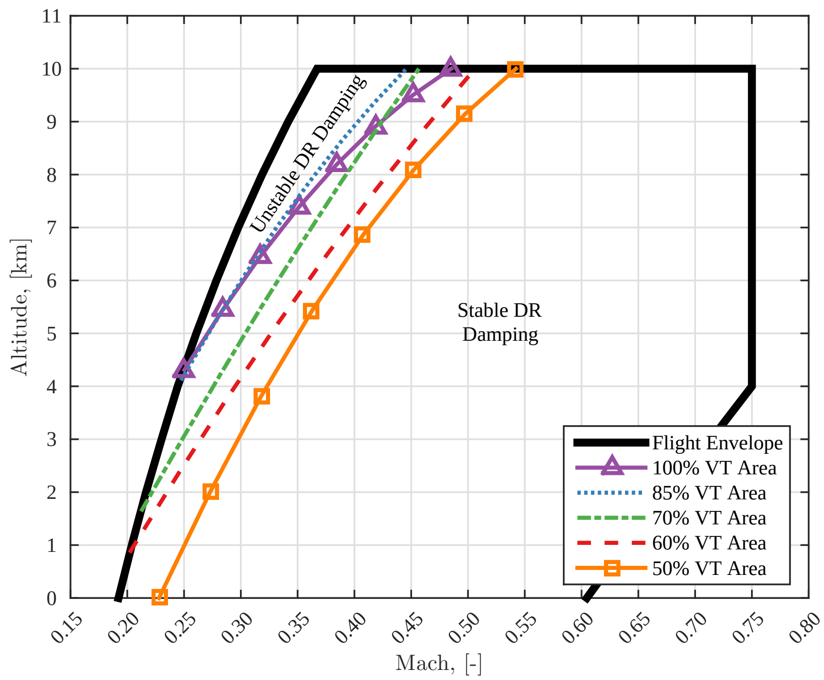

Figure 6.6: Fokker 100 Dutch roll damping ratio isobars for $\zeta_{DR} = 0$. Empty operational mass and inertia.

In the figure, the area left of each plot line indicates ζ_{DR} is less than zero, which means the Dutch roll mode is unstable in that portion of the flight envelope. For the original Fokker 100 design with the 100% VT area, the Dutch roll motion is only unstable at altitude above 4,000 m and near the aircraft's stall boundary. This particular area is outside of Fokker 100's typical operating conditions since it is close to the stall boundary and at altitudes which are greater than typical takeoff and landing altitudes. Since the unstable area it is not within typical operating conditions, it is not of major concern; however, the aircraft should not enter within that area of the flight envelope.

When examining figure 6.6, the line indicating the Dutch roll stability boundary moves deeper into the aircraft's flight envelope as the VT area is reduced, and flight conditions near the aircraft's stall boundary become unstable. For 50% VT area, there is an unstable Dutch roll mode at every altitude. This is particularly undesirable, because the aircraft's typical takeoff, climb, and landing flight conditions would have an unstable Dutch roll mode. For airports with altitudes above 1,000 meters, the 60% VT area and possibly the 70% VT area are predicted to have an unstable Dutch roll mode during takeoff and landing.

It should be reiterated that the stall boundary was selected calculated using a clean aircraft configuration. If high lift devices are used, then the stall boundary for the Fokker 100 will likely occur at a lower Mach numbers than the stall boundary indicated in figure 6.6. This indicates that low speed Dutch roll stability remains a concern for the 50% and 60% VT area designs. For this reason, these two VT designs will be considered as unacceptable designs. The 70% VT design has questionable Dutch roll stability at flight conditions corresponding to high altitude takeoff and landing, but other analyses will be completed before the 70% VT area is considered as an unacceptable design.

It is important for an aircraft to have a stable Dutch roll mode; however, poor Dutch roll damping can result in an aircraft design with undesirable flight characteristics. According to MIL-F-8785C, reference [59], a light to medium transport aircraft should have a value of ζ_{DR} greater than 0.08 in order for an aircraft to have level 1 flight qualities. Level 1 flight qualities indicate the aircraft can be flown without a large pilot workload. In figure 6.7, lines are plotted for each VT which correspond to expected ζ_{DR} values of 0.08. Areas of the flight envelope to the right of the lines indicate the Fokker 100 is expected to have ζ_{DR} values greater than 0.08 and level 1 flight characteristics.

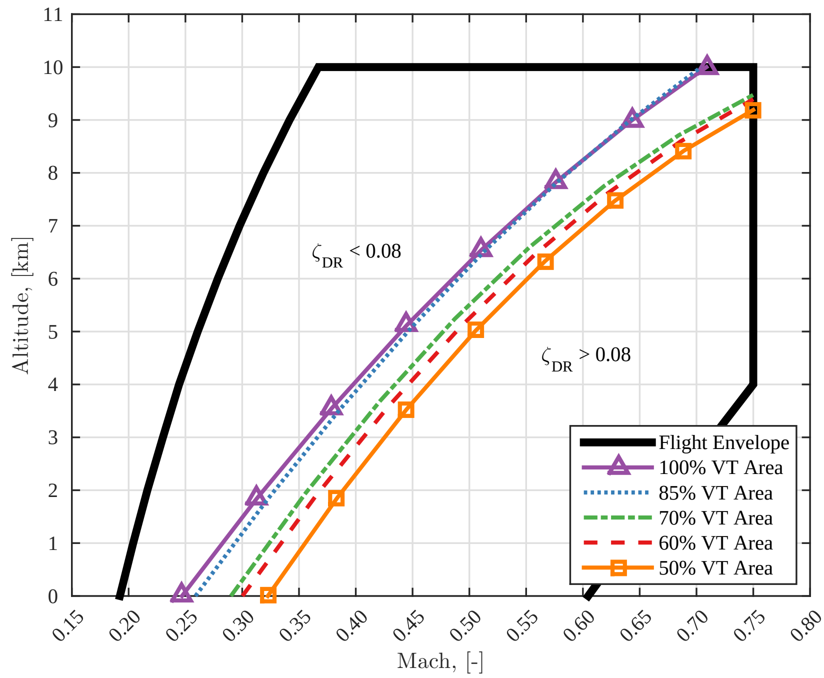

Figure 6.7: Fokker 100 Dutch roll damping ratio isobars for $\zeta_{DR} = 0.08$. Empty operational mass and inertia.

One important result which can be drawn from figure 6.7 is related to the Dutch roll damping coefficient during the aircraft's cruise condition. For a CTA, majority of its flight time is spent at cruise flight conditions, which is typically the upper right portion of the flight envelope. For both the 100% and 85% VT area, the upper right portion of the flight envelope has level 1 flight qualities with respect to the Dutch roll damping coefficient. It should be noted that the other VT designs can be equipped with artificial stability augmentation systems, such as a yaw damper, to improve the Dutch roll damping at cruise conditions. The concept of artificial stability will be discussed at a later point.

Now the Dutch roll frequency, ω_{DR} will be examined. For ω_{DR}, there are no strict requirements enforced within the Federal Aviation Requirements part 25 reference [58], which is used to assess the airworthiness of CTA; however, MIL-F-8785C, reference [59], provides requirements for ω_{DR}. In reference [59], a light to medium transport aircraft with a ω_{DR} greater than 0.4 rad/s is considered to have level 1 handling qualities. Values of ω_{DR} lower than 0.4 rad/s would produce level 3 handling qualities. Reference [31] also provides recommended values for ω_{DR}. According to this reference, the best level of ω_{DR} is between 1.8 and 2.3 rad/s. Now the value of ω_{DR} will be analyzed for the various VT designs.

In figure 6.8, isolines are plotted corresponded to ω_{DR} values equal to 0.4 rad/s. The areas to the right of the isolines indicates ω_{DR} is greater than 0.4 rad/s. No line for the 100% VT area is displayed, because ω_{DR} is greater than 0.4 rad/s at every point within the flight envelope. When examining the figure, the 60% and 50% VT areas have poor predicted Dutch roll frequencies in large sections of the flight envelope. The 60% and 50% VT area designs have already been shown to have unacceptable Dutch roll damping, and the Dutch roll frequency further confirms that these two VT designs produce poor Dutch roll stability. The 70% VT area also has relatively poor predicted Dutch roll frequency behavior; however, a deeper analysis of ω_{DR} for the various VT designs will be completed.

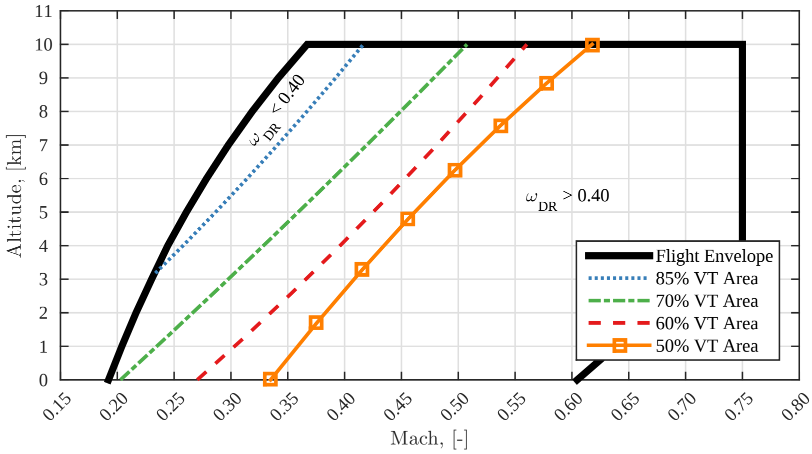

Figure 6.8: Fokker 100 Dutch roll frequency isobars, for ω_{DR} = 0.4 rad/s. Empty operational mass and inertia.

According to reference [31], the best level of ω_{DR} is between 1.8 and 2.3 rad/s; however, all flight conditions within the Fokker 100's flight envelope have a Dutch roll frequency less than 1.8 rad/s. This occurs for all VT designs. Using airworthiness criteria established in reference [31], the Fokker 100 has unacceptable predicted flight qualities with regards to the Dutch roll frequency. With this realization, it is beneficial to examine how the Dutch roll frequency impacts a pilot's opinion regarding the handling qualities of an aircraft.

In reference [31], multiple pilots used flight simulations to analyze the handing qualities of general aviation aircraft with various Dutch roll damping ratios and frequencies. For flight simulations with low Dutch roll frequencies, pilots claimed the aircraft had low directional stability, which resulted in poor heading control, large sideslip excursions, and roll and yaw trim problems. This comment is logical since Cn_{β}, the stability derivative most representative of directional stability, is strongly affected by the VT area. Based on these pilot comments, a method which may be used to improve the Dutch roll stability of the various aircraft designs, namely a yaw damper, will be discussed. Before this is completed, a summary of the dynamic stability up to this point will be given

An analysis of the Fokker 100's static and dynamic stability was presented. All the VT designs have been shown to have static stability and adequate flight qualities for the roll and spiral modes. In regards to the Dutch roll motion, the Fokker 100 designs with the 60% and 50% VT areas were shown to have poor predicted Dutch roll stability, and they are considered as unacceptable aircraft designs. The 70% area had questionable Dutch roll stability; however, additional analyses will be completed for the 70% VT area before it is considered to be an unacceptable design. For the 85% VT area, no major problems with the lateral-directional stability have been identified which would result in an unacceptable aircraft design. At this point, a compromise between the 85% and 70% VT area would likely produce an acceptable compromise between VT area and Dutch roll flight characteristics; however, the aircraft design would need to be equipped with a yaw damper to improve the Dutch roll flight characteristics at low altitudes and Mach numbers. Now the concept of yaw dampers will be introduced to see if the Dutch roll stability of the Fokker 100 can be improved.

6.5. YAW DAMPER

If the aircraft's trimmed flight condition is perturbed, then the perturbation may induce a yaw rate. The aircraft's directional stability is required to dampen the yaw rate; however, it has been demonstrated that an aircraft's lateral and directional stability are coupled. Due to the perturbation induced yaw rate, the aircraft will begin the Dutch roll motion [34]. One of the functions of the VT is to dampen the Dutch roll motion.

It has been shown that the aircraft's Dutch roll damping and frequency deteriorate as the VT area is reduced. In order for an aircraft to have level 1 handling qualities, which are associated with low pilot workloads and pleasant flight characteristics, the Dutch roll damping ratio and frequency should be greater than 0.08 and 0.4 rad/s, respectively [59]. To ensure the Dutch roll flight characteristics don't deteriorate to a level which makes the aircraft unflyable, an automatic flight control system, in the form of a yaw damper, should be designed for the aircraft. The design of a yaw damper is outside of the scope of the presented thesis research; however, the impact of the VT design on the Dutch roll motion and the necessity of a yaw damper will be briefly discussed.

If an aircraft is equipped with a yaw damper, its Dutch roll motion can be artificially damped through the deflection of the rudder. The yaw damper is equipped with a sensor that is designed to detect yaw rates. Through the sensing of the yaw rate, the control system can automatically deflect the rudder to dampen the Dutch roll motion [34].

One of the problems associated with reducing the VT area is the associated reduction in the aircraft's Dutch roll frequency. In reference [31] pilots associated poor heading control with low Dutch roll frequencies. This indicates that the reduction in Dutch roll frequency resulting from the reduction in VT area will worsen an aircraft's handling qualities. From a control systems viewpoint, the reduction Dutch roll frequency may be considered beneficial.

According to reference [32], the phase lag of a closed-loop control system increases as the frequency of the Dutch roll motion increases. The term 'closed-loop control system' indicates that the aircraft's yaw rate is sensed, and the the sensed yaw rate is fedback to a controller which sends control inputs to the rudder. The term lag is related to the delay between a control surface deflection and a control input. The first statement indicates that an increase in Dutch roll frequency necessitates an increase in the control system's frequency. It becomes more challenging to design a control system as its frequency requirements increase; therefore, it is beneficial to have a low frequency Dutch roll motion [32].

To summarize this section, the reduction in VT area results in a reduction of Dutch roll damping, and this reduction in Dutch roll damping necessitates the design of an automatic control system in the form of a yaw damper. The reduction in VT area also results in a reduction in the Dutch roll frequency, and this reduction in Dutch roll frequency is desirable from a control system design viewpoint.

In order to verify the feasibility of an aircraft designed with TVFC and an unconventionally small VT, a yaw damper must be designed. After a yaw damper is designed, the Dutch roll characteristics of the aircraft should be reassessed to ensure it has adequate flight qualities. A recommendation for future research is to have a yaw damper designed for each of the aircraft designs having a reduced VT area.

6.6. CONTROL EFFECTIVENESS RATIO

It has been mentioned the TVFC is expected to demonstrate its usefulness in low dynamic pressure flows, which is an area of the flight envelope where the effectiveness of aerodynamic control surfaces is reduced. This concept was demonstrated in figure 2.7 where the dimensional yawing coefficient for the rudder and TVFC was shown for an F-16 at sea level. In the figure, it shown that the TVFC had the larger dimensional yaw coefficient of the two control methods at Mach numbers below Mach 0.3 and sea level flight conditions.

The thrust vectoring proved to be an effective form of control for the F-16 at low Mach numbers; however, the effectiveness of the thrust vectoring must be demonstrated for the Fokker 100 and Tay 650 engine. To demonstrate the effectiveness of thrust vectoring a variable called the control effectiveness ratio, ξ, will be introduced. The control effective ratio is defined as follows:

$$\xi = \frac{\frac{\partial Cn}{\partial \delta_{TVFC}}}{\frac{\partial Cn}{\delta_r}} = \frac{Cn_{\delta_{TVFC}}}{Cn_{\delta_r}} \tag{6.10}$$

The physical meaning of the control effectiveness ratio is to determine which produces the larger yawing moment, either TVFC or the rudder, for a given control deflection angle. If the ratio is greater than one, then the thrust vectoring is more effective in creating a yawing moment than the rudder.

TVFC can be used during normal all-engines-operative (AEO) flight conditions as well as OEI flight conditions. For this reason, multiple control effectiveness ratios will be defined. ξ_{AEO} corresponds to the control effectiveness ratio when both of the Fokker 100 engines are used to produce a yawing moment, and ξ_{OEI} corresponds to the control effectiveness ratio when only one engine is used to produce a yawing moment.

Now that the definition and physical meaning of the control effectiveness ratio have been provided, it is beneficial to examine how this ratio varies within the aircraft's flight envelope. In figures 6.9 and 6.10 the control effectiveness ratio is plotted for the AEO and OEI flight conditions, respectively. In these figures, the control effectiveness ratio is calculated using the 100% VT area. The control effectiveness ratio was calculated for trimmed thrust flight condition. If a throttle setting is used which is greater than the trimmed thrust throttle setting, then it is possible to increase $Cn_{\delta_{TVFC}}$. This indicates that it is possible for ξ to be greater than the values shown in figures 6.9 and 6.10.

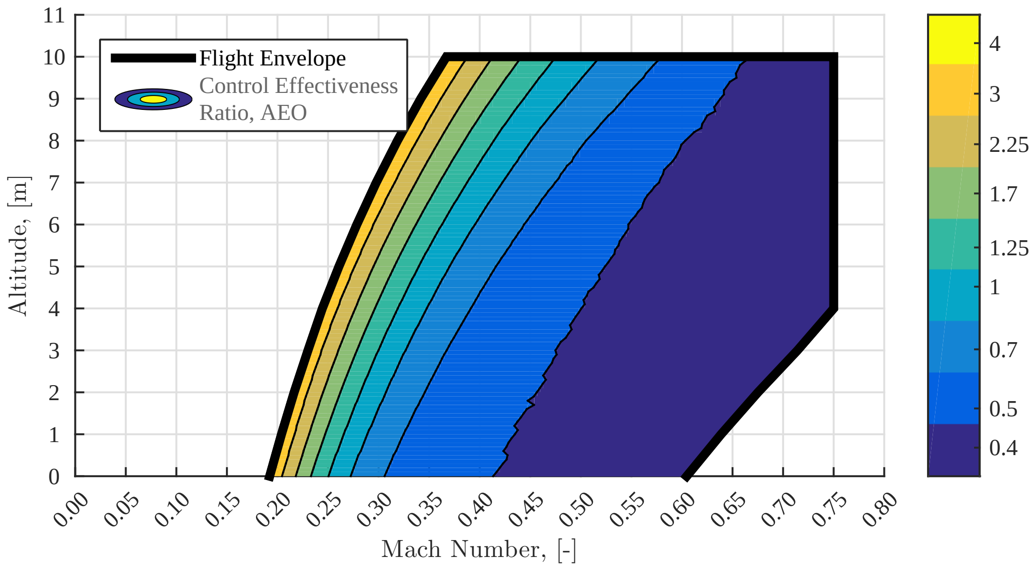

Figure 6.9: Control effectiveness ratio for all-engines-operative, trimmed thrust flight condition.

When examining figures 6.9 and 6.10, one may notice the two figures are quite similar. This is because ξ_{OEI} is half of ξ_{AEO}. Only one figure is required in order for to determine the control effectiveness ratio for both AEO and OEI flight conditions; however, multiple plots are generated for improved clarity and understanding.

From an examination of figure 6.9, it can be seen that ξ_{AEO} has a value greater than one near the flight envelope's stall boundary. This indicates that for a given control deflection angle, thrust vectoring produces a yawing moment larger than the rudder. The area of the flight envelope where ξ_{AEO} is greater than one is small; however, TVFC has shown to be an effective form of control in low dynamic pressure flows.

It should also be noted that ξ_{OEI} is greater than one in a small area of the flight envelope. This is important to notice since the thrust vectoring will be used provide trim yawing moments during OEI flight. At this point, using TVFC for trim during OEI conditions remains as a feasible idea. Now the OEI trim condition will be analyzed, and this will demonstrate or disprove the feasibility of using TVFC as a form of control during OEI flight.

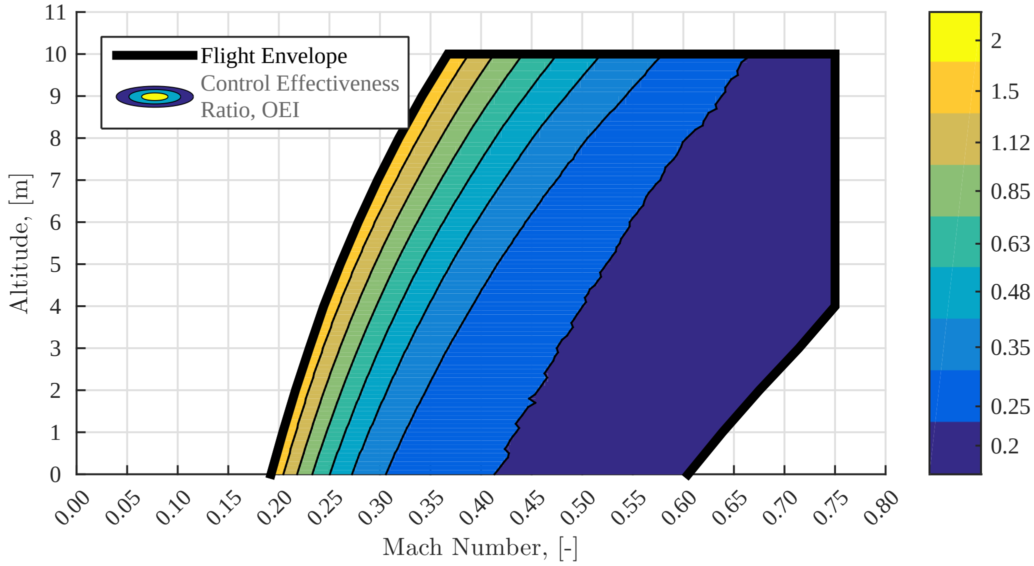

Figure 6.10: Control effectiveness ratio for one-engine-inoperative, trimmed thrust flight condition.

6.7. ONE-ENGINE-INOPERATIVE TRIM, BASELINE AIRCRAFT

It has been demonstrated that thrust vectoring can be an effective form of directional control in low dynamic pressure flows. One of the main research objectives is to demonstrate or disprove the feasibility of using TVFC during the occurrence of OEI flight conditions. This topic will now be discussed, but first it is important to reexamine the lateral-directional equations of motion.

The lateral-directional equations of motion are shown in equation set 6.1. In order to complete to OEI trim analysis, these equations must be adapted to reflect the trimmed flight condition.

In order for an aircraft to achieve the steady-state, trimmed flight condition, all aircraft accelerations, both linear and rotational, must equal zero. Additionally, the aircraft's rotational velocities must equal zero. Note that steady-state, trimmed flight does not require for linear velocities to be equal to zero. When the aircraft's linear accelerations, rotational accelerations, and rotational velocities are equal to zero, the lateral-directional equations of motion may be rewritten as follows:

$$Cy_\beta\beta + Cy_{\delta_a}\delta_a + Cy_{\delta_r}\delta_r + Cy_{\delta_{TVFC}}\delta_{TVFC} + mg\sin\phi\cos\theta = 0 \tag{6.11a}$$

$$Cl_\beta\beta + Cl_{\delta_a}\delta_a + Cl_{\delta_r}\delta_r + Cl_{\delta_{TVFC}}\delta_{TVFC} = 0 \tag{6.11b}$$

$$Cn_\beta\beta + Cn_{T_\beta}\beta + Cn_{\delta_a}\delta_a + Cn_{\delta_r}\delta_r + Cn_{\delta_{TVFC}}\delta_{TVFC} = 0 \tag{6.11c}$$

In the initial presentation of the equations of motion, the stability derivatives Cy_δ, Cl_δ, and Cn_δ were used to represent the sideforce, roll moment, and yaw moment for a given control deflection angle. In the equation set 6.11, these stability derivatives were expanded to denote the individual contributions of the aileron, rudder, and TVFC deflection angles to the aircraft's sideforce, rolling moment, and yawing moment.

Two final modifications will be made to the steady-state, lateral-directional equations of motion presented in the equation set 6.11. The first modification will replace $mg\cos\theta$ with the aircraft's lift coefficient, C_L. The other modification is made to the stability derivative Cn_{T_β}. This contribution of this stability derivative can be assumed to have a negligible contribution on the aircraft's yawing moment; however, it is important to recognize that the aircraft's engines produce a non-negligible yawing moment during the OEI flight condition. This allows for the the stability derivative Cn_{T_β} to be replaced with the stability derivative Cn_T, where Cn_T represents the yawing moment coefficient produced by the engines during the OEI flight condition. After these two modifications, the steady-state, lateral-directional equations of motion can be written as follows:

$$Cy_{\beta}\beta + Cy_{\delta_a}\delta_a + Cy_{\delta_r}\delta_r + Cy_{\delta_{TVFC}}\delta_{TVFC} + C_L\phi = 0 \tag{6.12a}$$

$$Cl_{\beta}\beta + Cl_{\delta_a}\delta_a + Cl_{\delta_r}\delta_r + Cl_{\delta_{TVFC}}\delta_{TVFC} = 0 \tag{6.12b}$$

$$Cn_{\beta}\beta + Cn_T + Cn_{\delta_a}\delta_a + Cn_{\delta_r}\delta_r + Cn_{\delta_{TVFC}}\delta_{TVFC} = 0 \tag{6.12c}$$

Equations set 6.12 can be used to trim an airplane; however, there are three equations and five unknown variables (β, ϕ, δ_a, δ_r, δ_{TVFC}). This indicates that equation set 6.12 is underdetermined, and an infinite amount of trim conditions exist. Clearly there is a dilemma when attempting to solve these equations of motions.

In order to solve this equation set, two of the unknown variables must be fixed. One of the variables which can be fixed is β. The aircraft's sideslip angle strongly impacts the aircraft's drag and required trim thrust. During the OEI flight condition, the operative engine will be operating near its fullest capacity. Any unnecessary drag contributions should be avoided. This indicates that β should be set equal to zero in order to avoid the drag increase caused by a sideslip angle. In the following OEI trim analyses, β is set equal to zero.

By setting β equal to zero, there are now four unknown variables and three equations. This still presents an infinite amount of possible trim solutions; however, by varying δ_{TVFC}, the impact of using thrust vectoring to trim the aircraft can be recognized. For example, δ_{TVFC} can be set equal to zero, and this would correspond to the trim condition of the baseline Fokker 100 which does not have thrust vectoring capabilities. By increasing δ_{TVFC}, the aircraft's OEI trim condition will change. This indicates that ϕ, δ_a, and δ_r will change when thrust vectoring is used to trim the aircraft, and the impact of thrust vectoring on the aircraft's trim condition can be recognized. By using the aforementioned knowledge, the OEI trim analysis can be completed.

In order to demonstrate the impact of thrust vectoring on the aircraft's trim condition, the concept of an aircraft's OEI flight envelope will be introduced. The OEI flight envelope corresponds to flight conditions where the aircraft can achieve trimmed flight after an engine failure. Typically the boundaries of the OEI flight envelope are determined when either the aircraft's maximum rudder deflection angle, stall angle, or maximum allowable thrust is reached. Using this knowledge, the OEI flight envelope for the 100% VT area has been determined for nozzle deflection angles, δ_{TVFC}. The results are shown in figure 6.11.

From an examination of figure 6.11, it can be seen that increasing δ_{TVFC} reduces the area of the OEI flight envelope. The cause for this reduction in OEI flight envelope is due to engine limitations. As the thrust vectoring nozzle is deflected, the engine's axial thrust is reduced. To account from this loss in axial thrust, the engine's throttle must be increased in order to maintain the steady-state flight condition. If the engine is already operating at its peak performance, then it is not possible for the engine's throttle to be increased. This is the cause for the change in the aircraft's OEI flight envelope as δ_{TVFC} is increased. It should also be noted that thrust losses are caused by the thrust vectoring, and these losses will impact the OEI flight envelope as well.

There is another peculiarity in the data presented in figure 6.11. As δ_{TVFC} is increased, the left boundary of the OEI flight envelope changes. For the flight envelope corresponding to all-engines-operative flight condition, this boundary is typically determined by the aircraft's stall behavior. For the OEI flight envelope, it may not be possible to achieve trimmed flight near the aircraft's stall boundary. This occurs because the aircraft would have to fly on the backside of the power curve in order to achieve trimmed flight near the stall boundary. In order to demonstrate the meaning of the phrase "backside of the power curve", figure 6.12 will be used.

In figure 6.12, the typical behavior of an aircraft's induced drag and parasite drag is plotted as a function of velocity. By summing the induced drag and parasite drag, an estimate of the aircraft's total drag can be determined. Notice there is a velocity where the total drag is minimized. If an aircraft achieves trimmed flight at a velocity which is less than the velocity were drag is minimized, then the aircraft is said to be flying on the backside of the power curve. The reason the left boundary of the OEI flight envelope changes is because the single operative engine cannot produce enough thrust to achieve trimmed flight on the backside of the power curve. Physically, trimmed flight on the backside of the power curve represents a speed instability; however, it is a feasible trimmed flight condition.

The effect of using TVFC on the Fokker 100's flight envelope has been analyzed, but the OEI trim condition must be further analyzed. To trim the aircraft, the three steady-state, lateral-directional equations of motion

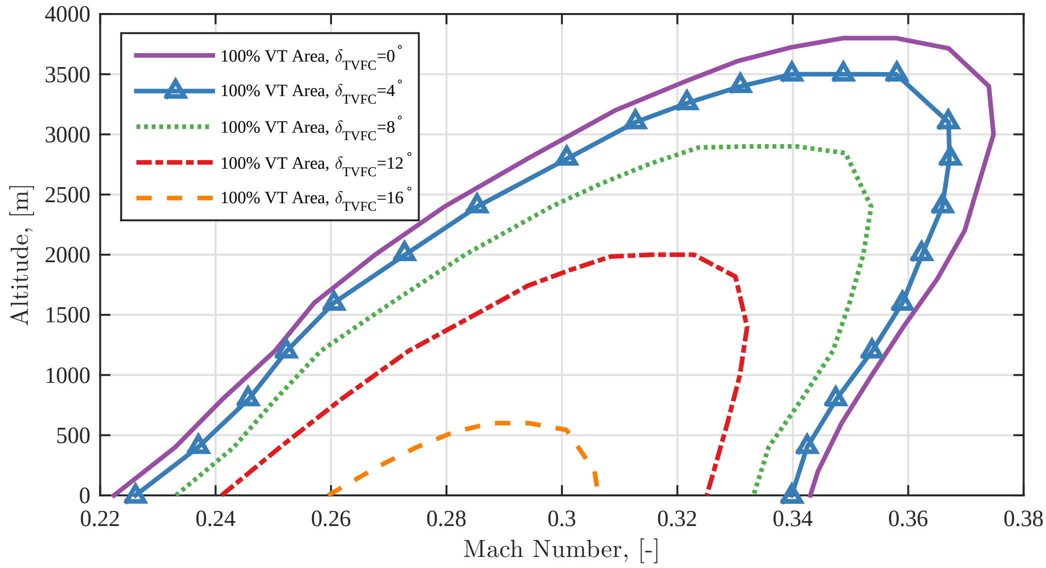

Figure 6.11: OEI envelope for the Fokker 100 with 100% VT area and various δ_{TVFC}

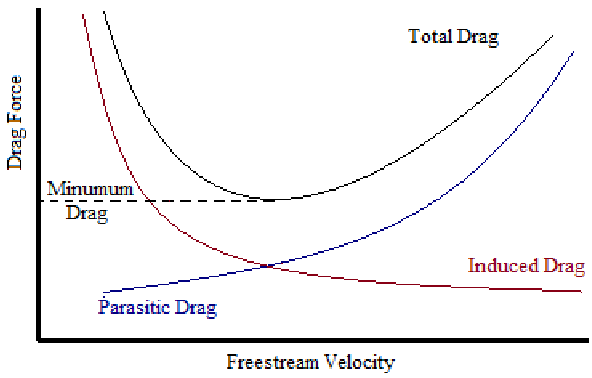

Figure 6.12: Induced and parasitic drag components

must be solved; however, this is challenging because there are three trim equations and five unknown variables. In figure 6.11, two of the five variables, β and δ_{TVFC}, were fixed, and the aircraft's OEI flight envelope was plotted. This figure demonstrated that trimmed, OEI flight can be achieved using both TVFC and the rudder; however, the trim condition of the aircraft has not been fully analyzed. An analysis of the impact of thrust vectoring on ϕ, δ_a, and δ_r must also be completed.

Now the impact of TVFC on the OEI trim variables ϕ, δ_a, and δ_r will be analyzed. For the analysis, figure 6.13 will be used, and the three plots on the left side will be compared to the three plots on the right side. Note that the plots on the left correspond to the OEI trim condition where δ_{TVFC}=0°, and the plots on the right correspond to the OEI trim condition where δ_{TVFC}=4°. It should also be mentioned the thrust vectoring is only used for directional trim in the following analyses. Any time there is a reference to δ_{TVFC}, this deflection angle is always in the y-axis, which means the thrust vectoring is not used for longitudinal trim.

First, the top two plots of figure 6.13 will be compared. These plots show the rudder deflection angle required for OEI, trimmed flight, $\delta_{r,OEI}$. As one can see, when TVFC is not used, δ_{TVFC}=0°, it is estimated that $\delta_{r,OEI}$ angles between 12.3° and 19.5° are required to trim the aircraft. When thrust vectoring is used to trim the aircraft, δ_{TVFC}=4°, it is estimated that $\delta_{r,OEI}$ angles between 10.5° and 18.9° are required to achieve trimmed flight during the OEI flight condition. By comparing these two plots, a reduction in $\delta_{r,OEI}$ is resultant when δ_{TVFC} is increased. This indicates the TVFC is providing the directional forces and moments required to trim the aircraft. By decreasing $\delta_{r,OEI}$, the rudder can then be used for providing control rather than trimming the aircraft.

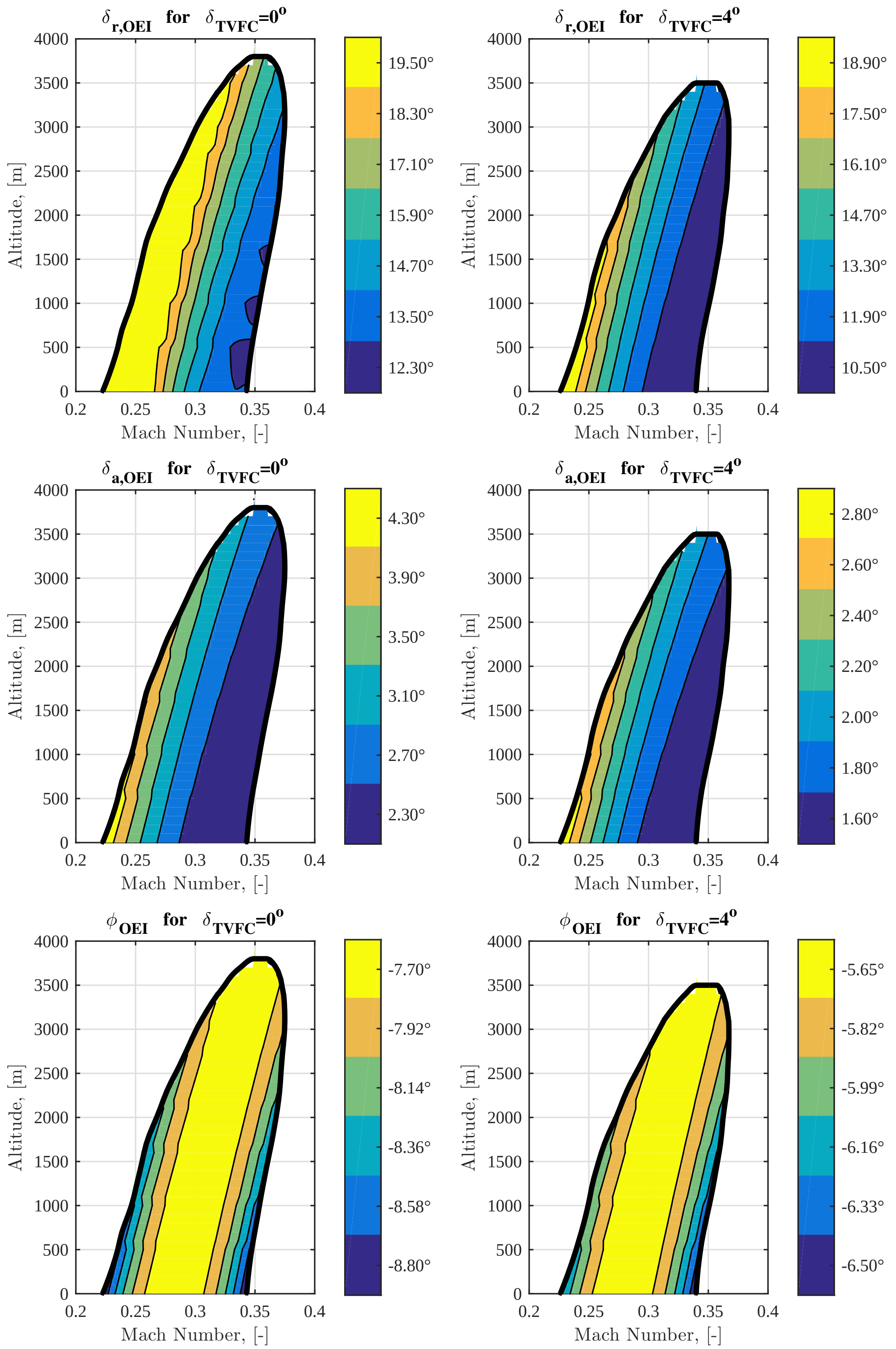

Figure 6.13: Fokker 100 OEI trim condition for nozzle deflection angle of δ_{TVFC}=0° (left) and δ_{TVFC}=0° (right). β=0°

Now the middle two plots of figure 6.13 will be compared. These plots show the aileron deflection angle required for OEI, trimmed flight, $\delta_{a,OEI}$. Through a comparison of these two plots, it can be seen that $\delta_{a,OEI}$ decreases when thrust vectoring is used to trim the aircraft during the OEI flight condition. The cause for this reduction in $\delta_{a,OEI}$ can be attributed to the difference in Cl_{δ_r} and $Cl_{\delta_{TVFC}}$. Due to the location of the rudder and TVFV, both of these control methods will create a rolling moment when deflected. However, the rolling moment arm length of the rudder is greater than the rolling moment arm length of the engine. This difference in rolling moment arm length causes Cl_{δ_r} to be greater than $Cl_{\delta_{TVFC}}$. The ailerons are required to balance the rolling moments caused by the rudder and TVFC. Since the vectored thrust creates a rolling moment smaller than the rudder, the required value of $\delta_{a,OEI}$ decreases.

Lastly, from a comparison of the bottom two plots, it can be seen that the bank angle required for OEI, trimmed flight, ϕ_{OEI}, is reduced when δ_{TVFC} is increased from 0° to 4°. This is beneficial because airworthiness standards presented in the MIL-F-8785C state that ϕ_{OEI} should not exceed 5°. The MIL-F-8785C has been used to judge the airworthiness of military aircraft in the past; however, this requirement is not always applied to CTA. Regardless, it has been shown that using thrust vectoring to trim the aircraft during OEI flight conditions allows for a reduction in ϕ_{OEI}, and this is predicted to improve an aircraft's airworthiness.

6.8. ONE-ENGINE-INOPERATIVE TRIM WITH REDUCED VERTICAL TAIL AREA

The impact of thrust vectoring on the OEI, trimmed flight condition has been demonstrated for the 100% VT area. It has been shown that thrust vectoring will reduce the OEI flight envelope; however, thrust vectoring has a positive impact on the OEI, trimmed flight condition because it allows for a reduction of ϕ_{OEI}, $\delta_{a,OEI}$, and $\delta_{r,OEI}$. Now it is beneficial to examine how the OEI flight envelope is affected by changes in the VT area. This task will be completed by analyzing the OEI flight envelope for the 70% and 85% VT areas.

Figure 6.14 shows the estimated OEI flight envelope for the 70% and 85% VT area designs. The estimated OEI flight envelope for the 100% VT area is also plotted so it may be used for comparison purposes++. In this figure, it is shown that the 85% VT area can provide trimmed OEI flight without the assistance of the TVFC, i.e. δ_{TVFC}=0°; however, the directional maneuverability would likely required for control to be provided by the TVFC. For the 85% VT area and δ_{TVFC}=4°, the OEI flight envelope is slightly smaller than the OEI flight envelope of the 100% VT area.

Perhaps the most interesting feature in this plot is the estimated OEI flight envelope for the 70% VT area and δ_{TVFC}=2°. For this case, the aircraft can be trimmed at higher altitudes when compared to the aircraft with the 100% VT area. The cause for this improvement in the OEI flight envelope can be attributed to a reduction in parasite drag resulting from a reduction in VT area. It is also possible that trim drag can be the cause for this increased OEI flight envelope. It has been shown that using thrust vectoring to trim an aircraft during OEI flight conditions allows for a reduction in $\delta_{a,OEI}$ and $\delta_{r,OEI}$. Lastly, it is desirable for aircraft to fly at high altitudes in order to minimize its fuel consumption and maximize its range. It may be possible that the 70% VT area has a longer range when compared to the 100% VT area for OEI flight conditions. The aforementioned statement has not been verified.

Based on the OEI analysis presented, both improvements and degradations in the aircraft's OEI trim were recognized. Deflecting the nozzle will result in a reduction of axial thrust, and this may reduce the area of the aircraft's OEI flight envelope. However, reducing the VT area results in a reduction of parasite drag, and it is feasible for the drag reduction to compensate for the loss in axial thrust due to a vectored nozzle. In the end, the OEI flight envelope may improve through the addition of TVFC and a reduction in VT area. Lastly, it was shown that using TVFC to provide OEI trim may improve an aircraft's airworthiness by reducing the aircraft's trimmed bank angle, aileron deflection angle, and rudder deflection angle.

In figure 6.14, it has been shown that the 70% and 85% VT area designs will have OEI flight envelopes comparable to the OEI flight envelope of the original 100% VT area. The bank angle and control deflection angles required for trimmed OEI flight may be reduced as δ_{TVFC} is increased, and this prediction can allow for improvements in the OEI trim condition. Based on these results, a VT area between 70% and 85% of the original VT area should allow for acceptable trimmed OEI flight characteristics.

It has been demonstrated that OEI trimmed flight with an unconventionally small VT and TVFC is feasible; however, additional OEI flight analyses must be completed. In particular the OEI and crosswind condition

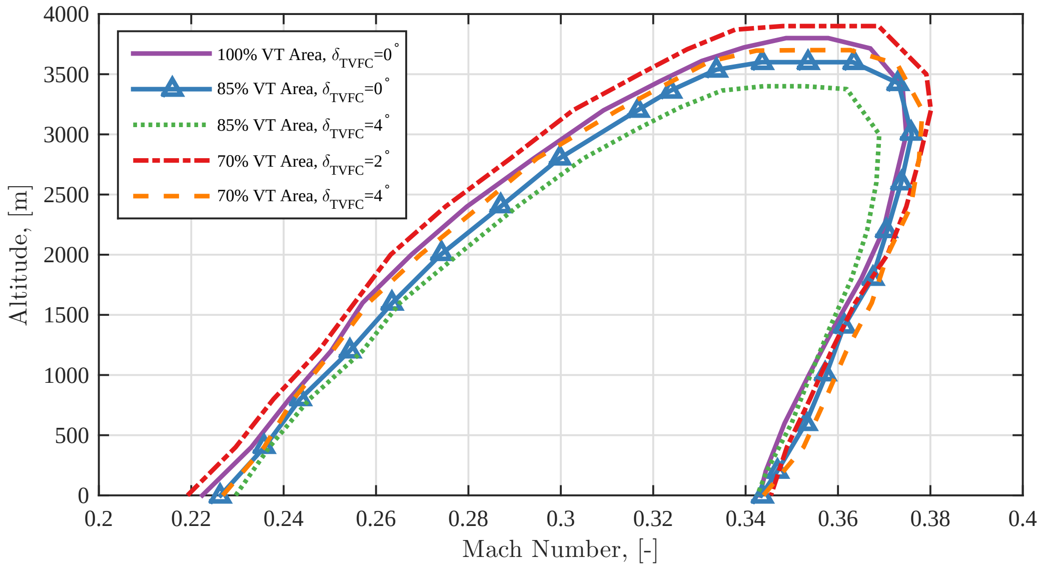

Figure 6.14: OEI flight envelope for various VT areas and δ_{TVFC}

must be analyzed in order to demonstrate and disprove the feasibility of the proposed aircraft design.

6.9. ONE-ENGINE-INOPERATIVE, CROSSWIND TRIM

The flight condition which typically determines the design of the VT is the OEI and crosswind flight condition. To be more specific, the flight condition where the crosswind comes from the direction of the failed engine is the critical condition which may determine the VT design. When the crosswind comes the direction of the failed engine, the rudder must balance both the yawing moment created by the asymmetric thrust as well as the yawing moment created by the crosswind and the aircraft's directional stability. This flight condition must be analyzed in order to demonstrate or disprove the design of an aircraft with an unconventionally small VT and TVFC.

In reference [59], light to medium transport aircraft are considered to have level 1 flight qualities if the aircraft can takeoff and land with normal pilot skill in 30 knot wind ($\approx 15.5 m/s$) coming from a 90° angle relative to the aircraft's heading angle. This criteria has been used to determine the flight qualities of military transport aircraft in the past, and it will now be used to analyze the flight qualities of the proposed thrust vectoring aircraft design.

To analyze the OEI, crosswind flight condition, an attempt to achieve steady-state, trimmed flight for the Fokker 100 aircraft model was made; however, the aircraft model could not achieve steady-state trimmed flight for the OEI and 15.5 m/s crosswind flight conditions. The cause for the models inability to achieve trimmed flight for the specified flight condition has yet to be determined. Because of this deficiency in the aircraft model, the OEI and crosswind flight condition was analyzed using 5 m/s crosswinds rather than 15.5 m/s crosswinds. The results of this analysis will now be discussed.

In table 6.4, values of δ_{TVFC}, δ_a, δ_r, and ϕ are shown which correspond to trimmed flight with OEI and 5 m/s crosswinds coming from the direction of the failed engine. Similar to previous analyses, the aircraft was trimmed at a sideslip angle of 0° in order to minimize the aircraft's drag.

When analyzing the results shown in table 6.4, it can be seen that δ_a and δ_r decrease as δ_{TVFC} increases. Similar results have been demonstrated for the OEI flight condition when there is no crosswind.

In addition to displaying the control surface deflection angles and trimmed bank angle, table 6.4 shows how the engine's turbine inlet temperature, T_{T4}, varies with the thrust vectoring deflection angle. It can be seen that T_{T4} decreases as δ_{TVFC} increases. For the developed aircraft model, T_{T4} is one of the variables influencing the aircraft's ability to achieve trim flight during OEI and crosswind flight conditions. Attention must be

VT Area	Flight Condition			Trim Variables					Engine Data
	Mach	Altitude	Crosswind	δ_{TVFC}	δ_r	δ_a	β	ϕ	T$T4$
% of original	[-]	[m]	[m/s]	[deg	[deg]	[deg]	[deg]	[deg]	[K]
100	0.30	1,000	5.0	0.0	13.8	2.21	0.0	-6.11	1105
100	0.30	1,000	5.0	4.0	9.40	1.26	0.0	-3.85	1097
100	0.30	1,000	5.0	8.0	5.28	0.37	0.0	-1.73	1093
100	0.30	1,000	5.0	12.0	1.36	-0.49	0.0	0.27	1090
100	0.30	1,000	5.0	13.0	0.40	-0.68	0.0	0.78	1089
100	0.30	1,000	5.0	14.0	-0.53	-0.88	0.0	1.23	1089
100	0.30	1,000	5.0	15.0	-1.44	-1.07	0.0	1.70	1088
100	0.30	1,000	5.0	16.0	-2.34	-1.26	0.0	2.15	1088
100	0.30	1,000	5.0	17.0	-3.22	-1.45	0.0	2.60	1089

Table 6.4: Lateral-directional trim for OEI flight with crosswind from direction with failed engine

given to ensure the engine's turbine inlet temperature does not exceed the maximum allowable turbine inlet temperature of 1123 K [28] in order to achieve trimmed flight. According to [28], the engine's operation time is limited to 10 minutes maximum at this temperature.

As stated, the data presented in table 6.4 shows that T_{T4} decreases as δ_{TVFC} increases. The decrease in T_{T4} occurs until δ_{TVFC} reaches a value of approximately 14°. This result is particularly interesting because an increase in δ_{TVFC} is associated with an increase in nozzle performance losses. To account for the thrust losses due to vectoring the engine's nozzle, it can be expected that an increase in δ_{TVFC} results in an increase in T$T4$. This can be expected because the engine's throttle must be increased in order to overcome the thrust losses due to an increase in δ_{TVFC}. However, the data shown in table 6.4 does not verify this logic.

The cause for the reduction in T_{T4} can be associated with the reduction in the aircraft's trim drag, which is drag caused by deflected control surfaces. In table 6.4, it has been shown that the rudder and aileron trim deflection angles decrease as δ_{TVFC} increases during OEI, crosswind flight conditions. The reduction in δ_a and δ_r results in a reduction in trim drag.

The reduction in trim drag also impacts the aircraft's engine. Since there is a reduction in trim drag, the thrust required for trimmed flight is reduced. A reduction in thrust required results in a reduction of engine mass flow rate. The inlet ram drag of an aircraft engine is directly related to the engine's inlet mass flow rate, and a decrease in inlet mass flow rate results in a decrease of inlet ram drag. With this realization, an increase in δ_{TVFC} may result in a decrease in trim drag and a decrease in inlet ram drag. Table 6.5 shows how the engine's mass flow rate and ram drag decrease as δ_{TVFC} increases.

VT Area	Flight Condition			Trim Variables			Engine Data	
	Mach	Altitude	Crosswind	δ_{TVFC}	δ_r	δ_a	$\dot{m}$	Ram Drag
% of original	[-]	[m]	[m/s]	[deg]	[deg]	[deg]	[kg/s]	
100	0.30	1,000	5.0	0.0	13.8	2.21	131.9	13.29
100	0.30	1,000	5.0	4.0	9.40	1.26	130.5	13.06
100	0.30	1,000	5.0	8.0	5.28	0.37	129.8	12.98
100	0.30	1,000	5.0	12.0	1.36	-0.49	129.4	12.94
100	0.30	1,000	5.0	13.0	0.40	-0.68	129.2	12.92
100	0.30	1,000	5.0	14.0	-0.53	-0.88	129.1	12.91
100	0.30	1,000	5.0	15.0	-1.44	-1.07	129.0	12.90
100	0.30	1,000	5.0	16.0	-2.34	-1.26	129.0	12.90
100	0.30	1,000	5.0	17.0	-3.22	-1.45	129.0	12.91

Table 6.5: Engine data for OEI flight with crosswind from direction with failed engine

This result is remarkable, because it indicates that thrust vectoring during OEI and crosswind flight reduces the aircraft's trim drag and ram drag. Due to these reductions in drag, the thrust required to achieve trimmed flight during OEI and a crosswind coming from the direction of the inoperative engine may be reduced.

A reduction in trim drag due to thrust vectoring is feasible; however, it is important to consider if this reduction in trim drag is greater than the thrust losses due to vectoring the engine's nozzle. If the reduction in trim drag is greater than the aforementioned thrust losses, then the thrust required to achieve trimmed flight during OEI and a crosswind may be reduced. Additionally, the aircraft's ram drag may be reduced. With this realization, the ability of VSAERO to accurately predict the increase in drag due to a control surface deflection must be considered. An analysis related to VSAERO and its ability to predict trim drag has not been completed for the present study. The explanation relating T_{T4} to a reduction in trim drag and inlet ram drag is feasible; however, this explanation should be verified.

There is a coupling between the aircraft's control deflection angles, engine performance, and thrust vectoring angle during OEI flight with a crosswind coming from the side of the inoperative engine. The analysis of the OEI flight condition presents some complexities, and a more detailed analysis of this flight condition should be completed. For the design of a thrust vectoring aircraft with a unconventionally small VT area to be considered feasible, and additional studies must be completed. In particular, trim drag analyses should be completed.

It has been shown that thrust vectoring may allow for reductions in control surface deflection angles required for trimmed OEI flight conditions. Additionally, it is feasible that an aircraft's OEI flight envelope is not significantly affected by using thrust vectoring to achieve trimmed flight. The OEI crosswind flight condition is shown to have some complexities, and a more detailed analysis should be completed with regards to the aircraft's trim drag.

6.10. DEEP STALL

The Fokker 100 aircraft has T-tail configuration, and redesigning the VT will impact the location of the horizontal tail (HT). As the VT area is reduced, its span is reduced. This reduction in VT span will change the location of the HT in relation to the aircraft's wing. If the VT span is reduced significantly, then the HT has the potential of becoming enveloped in the wing's wake during a stall. If this occurs, the HT control effectiveness will be reduced, and the aircraft may lose its ability to pitch down. This phenomenon is called deep stall, and it is important to analyze the deep stall characteristics of the Fokker 100 and the five VT designs.

Since a preliminary design of a thrust vectoring aircraft is being completed, a low fidelity method can be used to analyze the deep stall characteristics. In reference [30], an equation has been developed so to predict the angles of attack which define the region where the deep stall phenomenon could occur. If the aircraft is flown at an angle of attack between the angles defining the deep stall region, then the aircraft has the possibility of entering deep stall.

The method which estimates the stall region uses eight geometric angles formed between the wing and horizontal tail. Figure 6.15 show the eight geometric angles, and they are defined as follows

$\psi_{LE_wLE_{HT_r}}$ = angle between wing leading edge and HT root leading edge
$\psi_{LE_wLE_{HT_t}}$ = angle between wing leading edge and HT tip leading edge
$\psi_{LE_wTE_{HT_r}}$ = angle between wing leading edge and HT root trailing edge
$\psi_{LE_wTE_{HT_t}}$ = angle between wing leading edge and HT tip trailing edge
$\psi_{TE_wLE_{HT_r}}$ = angle between wing trailing edge and HT root leading edge
$\psi_{TE_wLE_{HT_t}}$ = angle between wing trailing edge and HT tip leading edge
$\psi_{TE_wTE_{HT_r}}$ = angle between wing trailing edge and HT root trailing edge
$\psi_{TE_wTE_{HT_t}}$ = angle between wing trailing edge and HT tip trailing edge

The stall region is defined between the minimum and maximum angle from the eight geometric angles. Using the method developed in reference [30], the deep stall region for each of the five aircraft designs has been calculated. Table 6.6 displays the results.

In reference [3], flight tests showed the Fokker 100 could rotate to an α of 12.6° during takeoff. At this α, flow separation of the main wing was minimal, but the aircraft's α was limited due to the aircraft's geometry and the possibility of tail strike. This indicates that the Fokker 100 stall α is greater than 12.6°.

In table 6.6, the angles used to define the deep stall region are bold. For the 50% VT area, the deep stall region is predicted at α angles between 13.0° and 23.8°. The α of 13.0° is still greater than the 12.6° angle

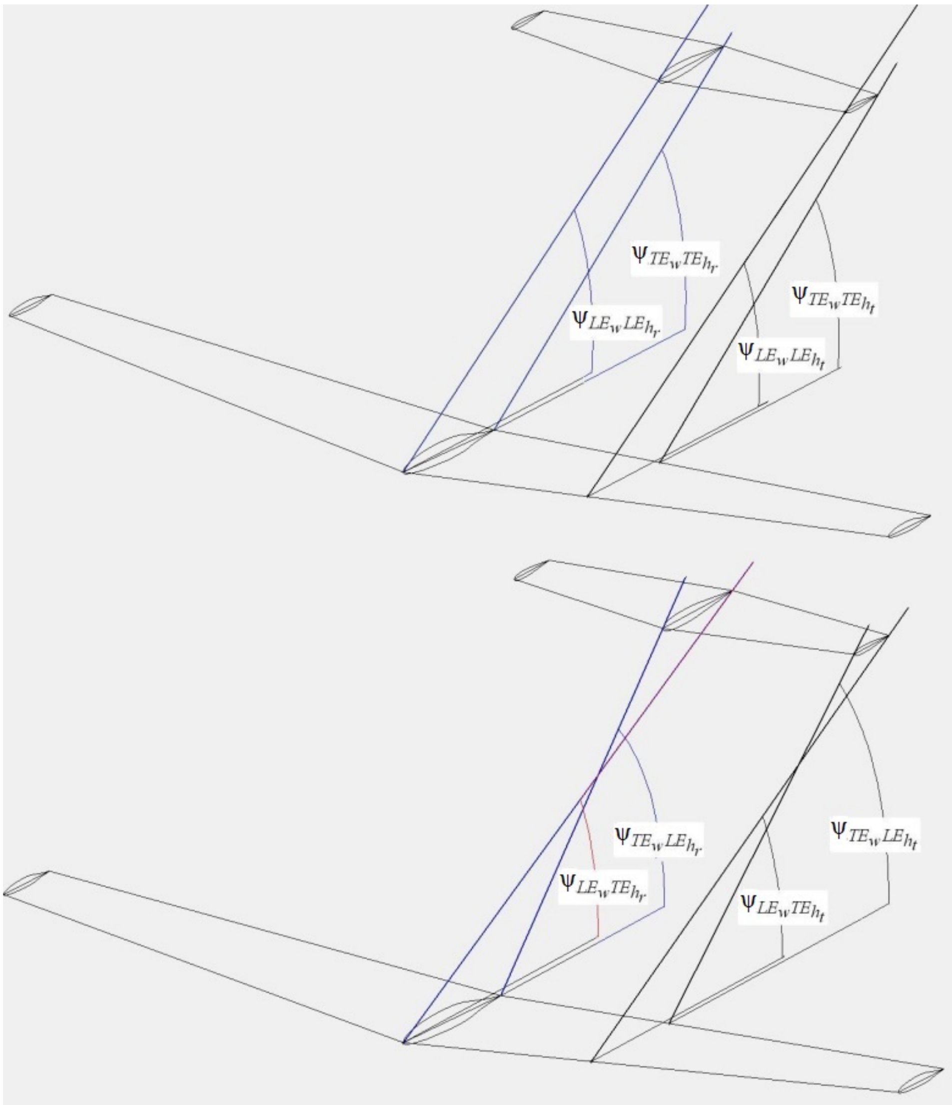

Figure 6.15: Geometric angles used to estimate the deep stall region [30]

of attack the actual Fokker 100 achieved during takeoff flight tests. Since it is likely that the Fokker 100 can achieve α angles greater than 12.6°, the pilot should be warned, such as with a stick-shaker, if the aircraft's α approaches the lower deep stall boundary. Even for the larger VT designs, the pilot should be warned of the deep stall possibility.

Although a reduction in VT area may increase the likelihood of a deep stall, there are control methods for the aircraft to recover from a deep stall. In fact, TVFC can improve the safety of a T-tail aircraft. In the occurrence an aircraft accidentally enters a deep stall, the TVFC could be used for longitudinal control, and it could create the nose-down pitching moment needed for stall recovery.

In summary, the deep stall is a dangerous aerodynamic phenomenon which affects T-tail aircraft. Reducing the VT area and span increases the likelihood of an aircraft entering a deep stall; however, there are methods to ensure the aircraft's safety is maintained. Pilot warning systems can ensure a deep stall does not occur, and if an aircraft accidentally enters a deep stall, the TVFC can be used to recover from the stall. This concept of using TVFC to recover from a deep stall has not been verified with the developed aircraft models.

VT Area % of original	$\psi_{\mathrm{LE}_w \mathrm{LE}_{HTr}}$	$\psi_{\mathrm{LE}_w \mathrm{LE}_{HTt}}$	$\psi_{\mathrm{LE}_w \mathrm{TE}_{HTr}}$	$\psi_{\mathrm{LE}_w \mathrm{TE}_{HTt}}$	$\psi_{\mathrm{TE}_w \mathrm{LE}_{HTr}}$	$\psi_{\mathrm{TE}_w \mathrm{LE}_{HTt}}$	$\psi_{\mathrm{TE}_w \mathrm{TE}_{HTr}}$	$\psi_{\mathrm{TE}_w \mathrm{TE}_{HTt}}$
100	18.2°	21.1°	**15.7**°	19.6°	26.3°	**28.4**°	21.4°	25.7°
85	17.4°	20.2°	**15.0**°	18.7°	25.3°	**27.1**°	20.5°	24.6°
70	16.5°	19.1°	**14.2**°	17.7°	23.9°	**25.8**°	19.4°	23.4°
60	15.8°	18.4°	**13.6**°	17.0°	23.0°	**24.8**°	18.6°	22.5°
50	15.1°	17.6°	**13.0**°	16.3°	22.0°	**23.8**°	17.8°	21.5°

Table 6.6: Calculation of geometric angles used to estimate the deep stall region

7

Vertical Tail Loads and Weight Analysis

7.1. Vertical Tail Loads Analysis

A critical part of the thesis study is to analyze if the aircraft's structural mass, often referred to as the empty operational mass, can be reduced through the addition of TVFC. The aircraft engine's mass will increase due to the addition of TVFC; however, a redesign of the VT should allow for a reduction in VT structural mass. The net result may be a reduction in the aircraft's empty operational mass; however, a thorough mass analysis for the VT must be completed to test this theory.

Before the mass of the VT can be determined, the loads acting on the VT must be known. The VT loading can be determined with knowledge of the VT design requirements for an aircraft. These design requirements state the VT must provide the forces and moments to achieve the following:

1. Directional trim
2. Static and dynamic directional stability
3. Directional control

Explicit examples stemming from these design requirements would include the ability to trim the aircraft in the occurrence of one-engine-inoperative (OEI) flight. The ability of the VT to provide sufficient damping of the Dutch roll motion may be another specific application to the VT design requirements. One final example VT design requirement may be related to aircraft maneuverability, such as the aircraft's ability to achieve a specific yaw rate. With the aforementioned design requirements, the loading conditions on the VT can be predicted.

The loading condition producing the maximum VT loading is of particular interest because this condition is used to determine the VT mass. In general, there are only a few flight conditions which cause significant VT loading. These conditions occur when the aircraft has a large sideslip angle, large rudder deflection angle, or a combination of sideslip angle and rudder deflection angle. Large sideslip and rudder deflection angles most commonly occur during yawing maneuvers, OEI flight, and gusting conditions. In the following sections, the flight conditions producing significant VT loads will be discussed.

Note that the rigid-body aircraft assumption is used in the following load analyses. Aeroelasticity, flutter, buffeting, etc. are neglected. This assumption is used to simplify the load analysis.

7.1.1. Introduction on Vertical Tail Maneuvering Loads

Yawing maneuvers occur when there is an abrupt change in rudder deflection angle. Forces generated by the rudder cause the aircraft to sideslip. Based on FAR 25.351, reference [58], the VT must be designed to withstand the loads produced by three different yaw maneuvers. FAR 25.351 describes the maneuvers as follows:

1. With the airplane in unaccelerated flight at zero yaw, it is assumed that the cockpit rudder control is suddenly displaced to achieve the resulting rudder deflection, δ_r, as limited by the control system or by a 300 pound pilot force.

2. With the cockpit rudder control deflected to δ_r, it is assumed that the airplane yaws to the overswing sideslip angle.

3. With the airplane yawed to the static equilibrium sideslip angle corresponding to δ_r, it is assumed that the cockpit rudder control is suddenly returned to neutral.

The first two described maneuvers are demonstrated in figure 7.1, which shows an aircraft's lateral-directional dynamic response to a rudder input, δ_r, is shown. At a time of one second, the rudder is deflected to some specified angle. This maneuver will now be referred to as maneuver I. Since the maximum VT loading condition is of interest, δ_r for maneuver I should correspond to the maximum allowable rudder deflection angle, $\delta_{r,max}$ for a given altitude and Mach number combination.

The second maneuver occurs shortly after the rudder is deflected to its maximum allowable deflection angle. For maneuver II, the aircraft will begin to slip. At some point, the aircraft will reach a maximum sideslip angle, β_{max}. In figure 7.1, the aircraft reaches β_{max} around 5 seconds. When β_{max} is achieved, the aircraft will have some bank angle, yaw rate, and roll rate. For this maneuver, the rudder deflection angle, sideslip angle, yaw rate, and roll rate should be determined so that they can be used for the VT load estimation.

The third maneuver occurs after the aircraft reaches a steady-state sideslip angle, β_{ss}. This occurs around a time of 35 seconds and beyond. After the steady sideslip is achieved, the rudder is abruptly returned to its neutral position. The aircraft will still have some sideslip angle, but the rudder deflection angle will be approximately zero. The sideslip angle will be the most significant contributor to the VT loading. Figure 7.1 does not show the aircraft's rudder returning to its neutral position.

Note that in figure 7.1 there is some small aileron deflection angle. This deflection angle is used to balance the rolling moment created by the rudder. If the aileron was not deflected, then the aircraft may roll to a bank angle which is outside of the aircraft's normal flight conditions. Aileron deflection angles ensure realistic bank angles are maintained during the maneuvers.

As has been shown, determining β_{max}, β_{ss}, and the rotational rates for the various maneuvers requires the simulation of the aircraft's dynamics. After δ_r, β_{max}, β_{ss}, and the maneuver rotational rates are determined, the VT maneuvering loads can be determined. To determine the maneuvering loads, it is required to complete aerodynamic simulations corresponding to each maneuver. This task can be completed using the computer program VSAERO. The capabilities and limitations of VSAERO have been discussed in chapter 5.

Completing the aircraft dynamic analyses and aerodynamic simulations can be readily completed with the developed Fokker 100 models; however, these analyses can be relatively time intensive. For example, the described maneuvering loads should be completed at many different altitude and Mach number combinations in order for the worst case maneuver loads to be recognized. This would require a vast amount of dynamic and aerodynamic analyses. To reduce the time intensive nature of the maneuvering load analysis, a simplified method will be used determine the maneuvering loads. This simplified method will now be discussed.

7.1.2. SIMPLIFIED METHOD FOR ESTIMATING MANEUVERING LOADS

In chapter 5, it was discussed that the S&C derivatives are impacted by the flow's Mach number; however, the derivatives do not appear to be influenced by the altitude for a specified Mach number. Consider the S&C derivatives Cy_β and $Cy_{\delta r}$, shown in figures 5.5. These two derivatives are reflective of the sideforce due to a sideslip angle or rudder deflection, and they are closely related to the VT loading due to a sideslip or rudder deflection. Since Cy_β and $Cy_{\delta r}$ do not vary significantly with altitude, one could assume the VT loads due to a change in β or δ_r will not vary with altitude. A similar argument can be created for the bending and torsion moments due to rudder deflection and the plots of $Cl_{\delta r}$ and $Cn_{\delta r}$. The rolling and yaw moments created by a rudder deflection are related to the bending and torsion moments experienced at the VT root, respectively. Since $Cl_{\delta r}$ and $Cn_{\delta r}$ do not vary significantly with altitude, the VT bending and torsion moments created by

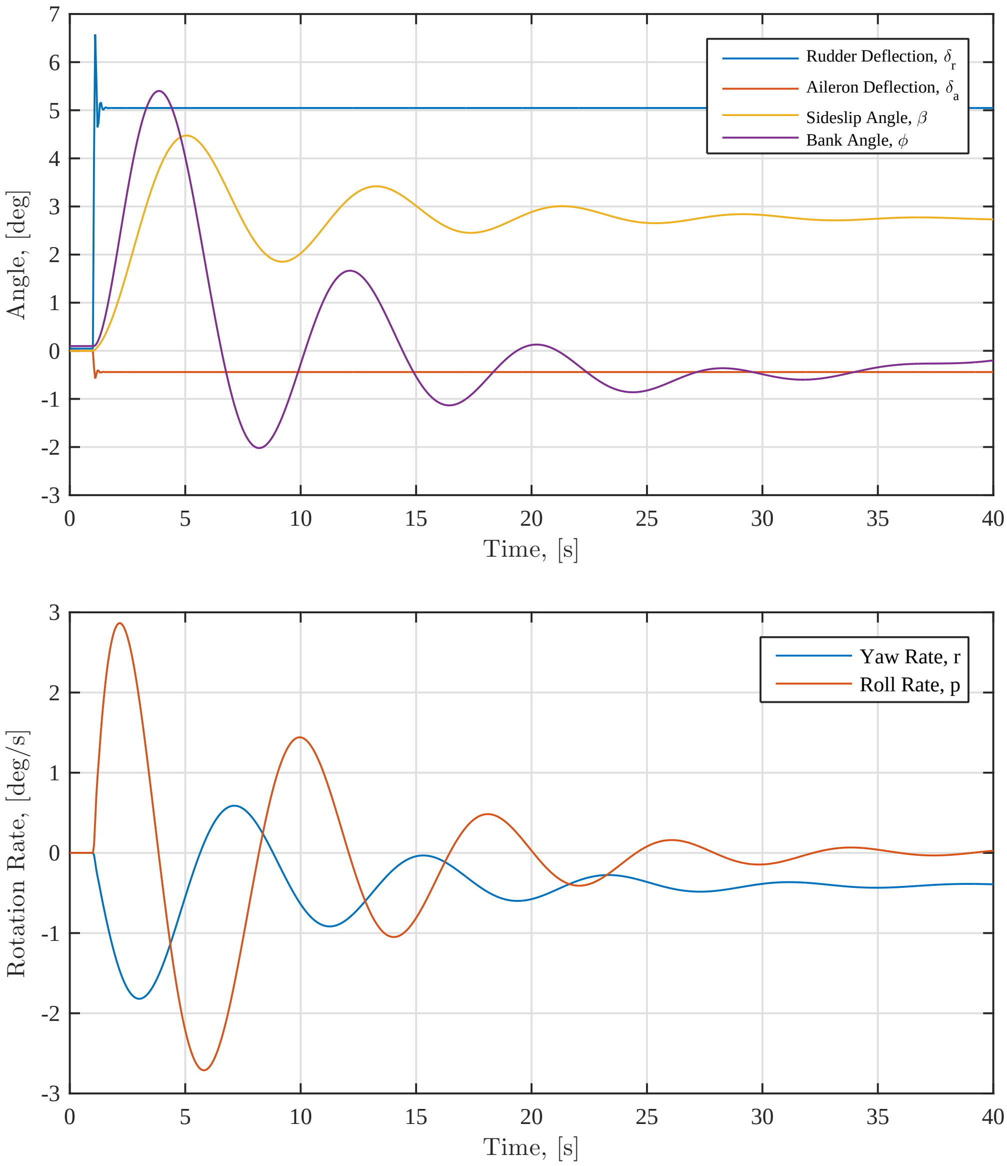

Figure 7.1: Aircraft sideslip response due to rudder deflection

a rudder deflection will likely not vary with altitude. With these realizations, a simplified approach can be introduced to calculate the VT loading. For the simplified approach, non-dimensional loading derivatives will be introduced.

Before the simplified approach is introduced, the assumption that rotational rates are not a significant contributor to the VT loading will be made. For maneuver I and maneuver III, the aircraft's yawing and rolling are approximately zero; however, maneuver II has a non-negligible yawing and rolling rate. If maneuver II is shown to be the worst case loading maneuver, then this assumption will have to be readdressed. With this assumption that the rotational rates do not cause significant VT loads, the 3 maneuvering loads can be represented with figure 7.2.

Consider the following equations, which calculate the non-dimensional loading derivatives due to a sideslip angle and rudder deflection [46]:

$$C_{\mathfrak{L}_{\delta\beta}} = \frac{1}{ql}\frac{\delta\mathfrak{L}}{\delta\beta} \tag{7.1a}$$

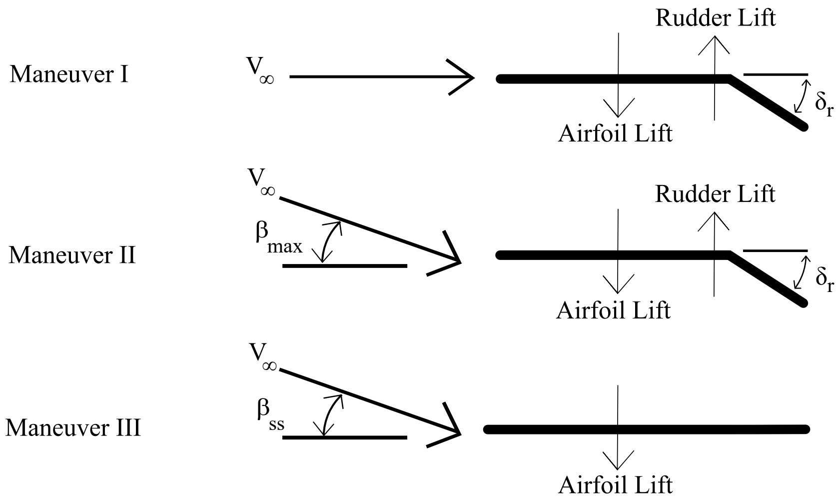

Figure 7.2: Definition of the maneuvers described in FAR 25.351

$$C_{\mathfrak{L}_{\delta r}} = \frac{1}{ql}\frac{\delta \mathfrak{L}}{\delta r} \tag{7.1b}$$

In equation the above equations, $\mathfrak{L}$ is either a shear, bending moment, or torsion load at the root of a lifting surface, such as a VT. The variable l is a characteristic length, and q is the flow's dynamic pressure. To determine the value of these loading derivatives, aerodynamic simulations should be completed, and the VT loads should be calculated. This process is similar to calculating S&C derivatives. It should be noted that the bending moment and torsion loads are calculated with respect to the VT root.

The primary assumption of the simplified maneuver loads approach is that $C\mathfrak{L}_\beta$ and $C\mathfrak{L}_{\delta r}$ vary only with Mach number and not altitude. This is based on the realization that Cy_β, $Cy_{\delta r}$, Cl_β, $Cl_{\delta r}$, Cn_β, and $Cn_{\delta r}$ vary with Mach number and not altitude. It may be argued that this assumption is not valid for the bending moment and torsion moment loads because Cl_β, $Cl_{\delta r}$, Cn_β, and $Cn_{\delta r}$ are calculated with respect to the aircraft's center of gravity and not the root of the VT. In spite of this argument, the assumption regarding the loading derivatives will still be made in order to simplify the VT loads analysis. Further analysis should be completed to demonstrate the validity of this assumption, and this assumption will be readdressed at the end of this section.

Now consider maneuver I through III as discussed in FAR 25.351. If one assumes the VT loading, $\mathfrak{L}$, varies linearly with β and δr, then principle of superposition can be used when calculating the loads for the three maneuvers. This following equations are resultant of this assumption [46]:

$$\mathfrak{L}_{mI} = qlC_{\mathfrak{L}_{\delta r}}\delta_{r,max} \tag{7.2a}$$

$$\mathfrak{L}_{mII} = qlC_{\mathfrak{L}_{\beta}}\beta_{max} + qlC_{\mathfrak{L}_{\delta r}}\delta_{r,max} \tag{7.2b}$$

$$\mathfrak{L}_{mIII} = qlC_{\mathfrak{L}_{\beta}}\beta_{ss} \tag{7.2c}$$

Finally, the method used to determine the value of $\delta_{r,max}$ must be explained. The value of $\delta_{r,max}$ can be selected to ensure the aircraft can be trimmed in the occurrence of OEI crosswind flight conditions. Therefore, a value of $\delta_{r,max}$ which is equal to $\delta_{r,OEI}$ can be used in the maneuver load equations. It must be noted that calculating $\delta_{r,OEI}$ is not feasible for some flight conditions. For example, it is not possible to trim the Fokker 100 at an altitude of 6,000 meters with a Mach number above 0.6 using only one engine. This is not possible because the single aircraft engine cannot produce enough thrust to achieve this flight condition. It is possible for the Fokker 100 to achieve the aforementioned flight condition using both engines; therefore, a different criteria must be used to select $\delta_{r,max}$ when it is illogical to use the OEI criteria.

When OEI flight is not feasible, the criteria used to determine $\delta_{r,max}$ can be selected to meet a specific aircraft handling quality. When the rudder is deflected, it will produce a yaw rate, r. If the rudder is undersized or its deflection angle is too small, then the aircraft's yaw response to δ_r will be sluggish; therefore, $\delta_{r,max}$ can be selected so the aircraft can achieve a specific yaw rate.

Since the determination of $\delta_{r,max}$ has been based on the OEI flight condition, the aircraft's yaw response within this section of the flight envelope can be examined. The yaw rates induced by $\delta_{r,OEI}$ in the flight envelope section where OEI trimmed flight is feasible can then be used to establish yaw rate requirements in the sections of the flight envelope where OEI trim flight is not feasible. Consider table 7.1, which shows the rudder required for OEI flight at an altitude of 2000 meters and various Mach numbers. The table also shows the maximum yaw rate achieved, r_{max}, if the rudder is deflected to $\delta_{r,OEI}$ when all engines are operative. As one can see, at an altitude of 2000 m and a Mach number of 0.38, a maximum yaw rate of $3.43\frac{deg}{s}$ can be achieved after a rudder input of 13.1^o. For flight conditions at an altitude of 2000 meters where trimmed OEI flight is not feasible, i.e. Mach numbers greater than Mach 0.38, $\delta_{r,max}$ should be selected such that a yaw rate of $3.43\frac{rad}{s}$ can be still be achieved. Table 7.1 contains data for $\delta_{r,max}$ such that the desired r_{max} value of $3.43\frac{deg}{s}$ can be achieved for Mach numbers above 0.38.

In appendix A, a table containing the data used to determine $\delta_{r,max}$ is shown. It has been created using the method which has just been discussed.

Altitude [m]	Mach [-]	$\delta_{r,OEI}$ [deg]	$\delta_{r,max}$ [deg]	r_{max} [deg/s]
2,000	0.30	20.0	20.0	3.67
2,000	0.32	16.5	16.5	3.37
2,000	0.35	14.3	14.3	3.33
2,000	0.38	13.1	13.1	3.43
2,000	0.42	-	11.8	3.43
2,000	0.58	-	8.70	3.43

Table 7.1: Rudder deflection required for trimmed, OEI flight

Once $\delta_{r,max}$ is known, the aircraft's dynamic analysis can be completed, and β_{max} and β_{ss} can be estimated. With these known variables, equation set 7.2 can be used to estimate the maneuver I through III loads. By calculating the maneuver loads for many different altitude and Mach number combinations, the maximum maneuver load can be determined. Since a rather crude method has been used to estimate the VT loads, the accuracy of the results can be improved with aerodynamic simulations. The aerodynamics of the maneuver producing the worst case load can be simulated using VSAERO. To clarify these statements, equation set 7.2 can be used to estimate which maneuver will produce the worst case loads, and the aerodynamics causing the worst case load can be simulated with VSAERO.

The method estimating the VT loads analysis uses tools of varying fidelity. The equation set 7.2 has a relatively low fidelity and the aerodynamic simulations has a relatively high fidelity. This allows for the VT maneuver loads analysis to be completed in an efficient manner.

Now it's beneficial to briefly summarize the process used to calculate the maneuver loads. The FAR 25.351 describes the maneuvers an aircraft is required to perform, and equation 7.2 presents a simplified method of calculating the maneuver loads. The maneuver loads must be calculated for various altitudes and Mach numbers. When it is feasible for the aircraft to achieve OEI trimmed flight, $\delta_{r,max}$ will equal $\delta_{r,OEI}$, and the maneuvers can be simulated. When OEI trimmed flight is not feasible, $\delta_{r,max}$ will be selected to achieve a maximum yaw rate, and this maximum yaw rate has been selected by analyzing the aircraft's yaw maneuvers within the OEI portion of the flight envelope. Lastly, β_{max} and β_{ss} are determined from an aircraft dynamics analysis following a rudder input. Once the maneuver producing the worst case loads is identified, aerodynamic simulations can be used to improve the accuracy of the estimated worst case maneuver loads. In appendix A, results from the maneuvering loads analysis are presented for the 100% VT area.

7.1.3. REEXAMINATION OF THE MANEUVERING LOAD ASSUMPTIONS

Earlier in this section, an assumption was made stating that the loading coefficients $C\mathfrak{L}_\beta$ and $C\mathfrak{L}_{\delta r}$ will not vary significantly with altitude for a given Mach number. This assumption has been made by the author of this thesis report, and the assumption has not been supported by analysis or literature. Now that the process used for the maneuvering loads analysis has been described, a reexamination of this assumption will be completed.

It must be reiterated that the loading coefficients $C\mathfrak{L}_{\beta}$ and $C\mathfrak{L}_{\delta r}$ are used in equation set 7.2. This equation set can be used to estimate the VT loading; however, the loads estimated with this equation are not used to estimate the VT mass. The equations are used to determine the flight condition where the worst case maneuver loads occur. Based on this result, the worst case maneuver loads are estimated using aerodynamic simulations, i.e. VSAERO. So one must consider how $C\mathfrak{L}_{\beta}$ and $C\mathfrak{L}_{\delta r}$ are being used in the load analysis to determine if the assumption is reasonable. In conclusion, the author of this research made the assumption that $C\mathfrak{L}_{\beta}$ and $C\mathfrak{L}_{\delta r}$ do not vary with altitude, and the author considers this assumption to be sufficiently accurate for estimating the flight condition where the worst case maneuver loads occur.

If one is unswayed by the argumentation supporting this assumption, then it is beneficial to examine the flight condition, altitude and Mach number combination, where maneuvers I through III produce the largest VT loading. Due to the length of the loading results, the tables containing the maneuvering load data calculated using equation set 7.2 are placed in tables A.2 through A.4 of the appendix. By examining this table one would recognize the worst case loading condition occurs at an altitude of 3,850 meters and Mach 0.75. This particular flight condition is located on the boundary of the flight envelope where the aircraft's maximum operational velocity, V_{MO}, intersects with the aircraft's maximum operational Mach number, M_{MO}. This can be verified by examining the flight envelope plotted in figure 5.4. This location in the flight envelope is important because this is where dynamic pressure is the largest [3]. The loading acting on the VT and the freestream's dynamic pressure are strongly related, and an increase in dynamic pressure will result in an increase in VT loading. With this realization, the assumption that $C\mathfrak{L}_{\beta}$ and $C\mathfrak{L}_{\delta r}$ do not vary with altitude appears to be reasonable, because these variables determined that the worst case maneuver loads occur at point in the flight envelope where dynamic pressure is the greatest. With this realization, the author of this research considers the assumption to be reasonable.

7.1.4. VERTICAL TAIL ONE-ENGINE-INOPERATIVE LOADS

The aircraft's maneuvering loads have been discussed; however, there are other loading conditions which may impact the VT mass. In particular, the loads acting on the VT after an engine failure must be determined. The OEI loading cases presented in this section differ slightly from the maneuvering loading cases, and the topic will be discussed. First, FAR 25.367 will be discussed to help formulate the background of the OEI loading cases.

The FAR 25.367 contains the engine out maneuvering requirements for transport aircraft. Based on these regulations, three loading conditions can be defined. The first OEI loading condition, OEI_{I}, occurs when an engine fails and the aircraft yaws to some maximum sideslip angle while there is no pilot response. The second OEI loading condition, OEI_{II}, occurs when the engine fails and the aircraft yaws; however, for this condition, the pilot applies a corrective rudder input 2 seconds after the failure. The third OEI loading condition, OEI_{III}, occurs when the aircraft has a failed engine and the proper rudder deflection is applied to achieve zero sideslip angle. Note that the loading for OEI_{III} is identical to the maneuver I loading, $\mathfrak{L}_{mI}$, because $\delta_{r,max}$ was selected to achieved trimmed, OEI flight.

As with the maneuvering loads, the OEI loads can be calculated using a simplified approach. The equations used to calculate the loads for the three OEI maneuvers are as follows:

$$\mathfrak{L}_{OEI,mI} = qlC_{\mathfrak{L}_{\beta}}\beta_{oy} \tag{7.3a}$$

$$\mathfrak{L}_{OEI,mII} = qlC_{\mathfrak{L}_{\beta}}\beta_{OEI} - qlC_{\mathfrak{L}_{\delta_r}}\delta_{r,OEI} \tag{7.3b}$$

$$\mathfrak{L}_{OEI,mIII} = qlC_{\mathfrak{L}_{\delta_r}}\delta_{r,OEI} \tag{7.3c}$$

In the above equation β_{oy} is the maximum sideslip angle, commonly called the overyaw angle, caused by the asymmetric thrust and no corrective pilot input. This is similar to β_{max} which is used for maneuver II; however, the sideslip angle is produced from the engine failure rather than an abrupt rudder input. β_{OEI} is the sideslip angle occurring 2 seconds after the engine failure. These two sideslip angles are determined from an aircraft dynamics analysis. Completing the OEI loads analysis is similar to completing the maneuver loads analysis following a rudder control input. The primary difference is that asymmetric thrust causes the maneuver to be initiated rather than a rudder control input.

Calculating the OEI loads with equation 7.3 must be completed carefully, because the dynamic analysis required to obtain β_{oy} and β_{OEI} poses some complications. For the dynamic analysis, the transient drag build-up and thrust decrease of the failed engine needs to be taken into consideration. It is assumed the thrust decreases linearly from the original thrust to no thrust over the period of one second. The drag build-up is also assumed to occur over the period of one second. This assumption is made because transient response data for the Tay 650 engine was not found in literature.

As with the maneuver loads analysis, the OEI loads should be completed for varying altitude and Mach number combinations. The combination of altitude, Mach number, β_{oy}, and β_{OEI} producing the largest OEI loads should be obtained. By knowing the worst case loading condition, aerodynamic simulations can be completed with VSAERO to improve the accuracy of the worst case OEI load.

For the OEI loads analysis, it is assumed VT loading due to rotational rates will be negligible. The estimation $\mathfrak{L}_{OEI,mII}$ will be affected by this assumption. If $\mathfrak{L}_{OEI,mII}$ causes the largest OEI maneuver loads, then the loading due to rotational rates should be taken into account during the aerodynamic simulations used for the VT load estimate. The assumption that the loading coefficients $C_{\mathfrak{L}_\beta}$ and $C_{\mathfrak{L}_{\delta r}}$ do not vary with altitude is also used. For more information regarding the impact of this assumption, the reader to referred to section 7.1.3.

Results of the OEI loading analysis and 100% VT area are displayed in tables A.5 and A.6 of the appendix.

7.1.5. VERTICAL TAIL GUST LOADS

Wind gusts often cause a VT to experience large loads. Calculation of the loads should be completed to ensure the VT is strong enough to withstand the gust loads. An analytical method to calculate gust loads is provided in reference [46]. The gust load equation may be calculated with the following equation:

$$\mathfrak{L}_{gust} = \frac{K_g U_{de} V_e C_{L\alpha v} S_v}{498} \tag{7.4a}$$

where K_g is the gust alleviation factor,

$$K_g = 0.88 \frac{\mu_v}{5.3 + \mu_v} \tag{7.4b}$$

and μ_v is the VT's lateral mass ratio

$$\mu_v = \frac{2 I_z}{\rho \bar{c}_v C_{L\alpha v} S_v l_v^2} \tag{7.4c}$$

In the above equations, U_{de} is the derived gust velocity (ft/s, eas), and FAR 25.341 provides the criteria used to calculate U_{de}. V_e is the aircraft's equivalent airspeed (knots, eas), $C_{L\alpha v}$ is the VT's lift curve slope (per radian), S_v is the VT planform area (ft^2), I_z is the aircraft's yawing moment of inertia (slug·ft^2), $\bar{c_{vt}}$ is the VT's mean aerodynamic chord (ft), and l_{vt} is the distance from the aircraft's center of gravity to the VT's center of lift (ft).

Equation set 7.4 provides a simplistic method of calculating the lateral-gust loads. Another method to calculate the gust loads is to simulate the aircraft's dynamics due to a gust response. After the aircraft's gust response is known, such as the sideslip angle and rotational rates, VSAERO simulations can be used to calculate the gust loads. The simplified method was selected as a first approximation of the gust loads.

The results of this gust loading analysis for the 100% VT area are displayed in table A.7 of the appendix.

7.1.6. VERTICAL TAIL LOADING RESULTS

Upon completion of the simplified VT load calculations, the flight maneuver producing the worst case VT loads can be determined. Up to this point, all the load analyses have used simplified equations to determine the worst case loading. Through the use of equation sets 7.2, 7.3, and 7.4, the flight condition (altitude, Mach number, sideslip angle, rudder deflection angle, and rotational rates) producing the worst case loads can be simulated with aerodynamic analysis software.

In appendix A the results of the simplified loading analysis for the 100% VT area are shown. Through an examination of all the VT loads for the various altitudes and Mach numbers, it is shown that the OEI_{II} loading condition at an altitude of 3,850 meters and Mach 0.75 produces the worst case VT loads. For OEI_{II}, the engine fails and the aircraft because to yaw. Two seconds after the engine failure, the pilot applies maximum rudder to correct the yawing motion. During the simplified analysis the aircraft's yaw rate was assumed to have a negligible impact on the VT loads; however, for the aerodynamic simulations, the yaw rates have not be neglected. The aerodynamics for this worst case loading condition have been simulated for all five of the aircraft designs using VSAERO. Table 7.2 displays the results.

	Flight Condition					Aerodynamic Loads		
VT Area	Altitude	Mach	$\delta_{r,OEI}$	β_{OEI}	r_{OEI}	Shear	Bending	Torsion
% of original	[m]	[-]	[deg]	[deg]	[deg/s]	[kN]	[kN·m]	[kN·m]
100	3,850	0.75	7.90	2.76	2.64	-102	-176	22.4
85	3,850	0.75	7.90	2.81	2.51	-87.9	-139	18.8
70	3,850	0.75	7.90	3.07	2.90	-77.3	-109	16.0
60	3,850	0.75	7.90	3.38	3.31	-71.1	-91.9	13.9
50	3,850	0.75	7.90	3.56	3.60	-32.6	-35.9	1.98

Table 7.2: Worst case VT loads. OEI_{II} loading case at an altitude of 3,850 meters and Mach 0.75

It is important to verify the results shown in table 7.2. In order to determine the flight condition producing the worst case loads, the simplistic method was used. The simplistic method made use of equation sets 7.2 and 7.3. A few assumptions were made when these equation sets were used. For the first assumption, it was assumed the rotational rates had a negligible effect on the VT loads. The second assumption stated that $C_{\mathfrak{L}_\beta}$ and $C_{\mathfrak{L}_{\delta r}}$ do not significantly change with altitude. With these assumptions and equation sets 7.2 and 7.3, the VT maneuvering and OEI loads were estimated. These VT loads obtained with the simplistic method are displayed in appendix A.

In table 7.2, the VT loads were estimated using aerodynamic simulations in VSAERO. The aircraft's yaw rate was included in these simulations. To check the results shown in table 7.2, the loads corresponding to the 100% VT area will be compared to the loads calculated with the simplistic method for the 100% VT area. Table 7.3 displays the results.

	Flight Condition					Aerodynamic Loads		
VT Area	Altitude	Mach	$\delta_{r,OEI}$	β_{OEI}	r_{OEI}	Shear	Bending	Torsion
% of original	[m]	[-]	[deg]	[deg]	[deg/s]	[kN]	[kN·m]	[kN·m]
VSAERO Simulations								
100	3,850	0.75	7.90	2.76	0.00	-102	-176	22.4
Simplistic Method (equation set 7.3)								
100	3,850	0.75	7.90	2.76	2.64	-97.8	-169	29.5

Table 7.3: Comparison between the estimated worst case loads for VSAERO and the simplistic method

As one can see, the loads calculated with the simplified method and the aerodynamic simulations are in good agreement. Using the aerodynamic results as the reference loads, the shear, bending, and torsion loads calculated with the simplistic method have errors of 4.1%, 4.0%, and 32%, respectively. It should also be noted that the simplistic method estimates that the worst case loads occur at an altitude of 3,850 meters and Mach 0.75. This location in the flight envelope is where the freestream's dynamic pressure is the largest [3]. Since the simplistic method (1) estimated loads which agree with the VSAERO simulation and (2) estimated that the worst case loads occur at a flight condition where the dynamic pressure is the largest in the flight envelope, the simplistic method is verified to produce reliable results.

Now that the worst case VT loads are estimated, the VT structural mass analysis can be completed. That is the next discussion topic.

7.2. VERTICAL TAIL MASS ANALYSIS

There are various methods to estimate a VT's mass, but the method selected for the analysis is a program named Elham Modified Weight Estimation Technique (EMWET). EMWET uses a finite element method to estimate the mass of an aerodynamic lifting body [38]. To use EMWET for the mass estimation, the lifting body's planform, airfoils, materials, and loads must be known.

In addition to estimating the VT mass, it is crucial to analyze how the HT mass is influenced by the redesign of the VT. For example, the scaling method used to redesign the VT results in a reduced chord length at each spanwise position. The HT mass is impacted by the reduction in VT chord length because the volume used to connect the two bodies is reduced.

To analyze the mass of the HT, it is important to determine how the HT is mounted to the VT. One of the inputs required to calculate the lifting body's mass is the location of the spars. Spars are structural part of a lifting body, and they are used to carry the aerodynamic loads encountered during flight. Since the spars are used to carry the aerodynamic loads for both the VT and HT, it was assumed the VT and HT spar intersect. The point of intersection between the spars determines how the HT is mounted to the VT. Figure 7.3 demonstrates this concept. As the VT is redesigned, the location of its spars will be repositioned which in turn causes the HT spars to be repositioned. Lastly, when the spar locations are determined, their position must allow for a realistic VT and HT design. For example, the VT spar must not interfere with the deflection of the rudder.

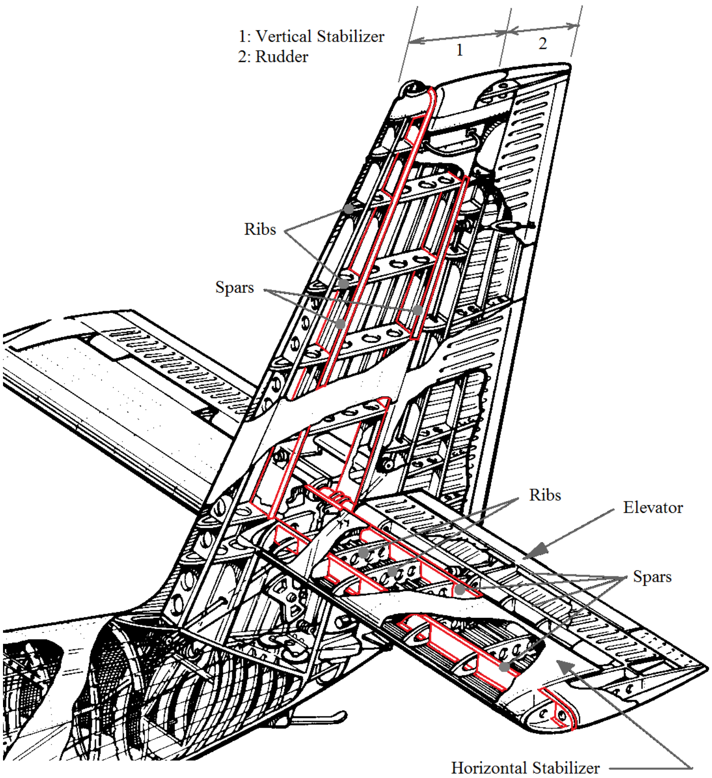

Figure 7.3: VT and HT spar location [60]

When EMWET is used for the VT mass estimation, it is unlikely that EMWET will estimate a VT mass that is exactly equal to the mass of the actual Fokker 100 VT. For this reason, a correction factor will be needed to correct for the difference between the estimated VT mass and the actual VT mass. The following equation demonstrates how the correction factor, k, can be used to correct the estimated mass of the original 100% VT area, $m_{100,est}$, so that it matches the mass of the real VT, $m_{100,real}$.

$$m_{100,est} \cdot k = m_{100,real} \tag{7.5}$$

When the VT area is reduced, the estimated VT mass will change, and this estimated VT mass must be multiplied by the correction factor so that it better estimates the mass of the real VT with a reduced area. This following equation demonstrates how the concept would be applied to the estimated mass of the 85% VT area.

$$m_{85,est} \cdot k = m_{85,real} \tag{7.6}$$

The difference between $M_{100,real}$ and $M_{85,real}$ would estimate the VT mass reduction resulting from the reduction in VT area. This concept is straightforward; however, one must consider how the correction factor k influences the VT mass estimation. For example, the spar locations of the actual Fokker 100 are unknown; therefore, the spar locations are a design variable for the VT. By changing the spar position, the estimated VT mass will change, and this results in a change in the correction factor. At this point it is unknown if the correction factor has an influence on the results of the mass estimation. Consider the following equations which demonstrate the correction factor concept for the 100% VT area, and there are two different mass estimations for this VT design.

$$m_{100,est_1} \cdot k_1 = m_{100,real} \tag{7.7a}$$

$$m_{100,est_2} \cdot k_2 = m_{100,real} \tag{7.7b}$$

Because the two mass estimations are different, there will be two different correction factors. Now one must consider how the correction factor influences the mass estimation if the VT area is reduced. The following equations represent this concept:

$$m_{85,est_1} \cdot k_1 = m_{85,real_1} \tag{7.8a}$$

$$m_{86,est_2} \cdot k_2 = m_{85,real_2} \tag{7.8b}$$

At this point, it is unknown if $m_{85,real_1}$ is equal to $m_{85,real_2}$. With this realization, an analysis of the correction factor and its impact on the mass estimation was completed.

For the analysis of the correction factor, the spar placement within the VT was varied, and the VT area was reduced. Table 7.4 displays the results. The real mass of the Fokker 100 VT is 365 kg, and this value was obtained from reference [3].

VT Area % of original	Front Spar Location [% chord position]	Rear Spar Location [% chord position]	m_{est} [kg]	k [-]	M_{real} [kg]
100	20	70	328.8	1.110	365.0
70	20	70	181.1	1.110	200.9
			Mass Reduction [kg]:		164.1
100	30	70	291.4	1.253	365.0
70	30	70	160.4	1.253	201.0
			Mass Reduction [kg]:		164.0
100	30	75	304.6	1.198	365.0
70	30	75	167.7	1.198	200.9
			Mass Reduction [kg]:		164.1

Table 7.4: Analysis of the VT spar placement and correction factor on mass estimation

By examining table 7.4, one can see the spar placement impacts the estimated VT mass and the correction factor, k. When applying the correction factor to the 70% VT area, it can be seen that it produces the same

m_{real} irregardless of the spar placement and value of k. This proves the spar placement within the VT does not have an impact on the mass analysis. Also, it can be concluded that the mass reduction which results from a reduction in VT area does not depend of the VT spar placement.

Now that the impact of the correction factor is understood, EMWET can be used to complete the mass estimation of the VT and HT. The main purpose of the mass estimation analysis is to see if a net mass reduction for the VT and HT combination occurs from the reduction in VT area. The results of the mass estimation are displayed in figure 7.4.

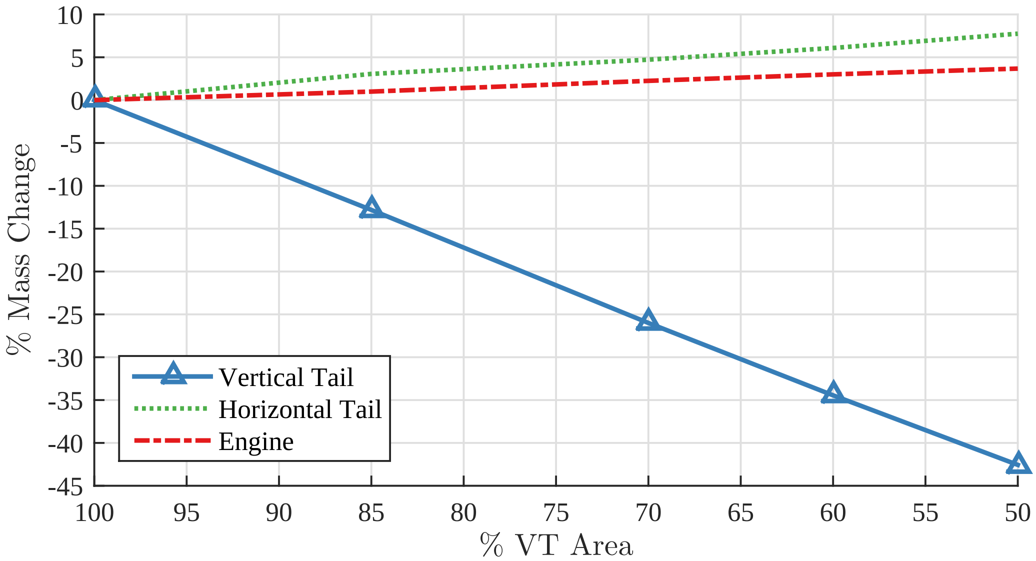

Figure 7.4: VT, HT, and engine mass shown for various VT areas

In figure 7.4, the estimated VT and HT masses are shown, and they are normalized by each of their original masses. By normalizing the VT and HT masses, the estimated percent mass change for each of the respective bodies can be seen as a function of VT area. For example, the 50% VT area design will result in an estimated VT mass reduction of approximately 43%, and the estimated HT mass will increase by approximately 8%

As seen in figure 7.4, reducing the VT area results in a decrease in VT structural mass. A reduction in VT area is also shown to impact the HT mass. As explained, the HT mass is impacted by the placement of its spars. When the VT area was reduced, the distance between the HT's front and rear spars is reduced. The repositioning of the HT's spar resulted in an increase in the HT mass.

A line corresponding to the normalized engine mass is also plotted in figure 7.4. The engine mass line has been calculated such that the net change in mass of the combined VT and HT bodies is added to the engine mass. For example, if the VT mass is reduced by 90 kg and the HT mass is increased by 20 kg, then there is a net mass reduction of 70 kg. This 70 kg can be added to the engine to account for the mass of the TVFC. This would indicate that the aircraft's empty operational weight would not change.

In section 4.3.4, the Tay 650 mass increment due to thrust vectoring was estimated. The results from this analysis are shown in table 4.3. By using this data and figure 7.4, the VT area which allows for a mass reduction large enough to account for the TVFC system weight addition can can be estimated.

The estimated engine mass increase would be between 2.7% and 4.6%. The 2.7% and 4.6% engine mass increase corresponds to thrust vectoring systems with 10° and 20° nozzle deflection angles, respectively By examining the line in figure 7.4 corresponding to the percent engine mass change, it can be seen that for the 50% VT area, the estimated engine mass can increase by slightly less that 5%, and this would indicate that the aircraft's empty operational mass would not change. This estimated percent engine mass increase is sufficient to account for the thrust vectoring system mass for both the 10° and 20° nozzle deflection angles for the 50% VT area.

Figure 7.4 can be used to calculate the estimated mass the VT for a given % VT area; however, the data is presented in the table 7.5 to provide transparency for the results

VT Area % of original	Estimated VT Mass [kg]	Correction Factor [-]	Corrected Mass [kg]	% Mass Change [%]
100	427	0.855	365	0.0
85	372	0.855	318	- 12.8
70	315	0.855	270	- 26.0
60	279	0.855	239	-34.4
50	245	0.855	209	-42.6

Table 7.5: VT mass estimation results

7.3. IMPACT OF VERTICAL TAIL MASS ON AIRCRAFT DYNAMICS

In section 6.4.1, a discussion about the coupling of an aircraft's dynamics, maneuvering loads, structural mass and inertia was presented. It was stated that the mass for the VT designs having a reduced area was unknown, and the VT mass would need to be estimated before the aircraft dynamics analysis was completed. An assumption was made which stated the VT mass scales linearly with VT area. For example, the 70% VT area design would have a mass which is 70% of the original VT mass. When examining figure 7.4, the aforementioned assumption was not correct; however, the assumption provided a good first estimation of the VT mass. This assumption is considered to be sufficiently accurate for the feasibility study being presented.

8

Performance Analysis

8.1. Parasite Drag Analysis

One of the research objectives is to determine how the reduction in VT area influences the aircraft's parasite drag coefficient. Parasite drag is consists primarily of skin-friction drag, which is related to the wetted surface area of an aircraft [15]. A reduction in parasite drag is expected to occur when the VT area is reduced, and the parasite drag must be estimated for the five Fokker 100 designs.

VSAERO was used to estimate the parasite drag for the aircraft designs. It should be noted that the VSAERO aircraft model does not include the engine's nacelles and pylons; therefore, the parasitic drag predicted by VSAERO is likely to underestimate the parasite drag of the actual Fokker 100. Fortunately parasite drag estimates for the Fokker 100 and its individual components are presented in reference [3]. By using this data, the parasite drag calculated by VSAERO can be corrected to include the drag contribution for the engine's nacelles and pylon.

In table 8.1, the parasite drag obtained using VSAERO simulations, $CD_{P,aero}$ is shown. The parasite drag coefficient was obtained at Mach 0.75, which is the typical cruise Mach number of the Fokker 100. Table 8.1 also contains the parasite drag coefficient for the Fokker 100 nacelles, $CD_{P,nac}$, and pylons $CD_{P,py}$. By summing the parasite drag coefficient obtained with VSAERO and the parasite drag coefficients for the nacelle and pylons, the total parasite drag coefficient, CD_0 can be estimated.

	Parasite Drag, Component			Total Estimated
VT Area % of original	VSAERO Aircraft $C_{D_{P,aero}} \cdot 10^4$, [-]	Nacelle $C_{D_{P,nac}} \cdot 10^4$, [-]	Pylon $C_{D_{P,py}} \cdot 10^4$, [-]	Parasite Drag $C_{D_0} \cdot 10^4$
100	172.8	16.4	2.0	191.2
85	170.9	16.4	2.0	189.3
70	169.4	16.4	2.0	187.8
60	168.3	16.4	2.0	186.7
50	166.2	16.4	2.0	184.6
C_{D_0} Estimated [3]: 191.6				
C_{D_0} Flight Test [3]: 188.0				

Table 8.1: Parasite drag estimation

To validate the estimation of the parasite drag coefficient, the estimated parasite drag coefficient for the 100% VT area will be compared to values obtained from reference [3]. In this reference, there are two difference parasite drag coefficients corresponding to the Fokker 100. One of the parasite drag coefficient has been estimated using empirical equations and the other has been obtained using flight test data. The values of these parasite drag coefficients are shown in table 8.1. When comparing the parasite drag coefficient which has been estimated with aerodynamic simulations, one can see it closely matches the reference values. It overestimates the parasite drag coefficient obtained using flight tests by 1.7%. This validates the parasite drag coefficient obtained using aerodynamics simulations.

By examining table 8.1 reduction in parasite drag results from a reduction in VT area. Since there is a reduction in parasite drag, it is beneficial to examine how the reduction in drag impacts the aircraft's mission fuel consumption. Now a mission performance analysis will be completed for the five different aircraft designs.

8.2. MISSION PERFORMANCE ANALYSIS

With the reduced VT area, the aircraft's parasite drag coefficient is reduced. To analyze the impact of the parasite drag coefficient on an aircraft's fuel consumption, a mission performance analysis can be completed for the different VT areas, and the impact of the parasite drag on the aircraft's mission fuel mass can be analyzed. For the mission analysis, the Fokker 100 was required to fly 2,900 km. The 2,900 km mission distance included a 200 km diversion to an alternate airport.

For the first mission performance analysis, it was assumed that the net mass reduction of the combined VT and HT bodies was equal to the engine mass addition due to the TVFC. For this analysis, the impact of the reduction in parasite drag on the aircraft's mission fuel weight weight can be recognized. The empty operational mass and payload mass used for the mission analysis are 24,541 kg and 11,108 kg, respectively [56]. This results in a max payload zero fuel mass of 35,649 kg. The results of the parasite drag and mission performance analyses are displayed in table 8.2.

VT Area % of original	Parasite Drag Coefficient [-]	Empty Mass + Payload Mass [kg]	Mission Fuel Mass Mass [kg]	Change in Mission Fuel Mass [%]
100	0.0191	35,649	7,003	0
85	0.0189	35,649	6,973	-0.43
70	0.0188	35,649	6,936	-0.96
60	0.0187	35,649	6,904	-1.41
50	0.0185	35,649	6,886	-1.67

Table 8.2: Analysis of parasite drag on mission fuel mass

Before the results are discussed, some additional information will be provided regarding the method used for the mission performance analysis. The entire mission was discretized into small flight segments. For each flight segment, the aircraft was trimmed using Phalanx, and the aircraft's specific fuel consumption at the trim point was obtained. This allowed for the fuel consumption each individual flight segment to be obtained. With knowledge of the fuel consumption for a given mission segment, the aircraft's fuel mass can be updated to reflect the fuel burnt throughout the mission. For the aircraft's cruise condition, the cruise Mach number was selected such that the aircraft's lift-to-drag ratio was maximized. This indicates that the cruise Mach number was not constant throughout the entire cruise segment. Additionally, the entire cruise segment was completed at an altitude of 10,000 m. Lastly, the mission fuel had to be determined with an iterative method. For example if the aircraft begins the mission with a fuel mass of 7,100 kg and ends the mission with 500 kg, then the starting mission fuel mass must be reduced. After the starting fuel mass is reduced, the mission analysis is completed again. This process was completed until the fuel mass at the end of the mission was $\pm$10 kg or less.

As indicated by the data in table 8.2, the mission fuel decreases as the VT area and parasite drag are reduced. It should be recognized the max payload zero fuel mass remains constant, thus the reduction in mission fuel mass is entirely from the reduction in parasite drag. The reduction in fuel mass is estimated to be less than one percent for the 70% VT area, but it allows for a slight improvement in the aircraft fuel consumption. Improvements in mission fuel consumption above one percent are unlikely since reducing the VT area below 70% produces highly undesirable lateral-directional S&C characteristics.

Now the results of the performance analysis will be completed which assumes the VT mass does not change as its area is reduced. The engine mass used for the simulations increased by 94 kg (2 x 47 kg) which corresponds to the mass increment due to a 10° thrust vectoring nozzle. The purpose of this analysis is to analyze if the estimated mass increment due to thrust vectoring will significantly impact the aircraft's mission fuel mass. Table 8.3 displays the results of the described mission performance analysis.

Thrust Vectoring System with 10° nozzle deflection angles				
VT Area % of original	Parasite Drag Coefficient [-]	Empty Mass + Payload Mass [kg]	Mission Fuel Mass [kg]	Change in Mission Fuel Mass [%]
100*	0.0191	35,649	7,003	0
85	0.0189	35,743	6,976	-0.39
70	0.0188	35,743	6,944	-0.84
60	0.0187	35,743	6,923	-1.14
50	0.0185	35,743	6,900	-1.47

Table 8.3: Analysis of parasite drag on mission fuel mass

From this analysis, it can be seen that the mission fuel mass decreases as the VT area and parasite drag is decreased. The reduction in mission fuel consumption is attributed to the reduction in parasite drag.

At the beginning of this report, it was assumed that a reduction in aircraft mission fuel consumption could be achieved if the reduction in VT mass was equal to the engine mass increase due to the addition of TVFC. By examining the data in table 8.3, this assumption may be considered inaccurate. The aircraft's max payload zero fuel mass increased due to the addition of TVFC; however, a reduction in mission fuel mass was achieved. This shows that even slight reduction in VT area, such as the 85% VT area, may reduce an aircraft's fuel consumption even after the addition of TVFC.

It is important to remember that the 50% and 60% VT areas had poor predicted dynamic stability, thus reductions in mission fuel mass greater than one percent are unlikely. The 70% VT area had a Dutch roll motion which was predicted to be unstable during flight conditions corresponding to landing and takeoff at high altitude (1000+ m) airports. With this statement, vertical tail designs where the VT area is less than 70% of the original VT area will produce unacceptable Dutch roll stability. When combining dynamic stability results with the mission performance results, reductions mission fuel consumption greater than one percent are unlikely.

9

Conclusions and Recommendations

9.1. Conclusions

The goal of the research was to assess the feasibility of a civil transport aircraft designed with thrust vectoring flight control (TVFC) and an unconventionally small vertical tail (VT) design. To guide the research, a research objective was formulated:

> *The research object is to investigate how the (1) lateral-directional stability and control, (2) parasite drag, (3) mission fuel consumption, and (4) empty operational weight of civil transport aircraft designed with thrust vectoring flight control and an unconventionally small vertical tail differ from a comparable, conventional civil transport aircraft design.*

To complete this research objective, the engines, aerodynamics, lateral-directional stability and control, and performance of an existing aircraft design, the Fokker 100, were modeled. This baseline aircraft model was modified such that it could have TVFC capabilities. The thrust vectoring engines were used for directional control. Because the thrust vectoring was used for directional control, the control power requirements of the VT were reduced. This reduction in control power necessitated a redesign of the VT, and four new VTs were designed. The areas of the redesigned VTs were 85%, 70%, 60%, and 50% the area of the baseline VT area, which corresponded to reductions in the vertical tail area of 15%, 30%, 40%, and 50%, respectively..

The a baseline engine, without TVFC, was modeled. The baseline engine model was the updated such that it could be used for the TVFC analysis. Engine performance losses were included in the model to improve the accuracy of the research. The mass addition due to the addition of thrust vectoring flight control was also estimated. It was estimated that the mass of a modern aircraft engine, equipped with thrust reversing capabilities, would increase between 2.7% and 4.6% due to the addition of thrust vectoring technology. This was considered to be a conservative estimate.

An aerodynamic analysis was completed for the five aircraft models. For the aerodynamic analysis, a program named VSAERO was used. With the results from the aerodynamic simulations, the lateral-directional static stability of the various aircraft models was analyzed. All five of the VT designs were shown to be have static lateral-directional stability.

After the completion of the static stability analysis, the lateral-directional dynamic stability of the five different aircraft designs was analyzed. The roll, spiral, and Dutch roll modes were included in the analysis. It was shown that the reduced VT mass and increased engine mass due to the addition of TVFC did not significantly affect the aircraft's roll mode. For the spiral mode, a reduction in VT area was shown to have a destabilizing effect; however, all five of the aircraft had satisfactory spiral flight characteristics. For the Dutch roll mode, a reduction in VT area was accompanied by a reduction in the damping and frequency of the Dutch roll motion. Based on the estimation of the Dutch roll damping coefficients, it was shown the 50% and 60% VT area designs would likely have an unstable Dutch roll mode at takeoff and landing conditions. The 70% VT area had questionable Dutch roll flight characteristics for flight conditions which are comparable to high altitude airports. The 85% VT area had acceptable Dutch roll flight characteristics throughout the aircraft's flight envelope. It has been recommended that a compromise between the 85% and 70% VT area would likely produce an acceptable compromise between the reduced VT area and Dutch roll flight characteristics; however, the aircraft design would required a yaw damper.

Following the lateral-directional stability analysis was a thrust vectoring control analysis. It has been demonstrated that thrust vectoring can be more effective than the rudder in generating yaw moments at low dynamic pressure flight conditions. A trim analysis for one-engine-inoperative (OEI) flight conditions was completed. The results of the analysis demonstrated that increasing the nozzle deflection angle to trim the aircraft during OEI flight conditions reduced the aircraft's OEI flight envelope, and this was attributed to a loss of axial thrust due to thrust vectoring for directional control. By using thrust vectoring to achieve OEI trim, it was shown that the aircraft's rudder deflection, aileron deflection, and bank angle could be reduced. Next, the impact of simultaneously reducing the VT area and using thrust vectoring on the aircraft's OEI flight envelope was discussed. Deflecting the nozzle will reduce the area of the aircraft's OEI flight envelope; however, reducing the VT area results in a reduction of parasite drag, and it is feasible for the parasite drag reduction to compensate for the loss in thrust due to vectoring the nozzle. In the end, the OEI flight envelope of an aircraft designed TVFC and a reduced in VT area may not differ significantly from the OEI flight envelope of the baseline aircraft without TVFC.

For the flight condition corresponding to OEI with a crosswind coming from the side of the inoperative engine, it was shown that the trim drag, thrust vectoring losses, and ram drag are closely coupled. Concrete conclusions are difficult to make due to the complexity of the required flight condition. It is recommended that a detailed trim drag analysis is completed in order to assess the feasible trim drag reduction associated with an increase in thrust vectoring deflection angle.

A discussion was presented regarding the deep stall characteristics of aircraft with T-tail configurations. Reducing the VT area increases the likelihood of an aircraft entering a deep stall; however, thrust vectoring can be used for longitudinal control and to aid the aircraft in recovering from the deep stall. No quantitative data was presented to verify this statement.

Vertical tail aerodynamic loading and mass estimations were also completed. For the loads analysis, maneuvering loads, OEI loads, and gust loads were considered. It was shown a sudden engine failure and the ensuing sideslip angle and pilot rudder input produced the worst case VT loads. With the estimated worst case loads determined, the mass of the various VT designs was estimated. It was demonstrated that the redesign of VT resulted in an increase of the horizontal tail (HT) mass. The net mass change of VT and HT was determined for each of the five VT designs, and the net weight reduction of the combined VT and HT bodies is comparable to the engine mass increment resulting from the addition of TVFC. The results from the mass analysis estimated that the engine mass should increase by less than 5% in order for there to be no change in the aircraft's empty operational mass.

Following the aerodynamic loading and mass analysis was an aircraft performance analysis. A part of this analysis required the estimation of the parasite drag coefficient for the five aircraft designs, and VSAERO simulations were used to complete this task. Because there was a reduction in parasite drag, an analysis of the aircraft's mission performance was completed to analyze the impact of the parasite drag coefficient on the aircraft's mission fuel consumption. It was shown that the parasite drag reduction associated with the 85% VT area resulted in a fuel mass reduction 0.43%.

It was originally assumed that a reduction in mission fuel consumption could be achieved if the reduction in VT mass was equal to the mass increase due to the addition of TVFC. This assumption was shown to be incorrect. It is feasible that an aircraft's mission fuel consumption is reduced through a reduction in VT area and parasite drag. This reduction in mission fuel mass can occur even the aircraft's empty operational mass increased after the addition of TVFC. For the aircraft design with the 85% VT area, a decrease in mission fuel mass of 0.39% is feasible after the addition of TVFC.

Further studies should be completed in relation to the design of an aircraft with TVFC and an unconventionally small VT. At the moment, this proposed aircraft design remains feasible, and it has been predicted that reductions in mission fuel mass can be associated with the aircraft design when compared to similar aircraft designs. Reductions in mission fuel mass greater than 1% are unlikely; however, these are feasible reductions in mission fuel mass for the thrust vectoring civil transport aircraft which has an unconventionally small vertical tail.

9.2. RECOMMENDATIONS

The results of the thesis research have been presented, and it is now beneficial to reflect on the results. The reflection on the results will come in the form of recommendations for future research related to thrust vectoring flight control and its application to civil transport aircraft.

Yaw Damper: In order to verify the feasibility of an aircraft designed with TVFC and an unconventionally small VT, a yaw damper must be designed. It has been demonstrated that a reduction in VT are will cause the Dutch roll flight characteristics of an aircraft to deteriorate. It is recommended that a yaw damper be designed for each of the aircraft designed with a reduced VT area.

OEI with Crosswind Trim: The trim of the aircraft with OEI and a crosswind was shown to be quite complex. A close coupling between the engine's thrust losses due nozzle deflection, trim drag, and ram drag was demonstrated. A detailed analysis of the aircraft's trim drag should be completed in order to see if thrust vectoring during OEI crosswind flight is feasible.

OEI Climb Performance: The rate of climb for an aircraft with OEI must be analyzed. There are specific requirements stated within the FAR 25 related to the OEI climb performance of CTA. High lift devices were not included in the aircraft aerodynamics model, and this prevented an analysis of the OEI climb performance. It should also noted that using TVFC is used to trim the aircraft during OEI flight condition will result in a reduction of axial thrust. The reduction in axial thrust and its impact on the OEI climb performance must be analyzed.

Improved TVFC Mass Estimate: The estimated mass addition due to TVFC was completed using reference data which is more than 20 years old. The mass estimation should be completed such that it reflects modern technology. It is also likely that the engine's pylon mass is impacted by the addition of TVFC. Using the thrust vectoring for directional control with cause the engine's pylon to experience either tensile or compressive forces, and the pylon's structure must be strengthened to account for these additional forces. This would result in an increase in engine pylon mass. There is clearly a deficiency in the method used to estimate the mass addition due to TVFC.

Thrust Vectoring for Longitudinal Control: It may be possible to redesign the horizontal tail if thrust vectoring is used for longitudinal control. Military aircraft have used thrust vectoring for longitudinal control for trimming the aircraft, and this resulted in a reduction in trim drag. It should be reiterated that thrust vectoring is relatively ineffective in high dynamic pressure flows when compared to the the effectiveness of aerodynamic control surfaces. Based on the author's intuition, it is unlikely that TVFC will provide performance benefits in the form of reduced trim drag during cruise flight; however, this statement must be validated.

Thrust Vectoring to Reduce Noise: If thrust vectoring is used for longitudinal trim during climb, then the nozzles would need to be deflected upwards. This would likely reduce the noise perceived by people on the ground because the nozzle is directed away from the earth.

Recovery from Deep Stall: In the occurrence an aircraft enters a deep stall, thrust vectoring for longitudinal control may be used to help the aircraft recover from the stall. An analysis of the thrust vectoring at high angles of attack and in aircraft stall conditions should be completed to verify this statement.

Crosswind Landing Analysis: In order for an aircraft to maintain a constant heading angle during a crosswind landing, the aircraft's rudder must be deflected. If the rudder is too small, then the aircraft may not be able to maintain a constant heading angle. This would indicate that TVFC would be needed to provide directional trim forces during the crosswind landing; furthermore, there would be some axial thrust component, so long as the nozzle is deflected less than 90°. CTA set the engine throttle to idle during a landing in order to minimize the landing speed and distance. Using TVFC during a crosswind landing would increase an aircraft's landing speed and distance. This change in aircraft landing performance should be analyzed.

Control Allocation Methods: If an aircraft is designed with TVFC and traditional aerodynamic control surfaces, then redundant forms of control exist. Detailed knowledge of the control effectors used for the TVFC and aerodynamic control should be obtained. Control allocation methods should be completed in order to ensure the proposed aircraft design has adequate control power throughout the flight envelope.

Bibliography

[1] van Weezepoel, P., Fokker 100 Front Schiphol Tower, [Cover photo]. http://www.dutch-aviation.nl/.

[2] Directorate-General for Research and Innovation EU, 2011. *Flightpath 2050, Europe's Vision for Aviation*, Publications Office of the European Union, Luxembourg.

[3] Obert, E., 2009. *Aerodynamic Design of Transport Aircraft*. Delft, Netherlands: Delft University Press.

[4] Gal-Or, B., 1998 Review of the Debate and the Development of Thrust Vectoring Technology. In: *Journal of Thermal Sciece*, v7(1).

[5] Whitford, R., 1987. *Design for Combat Aircraft*. Coulsdon, United Kingdom: Jane's Information Group.

[6] Mace, J., et al, 1989. Advanced Thrust Vectoring Nozzles for Supercruise Fighter Aircraft. In: AIAA (American Institute of Aeronautics and Astronautics), *AIAA/ASME/SAE/ASEE 25th Joint Propulsion Conference*. Monterey, California, 10-12 July, 1989. Washington, D.C.: AIAA.

[7] Gal-Or, B., 1990. *Vectored Propulsion, Supermaneuverability and Robot Aircraft* New York: Springer-Verlag.

[8] Peron, L.R., Carpenter, T., 1992. *Thrust Vectoring for Lateral and Directional Stability*. Edwards, California: National Aeronautics and Space Administration (NASA).

[9] Steer, A.J., 2000. Integrated Control of a Second Generation Supersonic Commercial Transport Aircraft Using Thrust Vectoring. *American Institute of Aeronautics and Astronautics*, DOI: 10.2514/6.2000-4109.

[10] Cohn, J.A., 1985. Axisymmetric Thrust Reversing Thrust Vectoring Exhaust System for Maneuver and Balanced Field Length Aircraft. In: AIAA (American Institute of Aeronautics and Astronautics), *AIAA/SAE/ASME/ASEE 21st Joint Propulsion Conference*. Monterey, California, 8-10 July, 1985. New York: AIAA.

[11] Pascoa, J.C., et al, 2013. A Review of Thrust-Vectoring in Support of a V/STOL Non-Moving Mechanical Propulsion System. *Central European Journal of Engineering*, v3(3), p374-388.

[12] Richey, G.K., Berrier, B.L., Palcza, J.L., 1977. Two-Dimensional Nozzle/Airframe Integration Technology - An Overview. In: AIAA (American Institute of Aeronautics and Astronautics), *AIAA/SAE 13th Propulsion Conference*. Orlando, Florida, 11-13 July 1977. New York: AIAA.

[13] Omoragbon, A.I., et al, 2013. Feasibility Study of a Thrust Vector Control Transport. In: ASEE (American Society of Engineering Education), *2013 ASEE Gulf-Southwest Annual Conference*. Arlington, Texas, 21-23 March, 2013. ASEE.

[14] Ikaza, D., 2000. Thrust Vectoring Nozzle for Military Aircraft Engines. In: *NATO R&T Organization Symposium on Active Control Technology for Enhanced Performance Operational Capabilities of Military Aircraft, Land Vehicles and Sea Vehicles*. Braunschweig, Germany, 8-11 May 2000.

[15] Raymer, D.P., 1992. *Aircraft Design: A Conceptual Approach*, 2nd ed. Washington, D.C.: American Institute of Aeronautics and Astronautics, Inc.

[16] Lichtsinder, A., Kreindler, E., Gal-Or, B., 1998. Minimum-Time Maneuvers of Thrust-Vectored Aircraft *Journal of Guidance, Control, and Dynamics*, v21(2).

[17] Alcorn, C.W., Croom, M.A., Francis, M.S., Ross, H., 1995. The X-31 Aircraft: Advances in Aircraft Agility and Performance. *Progress in Aerospace Science*, v32, p377-413.

[18] Francis, M.S., Henderson, E.D, 1994. X-31 Enhanced Fighter Maneuverability Demonstrator: Flight Test Achievements. *CAS-94-7.2.1, 19th ICAS Conference*. Anaheim, California, September.

[19] Vinayagam, A.K., Sinha, N.K., 2014. An Assessment of Thrust Vector Concepts for Twin-Engine Airplane. In: *Journal of Aerospace Engineering*, v228(6), p960-979.

[20] Gal-Or, B., 1996. Civilizing Military Thrust Vectoring Flight Control. *Aerospace America, American Institute of Aeronautics and Astronautics*, v34(n4), p20.

[21] Hienz, E., Vedova, R., 1984. Requirements, Definition and Preliminary Design for an Axisymmetric Vectoring Nozzle, to Enhance Aircraft Maneuverability. In: AIAA (American Institute of Aeronautics and Astronautics), *AIAA/SAE/ASME 20th Joint Propulsion Conference*. Cincinnati, Ohio, 11-13 June, 1984. New York: AIAA.

[22] Gal-Or, B., Sherbaum, V., Lichtsinder, M., 1995. Fundamentals of Catastrophic Failure Prevention by Thrust Vectoring *Journal of Aircraft*, v32(3).

[23] Capone, F. et al, 1992 Comparative Investigation of Multiplane Thrust Vectoring Nozzles. In: AIAA (American Institute of Aeronautics and Astronautics), *AIAA/SAE/ASME/ASEE 28th Joint Propulsion Conference and Exhibit*. Nashville, Tennessee, 6-8 July, 1992. Washington, D.C.: AIAA.

[24] Wilson, E.A., Adler, D., Bar-Yoseph, P., 2003. Thrust-Vectoring Nozzle Performance Modeling *Journal of Propulsion and Power*, v19(1).

[25] Hiley, P.E., Wallace, H.W., Booz, D.E., 1976. Nonaxisymmetric Nozzles Installed in Advanced Fighter Aircraft. *Journal of Aircraft*, v13(12) p1000-1006.

[26] Wilson, E.A., Adler, D., Bar-Yoseph, P., 2002. Geometric Evaluation of Axisymmetric Thrust-Vectoring Nozzle for Aerodynamic Performance Predictions *Journal of Propulsion and Power*, v18(3).

[27] Binder, N., Carbonneau, X., 2012. Performance of a Thrust-Vectoring Solution for Unmanned Air Vehicles *Journal of Propulsion and Power*, v28(5).

[28] E.063 Rolls-Royce Deutschland Tay Series Engine. EASA.E.063. Issue 4. June 2013.

[29] Sherbaum, V., Lichtsinder, M., 1998. Jet Deflection Angles in Military, Civil and RPV Thrust Vectoring Aircraft. *International Journal of Turbo and Jet Engines*, v15, p250-273.

[30] Anemaat, W.A.J., Kaushik, B., Po, K., 2011. A Method to Predict Deep Stall. In: AIAA (American Institute of Aeronautics and Astronautics), *AIAA Applied Aerodynamics Conference*. 27-30 June, 2011. Honolulu, Hawaii.

[31] Ellis, D.R., Seckel, E., 1969. Flying Qualities of Small General Aviation Airplanes. *Federal Aviation Administration*.

[32] Berger, T., Tischler, M.B., Hagerott, S.G., Gangsaas, D., Saeed, N., 2013. Lateral/Directional Control Law Design and Handling Qualities Optimization for a Business Jet Flight Control System. In: AIAA (American Institute of Aeronautics and Astronautics), *AIAA Atmospheric Flight Mechanics Conference*. 19-22 August, 2013. Boston, MA.

[33] Tucker, T., 1999. Touchdown: The Development of Propulsion Controlled Aircraft at NASA Dryden. *National Aeronautics and Space Administration*. Washington, D.C.

[34] Roskam, J., 1998. *Airplane Flight Dynamics and Automatic Flight Controls*. Lawrence: Design, Analysis and Research Corporation.

[35] Mulder, J.A., et al, 2013. *Flight Dynamics - Lecture Notes* Delft: Control and Simulation Division.

[36] Oates, G.C., 1985. *Aerothermodynamics of Aircraft Engine Components*. New York: American Institute of Aeronautics and Astronautics

[37] Mattingly, J.D., Heiser, W.H., Pratt, D.T., 2002. *Aircraft Engine Design*. Reston, Virginia, USA: American Institute of Aeronautics and Astronautics

[38] Elham, A., La Rocca, G., Vos, R., 2011. Refined Preliminary Weight Estimation Tool for Airplane Wing and Tail *SAE International Journal of Aerospace* October 2011.

[39] Voskuijl, M., La Rocca, G., Dircken, F., 2008. Controllability of Blended Wing Body Aircraft. *26th International Congress of the Aeronautical Sciences*. Anchorage, Alaska, 14-19 September 2008.

[40] Edmund, D.O., 2012. *A Velocity Decomposition Method For Efficient Numerical Computation of Steady External Flows*. Ph.D. Thesis, University of Michigan. Available at: <https://deepblue.lib.umich.edu/handle/2027.42/96152>

[41] General Electric F110 Turbofan. 2016. *Forecast International Powerweb* <http://www.fi-powerweb.com/Engine/General-Electric-F110.html>

[42] F404 Turbofan Engines. *General Electric Aviation* <https://www.geaviation.com/sites/default/files/datasheet-F404-Family.pdf>

[43] Sung, R., 2013. *A Comparative Study of the GSP 11 and GasTurb 11 on Their Respective Simulations for a Single-Spool Turbojet*. M.Sc. The University of Tennessee-Knoxville. Available at: <http://trace.tennessee.edu/cgi/viewcontent.cgi?article=2897&context=utk-gradthes>

[44] Sadraey, M.H., 2012. *Aircraft Design: A Systems Engineering Approach*. Wiley Publications.

[45] Lighthill, M. J., 1958. On Displacement Thickness. *Journal of Fluid Mechanics*, v4 p383-392.

[46] Lomax, T.L., 1996. *Structural Loads Analysis for Commercial Transport Aircraft: Theory and Practice*. Reston, VA.: American Institute of Aeronautics and Astronautics

[47] Levine, W.S., 1999. *Control System Applications* New York: CRC Press

[48] Torenbeek, E., 1982. *Synthesis of Subsonic Airplane Design*. Dordrecht: Springer Science + Business Media, B.V.

[49] Nicolosi, F., Vecchia, P.D., Ciliberti, D., 2014. Aerodynamic Interference issues in Aircraft Directional Control. *Journal of Aerospace Engineering*, v28(1).

[50] Gal-Or, B., 1990. Fundamental Concepts of Vectored Propulsion. *Journal of Propulsion* v6(6).

[51] Roskam, J., 1985. *Airplane Design Part I: Preliminary Sizing of Airplanes*. Ottawa: Roskam Aviation and Engineering Corporation.

[52] Carlson, J.R., 1992. A Nozzle Internal Performance Prediction Method. NASA-TP-3211, October 1992.

[53] Berrier, B.L., Taylor, J.G, 1990. Internal Performance of Two Nozzles Utilizing Gimbal Concepts for Thrust Vectoring. NASA-TP-2991, February, 1990.

[54] Mutluay, T., 2015. *The Development of an Inertia Estimation Method to Support Handling Quality Assessment*. M.Sc. Thesis, Delft University of Technology.

[55] Wei, J.H. 2016. *Parametric Modelling for Determining Aircraft Stability and Control Derivatives*. M.Sc. Thesis, Delft University of Technology.

[56] Jenkinson, L., Simpkin, P., Rhodes, D., 2001. Civil Jet Aircraft Design. *Butterworth-Heinemann*. Available at: <https://booksite.elsevier.com/9780340741528/appendices/data-a/table-8/table.htm>

[57] Nathman, J.K., 2014. *VSAERO - A Computer Program for Calculating The Nonlinear Aerodynamic Characteristics Of Arbitrary Configuration* v7.7. May, 2014.

[58] U.S. National Archives and Records Administration. *Code of Federal Regulations*. Title 14. Aeronautics and Space. Airworthiness Standards: Transport Category Airplanes. 2014.

[59] Anon., Military Standard, *Flying Qualities of Piloted Aircraft*. MIL-STD-1797A, 30 January, 1990. Unclassified.

[60] Aircraft Structure in the Empennage. Digital image. Free Aviation Study. N.p., 16 May 2015. Web. <http://aviationstudys.blogspot.nl/2015_05_10_archive.html>.

A

Appendix: Vertical Tail Loads Analysis

A.1. Maximum Rudder Deflection Angle

Altitude $[m]$	Mach $[-]$	$\delta_{r,OEI}$ $[deg]$	$\delta_{r,max}$ $[deg]$	Max Yaw Rate $[deg/s]$
0	0.20	-	-	-
0	0.25	20.0	20.0	3.18
0	0.31	14.2	14.2	3.19
0	0.35	12.6	12.6	3.34
0	0.42	-	10.3	3.37
0	0.58	-	7.6	3.36
0	0.75	-	-	-
2,000	0.30	20.0	20.0	3.67
2,000	0.32	16.5	16.5	3.37
2,000	0.35	14.3	14.3	3.33
2,000	0.38	13.1	13.1	3.43
2,000	0.42	-	11.8	3.45
2,000	0.58	-	8.70	3.43
2,000	0.75	-	-	-
3,850	0.30	-	20.0	2.68
3,850	0.42	-	13.0	3.46
3,850	0.58	-	9.80	3.45
3,850	0.75	-	7.90	3.44
6,000	0.30	-	20.0	3.05
6,000	0.42	-	15.2	3.46
6,000	0.58	-	11.4	3.44
6,000	0.75	-	9.20	3.44
10,000	0.42	-	17.2	3.50
10,000	0.58	-	15.7	3.46
10,000	0.75	-	12.8	3.42

Table A.1: Maximum allowable rudder deflection angles. δ_r was calculated such that trimmed OEI flight could be achieved. If trimmed flight could not be achieved with OEI, then yaw rate criteria was used to determine δ_r.

A.2. MANEUVER I LOADS ANALYSIS

Altitude $[m]$	Mach $[-]$	δ_r $[deg]$	Shear Loads $[kN]$	Bending Moment $[kN \cdot m]$	Torsion Moment $[kN \cdot m]$
0	0.30	14.2	16.1	28.3	-5.25
0	0.42	10.3	23.7	44.6	-10.9
0	0.58	7.60	45.3	79.8	-15.5
2,000	0.30	20.0	16.6	29.3	-5.44
2,000	0.42	11.8	21.3	40.1	-9.79
2,000	0.58	8.70	40.7	71.6	-13.9
3,850	0.30	20.0	13.1	23.2	-4.30
3,850	0.42	13.0	18.6	35.0	-8.53
3,850	0.58	9.80	36.3	63.8	-12.4
3,850	0.75	7.90	54.7	93.6	-17.7
6,000	0.30	20.0	9.87	17.4	-3.23
6,000	0.42	15.2	16.3	30.7	-7.49
6,000	0.58	11.4	31.7	55.7	-10.8
6,000	0.75	9.20	47.9	81.8	-15.4
10,000	0.42	17.2	10.3	19.4	-4.75
10,000	0.58	15.7	24.4	43.0	-8.35
10,000	0.75	12.8	37.9	64.8	-12.2

Table A.2: Maneuver I Loads - Rudder is abruptly deflected to $\delta_{r,max}$ as specified in table A.1.

A.3. MANEUVER II LOADS ANALYSIS

Altitude $[m]$	Mach $[-]$	δ_r $[deg]$	β_{OY} $[deg]$	Shear Loads $[kN]$	Bending Moment $[kN \cdot m]$	Torsion Moment $[kN \cdot m]$
0	0.30	14.2	10.7	-8.84	-16.5	2.86
0	0.42	10.3	8.70	-31.8	-55.8	7.46
0	0.58	7.60	6.15	-39.3	-71.5	8.36
2,000	0.30	20.0	15.8	-10.3	-19.2	3.35
2,000	0.42	11.8	10.4	-31.0	-54.4	7.49
2,000	0.58	8.70	7.28	-37.9	-68.7	8.26
3,850	0.30	20.0	14.3	-6.13	-11.5	1.98
3,850	0.42	13.0	11.7	-27.7	-48.7	6.76
3,850	0.58	9.80	8.43	-35.7	-64.9	7.90
3,850	0.75	7.90	5.98	-40.6	-72.5	8.67
6,000	0.30	20.0	13.9	-4.26	-8.03	1.38
6,000	0.42	15.2	13.3	-23.2	-40.7	5.56
6,000	0.58	11.4	10.1	-32.7	-59.4	7.33
6,000	0.75	9.20	7.10	-37.2	-66.2	8.02
10,000	0.42	17.2	13.5	-12.2	-21.3	2.71
10,000	0.58	15.7	13.9	-25.5	-46.2	5.71
10,000	0.75	13.0	9.89	-28.4	-50.7	6.08

Table A.3: Maneuver II Loads - Rudder is abruptly deflected to $\delta_{r,max}$ and aircraft yaws to β_{OY}.

A.4. MANEUVER III LOADS ANALYSIS

Altitude $[m]$	Mach $[-]$	β_{ss} $[deg]$	Shear Loads $[kN]$	Bending Moment $[kN \cdot m]$	Torsion Moment $[kN \cdot m]$
0	0.30	7.35	-17.1	-30.8	5.67
0	0.42	5.30	-33.9	-61.2	11.2
0	0.58	3.65	-50.2	-89.7	14.1
2,000	0.30	10.7	-18.3	-33.0	5.96
2,000	0.42	6.15	-30.8	-55.8	10.2
2,000	0.58	4.17	-45.0	-80.5	12.7
3,850	0.30	9.64	-13.0	-23.4	4.24
3,850	0.42	6.63	-26.3	-47.5	8.68
3,850	0.58	4.54	-38.8	-67.3	10.9
3,850	0.75	3.39	-54.1	-94.3	14.9
6,000	0.30	10.8	-10.9	-19.6	3.55
6,000	0.42	7.64	-22.7	-41.1	7.51
6,000	0.58	5.11	-32.7	-58.5	9.23
6,000	0.75	3.84	-46.0	-80.1	12.7
10,000	0.42	6.05	-10.1	-18.2	3.33
10,000	0.58	5.17	-18.6	-33.2	5.24
10,000	0.75	5.38	-36.1	-62.8	9.96

Table A.4: Maneuver III Loads - Rudder is deflected to $\delta_{r,max}$ and the aircaft achieves a steady sideslip angle of β_{ss}. After β_{ss} is achieved, the rudder deflection is abruptly set to 0°.

A.5. ONE-ENGINE-INOPERATIVE I LOADS ANALYSIS

Altitude $[m]$	Mach $[-]$	β_{OY} $[deg]$	Shear Loads $[kN]$	Bending Moment $[kN \cdot m]$	Torsion Moment $[kN \cdot m]$
0	0.30	3.97	-6.02	-10.8	1.96
0	0.42	3.35	-21.4	-38.7	70.7
0	0.58	3.72	-51.2	-91.6	14.4
2,000	0.30	4.99	-8.54	-15.4	2.78
2,000	0.42	3.95	-22.3	-40.3	7.36
2,000	0.58	3.87	-41.8	-74.7	11.8
3,850	0.30	5.10	-6.90	-12.4	2.25
3,850	0.42	3.96	-15.7	-28.4	5.18
3,850	0.58	3.81	-32.5	-58.2	9.17
3,850	0.75	3.39	-54.2	-9.43	14.9
6,000	0.30	6.55	-6.65	-12.0	21.7
6,000	0.42	4.40	-13.1	-23.7	4.35
6,000	0.58	3.90	-25.0	-44.7	7.05
6,000	0.75	3.50	-41.9	-73.0	11.6
10,000	0.42	7.60	-12.7	-22.9	4.18
10,000	0.58	4.40	-15.8	-28.3	4.46
10,000	0.75	3.71	-24.9	-43.4	6.87

Table A.5: One-Engine-Inoperative Loads I - Engine failure occurs and the aircraft yaws. No pilot correction occurs, and the aircraft yaws to some maximum overyaw angle, β_{OY}.

A.6. ONE-ENGINE-INOPERATIVE II LOADS ANALYSIS

Altitude $[m]$	Mach $[-]$	δ_r $[deg]$	β $[deg]$	Shear Loads $[kN]$	Bending Moment $[kN \cdot m]$	Torsion Moment $[kN \cdot m]$
0	0.30	14.2	1.24	-12.3	-21.8	4.03
0	0.42	10.3	1.67	-34.4	-63.9	14.4
0	0.58	7.60	2.68	-82.2	-146	25.9
2,000	0.30	20.0	1.51	-19.2	-34.0	6.28
2,000	0.42	11.8	1.74	-33.7	-62.7	14.2
2,000	0.58	8.70	2.39	-66.4	-118	21.2
3,850	0.30	20.0	1.37	-15.0	-26.5	4.90
3,850	0.42	13.0	1.45	-24.3	-45.3	10.4
3,850	0.58	9.50	2.07	-53.9	-9.54	17.4
3,850	0.75	7.90	2.70	-97.8	-169	29.5
6,000	0.30	20.0	1.58	-11.5	-20.3	3.75
6,000	0.42	15.2	1.45	-20.3	-37.9	8.80
6,000	0.58	11.4	1.73	-42.7	-75.5	13.9
6,000	0.75	9.20	2.36	-76.2	-131	23.3
10,000	0.42	17.2	1.55	-12.9	-24.1	5.60
10,000	0.58	15.7	1.34	-29.3	-51.6	9.71
10,000	0.75	13.0	1.68	-49.2	-84.5	15.3

Table A.6: One-Engine-Inoperative II Loads - Engine failure occurs and the aircraft yaws. The pilot applies the $\delta_{r,max}$ two seconds after the failure occurs.

A.7. GUST LOADS ANALYSIS

Altitude $[m]$	Mach $[-]$	Shear Load $[kN]$	Bending Moment $[kN \cdot m]$	Torsion Moment $[kN \cdot m]$
0	0.25	-27.2	-9.56	0.670
0	0.42	-57.6	-20.4	1.42
0	0.58	-90.4	-31.6	1.89
2,000	0.30	-24.0	-8.42	0.594
2,000	0.42	-50.7	-17.9	1.26
2,000	0.58	-79.5	-27.8	1.68
3,850	0.42	-44.6	-15.8	1.11
3,850	0.58	-69.8	-24.4	1.48
3,850	0.75	-101	-34.4	2.10
6,000	0.42	-39.1	-13.8	0.983
6,000	0.58	-61.2	-21.4	1.31
6,000	0.75	-88.7	-30.1	1.85
10,000	0.42	-30.8	-10.9	0.780
10,000	0.58	-48.1	-16.8	1.04
10,000	0.75	-69.6	-23.6	1.47

Table A.7: Gust load weight analysis based on FAR 25.341